GLASILO SLOVENSKIH TEKSTILCEV • SLOVENE JOURNAL FOR TEXTILE AND CLOTHING TECHNOLOGY, DESIGN AND MARKETING

tekstilec

4/2022 • vol. 65 • 243–328
ISSN 0351-3386 (tiskano/printed)
ISSN 2350 - 3696 (elektronsko/online)
UDK 677 + 687 (05)

Univerza *v Ljubljani*
Naravoslovnotehniška fakulteta

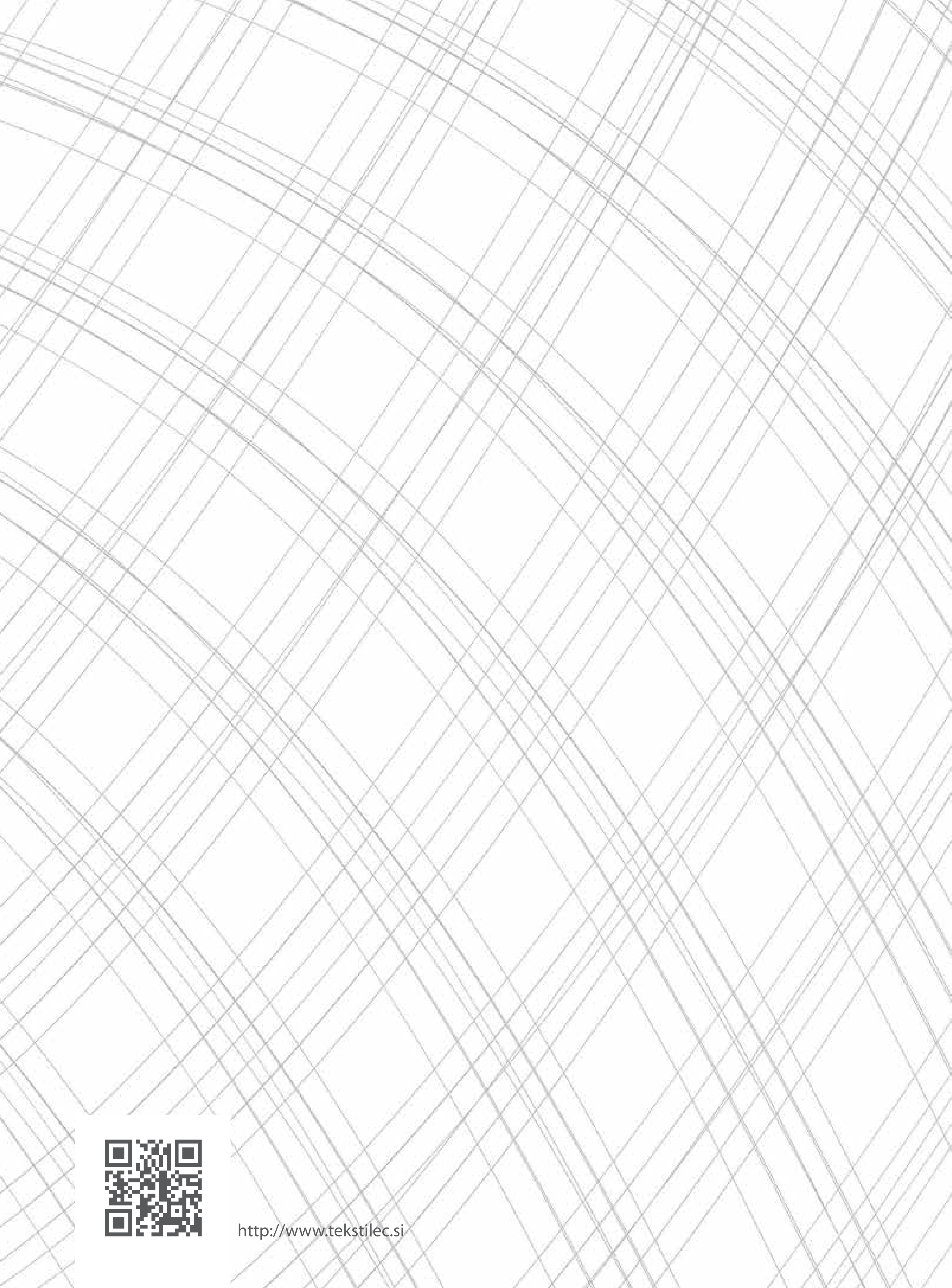

http://www.tekstilec.si

tekstılec (ISSN: 0351-3386 tiskano, 2350-3696 elektronsko) je znanstvena revija, ki podaja temeljne in aplikativne znanstvene informacije v fizikalni, kemijski in tehnološki znanosti, vezani na tekstilno in oblačilno tehnologijo, oblikovanje in trženje tekstilij in oblačil. V prilogah so v slovenskem jeziku objavljeni strokovni članki in prispevki o novostih v tekstilni tehnologiji iz Slovenije in sveta, prispevki s področja oblikovanja tekstilij in oblačil, informacije o raziskovalnih projektih ipd.

tekstılec *(ISSN: 0351-3386 printed, 2350-3696 online) the scientific journal gives fundamental and applied scientific information in the physical, chemical and engineering sciences related to the textile and clothing industry, design and marketing. In the appendices written in Slovene language, are published technical and short articles about the textile-technology novelties from Slovenia and the world, articles on textile and clothing design, information about research projects etc.*

Dosegljivo na svetovnem spletu/*Available Online at*
www.tekstilec.si

Crossref

Tekstilec je indeksiran v naslednjih bazah/*Tekstilec is indexed in*
Emerging Sources Citation Index – ESCI (by Clarivate Analytics):
Journal Citation Indicator, JCI (Material Science, Textiles): 2021: 0.34
Leiden University's Center for Science & Technology Studies:
2021: SNIP 0.726
SCOPUS/Elsevier (2021: Q3, SJR 0.312, Cite Score 1.9, H Index 13)
Ei Compendex
DOAJ
WTI Frankfurt/TEMA® Technology and Management/
TOGA® Textile Database
World Textiles/EBSCO Information Services
Textile Technology Complete/EBSCO Information Services
Textile Technology Index/EBSCO Information Services
Chemical Abstracts/ACS
ULRICHWEB – global serials directory
LIBRARY OF THE TECHNICAL UNIVERSITY OF LODZ
dLIB
SICRIS: 1A3 (Z, A', A1/2); Scopus (d)

tekstilec

Ustanovitelja / *Founded by*

- Zveza inženirjev in tehnikov tekstilcev Slovenije / *Association of Slovene Textile Engineers and Technicians*
- Gospodarska zbornica Slovenije – Združenje za tekstilno, oblačilno in usnjarsko predelovalno industrijo / *Chamber of Commerce and Industry of Slovenia – Textiles, Clothing and Leather Processing Association*

Revijo sofinancirajo / *Journal is Financially Supported*

- Javna agencija za raziskovalno dejavnost Republike Slovenije / *Slovenian Research Agency*
- Univerza v Ljubljani, Naravoslovnotehniška fakulteta / *University of Ljubljana, Faculty of Natural Sciences and Engineering*
- Univerza v Mariboru, Fakulteta za strojništvo / *University of Maribor, Faculty for Mechanical Engineering*

Izdajatelj / *Publisher*
Univerza v Ljubljani, Naravoslovnotehniška fakulteta /
University of Ljubljana, Faculty of Natural Sciences and Engineering

Revija Tekstilec izhaja pod okriljem Založbe Univerze v Ljubljani/
The journal Tekstilec is published by the University of Ljubljana Press

Sponzor / *Sponsor*
Predilnica Litija, d. o. o.

Naslov uredništva / *Editorial Office Address*
Uredništvo Tekstilec, Snežniška 5, SI–1000 Ljubljana
Tel./*Tel.*: + 386 1 200 32 00, +386 1 200 32 24
Faks/*Fax*: + 386 1 200 32 70
E–pošta/*E–mail*: tekstilec@ntf.uni–lj.si
Spletni naslov / *Internet page:*
http://www.tekstilec.si; https://journals.uni-lj.si/tekstilec

Lektor za slovenščino / *Slovenian Language Editor* Milojka Mansoor
Lektor za angleščino / *English Language Editor*
Barbara Luštek-Preskar, Glen Champagne

Oblikovanje platnice / *Design of the Cover* Tanja Nuša Kočevar
Oblikovanje / *Design* Miha Golob
Oblikovanje spletnih strani / *Website* Design Jure Ahtik

Tisk / *Printed by* PRIMITUS, d. o. o.

Revija Tekstilec izhaja štirikrat letno /
Journal Tekstilec appears quarterly

Revija je pri Ministrstvu za kulturo vpisana v razvid medijev pod številko 583. Letna naročnina za člane Društev inženirjev in tehnikov tekstilcev je vključena v članarino.
Letna naročnina za posameznike 38 €
za študente 22 €
za mala podjetja 90 € za velika podjetja 180 €
za tujino 110 €

Cena posamezne številke 10 €

Na podlagi Zakona o davku na dodano vrednost sodi revija Tekstilec med proizvode, od katerih se obračunava DDV po stopnji 5 %.

Imetnik računa / *Account holder*
Univerza v Ljubljani,
Naravoslovnotehniska fakulteta,
Askerceva 12, 1000 Ljubljana, SI-Slovenija

Transakcijski račun / *Bank Account*
SI56 01100–6030708186,
Banka Slovenije,
Slovenska 35, 1000 Ljubljana, SI-Slovenija

SWIFT / SWIFT Code: BSLJSI2X

tekstılec VOLUME 65 • TEKSTILEC 4 2022 ISSN 0351-3386 (tiskano/printed)
UDK 677 + 687 (05)

SCIENTIFIC ARTICLES/
Znanstveni članki

Jantera Sekar Tirta[1]*, Hoerudin*[2]*, Ida Nuramdhani*[1,3]
[1] *Politeknik STTT Bandung, Bandung, Indonesia*
[2] *Indonesian Center for Agricultural Postharvest Research and Development, Bogor, Indonesia*
[3] *Department of Textile Chemistry, Politeknik STTT Bandung, Bandung, Indonesia*

Fastness Improvement of a Crystalline Liquid Thermochromic Print on Cotton Fabric by the Application of Silica Nanoparticles from Rice-Husk

Izboljšanje obstojnosti termokromnega tiska s tekočimi kristali na bombažni tkanini z uporabo nanodelcev silicijevega dioksida iz riževih lupin

Original scientific article/*Izvirni znanstveni članek*
Received/*Prispelo* 7-2022 • Accepted/*Sprejeto* 11-2022

Corresponding author/*Korespondenčna avtorica:*
Ida Nuramdhani, S.Si.T., M.Sc., Ph.D.
E-mail: ida.nuramdhani@stttekstil.ac.id
ORCID ID: 0000-0002-1034-3598

Abstract

Most commercially available thermochromic dyes are not resistant to washing and rubbing when applied to textile materials. This is due to their low affinity for fibre. The addition of silica extracted from rice husk ash using the sol-gel method was performed to improve colour fastness and maintain the stability of thermochromic dyes printed on cotton fabrics. The rice husks used in this study were derived from the *Baroma* rice variety with silica content in ash and silica gel of 97.05% and 99.20%. The morphological structures and particle sizes of the silica obtained were analysed using a scanning electron microscope (SEM) and particle size analyser (PSA). The particle sizes of the silica product, thermochromic dye and silica-dye mixture were 53.64–60.66 nm, 2.603 nm and 5.827 nm, respectively. The printing process of silica: the dye mixture was applied to cotton fabric in a ratio of 1:1. Fluid of silica: the dye showed good stability until the seventh day of observation. Colour fastness to washing assessed using a staining scale was better with the addition of silica than without silica, i.e. 3–4. Similarly, fastness to rubbing was also better with the addition of silica, i.e. 3–4 dry rubbings and 3 wet rubbings. Moreover, the combination of silica, binder, PDMS and dye (in a ratio of 1 : 1 : 1 : 1) gave the best colour fastness to washing and rubbing.

Keywords: rice husk, silica, thermochromic dyes, liquid crystal, printing

Izvleček

Večina komercialno dostopnih termokromnih barvil, nanesenih na tekstilne materiale, ni odporna proti pranju in drgnjenju. To je posledica njihove nizke afinitete do vlaken. Dodatek silicijevega dioksida, ekstrahiranega iz pepela riževih lupin z metodo sol-gel, je bil namenjen izboljšanju barvne obstojnosti in ohranitvi stabilnosti termokromnega barvila, natisnjenega na bombažne tkanine. V tej študiji so bile uporabljene riževe lupine sorte riža Baroma z vsebnostjo silicijevega dioksida v pepelu in silikagelu 97,05 % in 99,20 %. Morfološke strukture in velikost delcev dobljenega silicijevega dioksida so bili analizirani s pomočjo vrstičnega elektronskega mikroskopa (SEM) in analizatorja velikosti delcev

(PSA). Velikosti delcev silicijevega dioksida, termokromnega barvila in mešanice silicijevega dioksida in barvila so bile 53,64–60,66 nm; 2,603 nm oziroma 5,827 nm. Tiskanje na bombažno tkanino je bilo izvedeno z mešanico silicijevega dioksida in barvila v razmerju 1:1. Tekoča mešanica silicijevega dioksida : barvilo je pokazala dobro stabilnost do sedmega dneva opazovanja. Barvna obstojnost pri pranju, ocenjena s prehodom barvila na spremljevalno tkanino, je bila ob dodatku silicijevega dioksida boljša kot brez silicijevega dioksida, tj. ocena 3–4. Podobno je bila tudi obstojnost pri drgnjenju boljša ob dodatku silicijevega dioksida, in sicer ocena 3–4 pri suhem in ocena 3 pri mokrem drgnjenju. Poleg tega je kombinacija silicijevega dioksida : veziva : PDMS (polidimetilsiloksana) : barvila v razmerju 1 : 1 : 1 : 1 dala najboljšo barvno obstojnost pri pranju in drgnjenju.

Ključne besede: riževe luščine, silicijev dioksid, termokromna barvila, tekoči kristal, tisk

1 Introduction

Thermochromic dyes, the most frequently used smart dyes among other developed chromic materials, change colour reversibly or irreversibly when the temperature of the surrounding environment changes [1], even in the context of a minor temperature change [2]. Based on their ability to respond to the stimuli of changing temperature, thermochromic dyes are divided into two types: leuco and crystalline liquid. As seen in Figure 1 [3], the leuco type exhibits a single colour change through a molecular rearrangement, while the crystalline liquid, which is made of a cholesteric liquid crystal, can demonstrate a spectrum of colour change [4]. The colour change shown by thermochromic liquid crystal (TLC) is initially colourless at room temperature, then red when the temperature increases to yellow, green, blue, and purple, and then colourless again, depending on the reflected wavelength at a certain temperature [5]. Both types of thermochromic dyes have been widely used in various smart textile applications, primarily for sensor applications or for aesthetic purposes in fashion products. For these purposes, the smart properties of the thermochromic dyes can be expanded if their technical properties can be improved.

One of the important properties to be improved in terms of thermochromic print on cotton is colour fastness. It is evident from available literature that some thermochromic dyes are susceptible to photochemical reactions, which causes colour fading, which in turn indicates a low affinity to fibres and poor fastness to light [6]. Some commercially available thermochromic dyes were also reported to be unwashable when applied to textiles [7, 8]. Previous studies reported that silica nanoparticles could effectively increase the fastness properties of thermochromic dyes, either by immobilizing the thermochromic dyes in the silica nanoparticles [9] or by coating the silica sol-gel on the surface of the thermochromic dye-printed textile materials [10]. Silica is generally prepared using vapor-phase reaction, sol-gel and thermal decomposition methods. Various techniques have been used to produce pure nano-sized silica with a high surface area using an

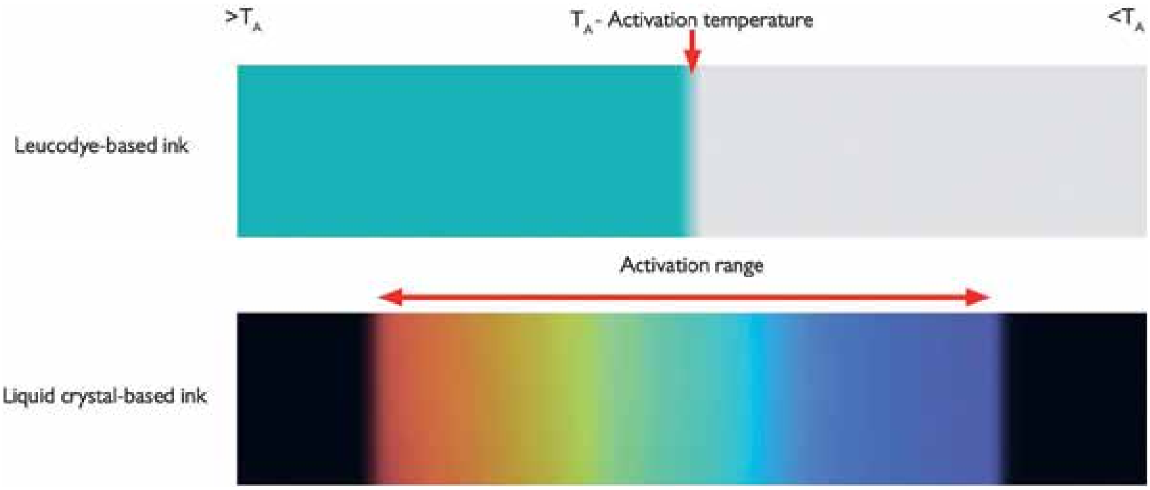

Figure 1: Changes in leuco and liquid crystal types of dyes [3]

easy-to-use alkaline extraction followed by an acid precipitation method. This method can be used conventionally and has the advantages of being simple, cost-effective, and reproducible. The results of previous studies indicate that the use of silica nanoparticles to improve the fastness of thermochromic dyes is still the subject of a great deal of additional study, and is thus the background of this study.

In this study, silica was synthesized from rice husk biomass. Using the proper preparation treatment of silica from rice, husks can be used in the textile sector. The utilization of rice husks is potentially promising, including in Indonesia, which is an agricultural country, with rice as one of its most important commodities. Based on the results of a BPS (Indonesian Central Bureau of Statistics) survey, Indonesia recorded very high grain production in 2021 of about 54.42 million tons of GKG (milled dry grain) [11]. From each rice milling process, rice husks usually account for between 20–30% of the initial weight of the grain. Rice husk waste is widely found in rural areas as a by-product of rice milling, and has great potential. The silica content in rice husk is 15–20% [12]. If the rice husk is converted into ash, the silica content is 99% [13]. The rice sample used in this study was the *Baroma* variety in the form of grain as shown in Figure 2. It was therefore necessary to carry out a milling process to separate the rice and rice husks.

Rice husk has many organic and inorganic compounds that are quite complex. Several steps are thus required to achieve pure silica form. The many methods used to obtain silica nanoparticles include the sol-gel method, reverse micro emulsion, and heat synthesis. The sol-gel method was used to produce pure silica because it can control particle size, size distribution and morphology through reaction parameters [14]. The silica used was the result of synthesis using sol-gel as shown in Figure 3. One of the potential uses of nanometre-sized silica in textile materials is to improve the properties or characteristics of various smart dyes.

Figure 3: Silica gel from a sol-gel synthesis process

The colouring of a textile material can be achieved using a dye that is applied through dyeing or by printing. Printing using a flatscreen is the oldest but easiest method because of its simple application [15]. In this study, a printing process was selected as the method of application of the thermochromic

a) *b)*

Figure 2: Rice grain (a) and rice husk (b) of the Baroma variety

dye. The effect of nano-silica from rice husks and its combination with other additives (binding agent and polydimethylsiloxane) to the fastness of the printing results was studied.

2 Materials and methods

2.1 Materials

Silica nanoparticle gels were synthesized from the rice husk of the Baroma variety obtained from the Indonesian Centre for Rice Research at the Ministry of Agriculture. The detailed process of making silica nanoparticles is not described in this study. However, the production steps referred to in [16, 17] are mentioned here, with some modifications. The resulting silica characterized using particle size analysis (PSA; Zetasizer Nano Range, Malvern Instrument) showed that the mean size of the silica obtained from the rice husk ash and from the sol-gel process were 30.06 nm–46.44 nm and 53.64–60.66 nm, respectively. The surface area, pore radius and silica pore volume analysed using Brunauer–Emmett–Teller analysis (BET Quantachrome QuadraWin ©2000-16, Quantachrome Instruments) gave the results of 224.1660 m^2/g, 4.16759 nm, and 0.4671 cm^3/g, respectively. The amorphous properties of the silica were shown using X-ray diffraction analysis (XRD Shimadzu XRD-7000). The thermochromic liquid crystal used for this study has the commercial name of Temperature Responsive Liquid Crystal Sprayable Ink, with an activation temperature of 24–29 °C. It is manufactured by Good Life Innovations Ltd (Special FX Creative). Stabiprint B–PK 400 binder (acrylic copolymers) was purchased from a local supplier. Polydimethylsiloxane (PDMS) linker was purchased from Wacker. The 100% black cotton fabric was obtained from the stock in our laboratory.

2.2 Methods

2.2.1 Preparation of the thermochromic print on cotton

Before being printed on the prepared cotton fabric, the thermochromic dye and mixtures thereof were stirred at 500 rpm for 60 minutes [18]. Flat screen printing was selected as the best method among others, such as padding or spraying to obtain an even distribution of the TLC ink on the fabric surface. The same method was also reported previously by other researchers [19]. The method was also suitable for the TLC used in this study, as suggested by the supplier, [20] and it demonstrated minimum viscosity for the flat screen-printing process, even without the addition of thickeners or other auxiliaries. The screen used was a monofilament polyester (70–80 threads/cm), as suggested in the product technical data sheet. Furthermore, the addition of binder and silica nanoparticles in the form of sol-gel could also increase the viscosity of the print paste. Four variations of mixture were prepared as follows: (1) V1: TLC (thermochromic liquid crystal) + binder; (2) V2: TLC + silica; (3) V3: TLC + binder + silica; and (4) V4: TLC + binder + silica + PDMS. In addition, printing fabric with only TLC (without binder) was also prepared for comparison purposes, particularly for testing the washing fastness. Printing the TLC with binder (V1) is a commonly applied composition. In V2, binder was not added to compare the effect between silica and binder to the washing fastness of the printed fabric. The mixture effect of binder and silica was represented in V3 and, finally, PDMS was added to the mixture of V3 to study its effect on improving the washing fastness of the printed fabric. All variations were prepared with a composition of each ingredient in a ratio of 1 : 1. The prepared mixtures (Table 1) were then flat screen printed using a T80 screen. Each printed fabric was then dried at a tem-

Table 1: Variations of printing paste mixtures

Printing paste	Concentration (g/100 g)				
	TLC	Binder	Silica	PDMS	Distilled water
Blank	50.0	/	/	/	50.0
V1	33.3	33.3	/	/	33.3
V2	33.3	/	33.3		33.3
V3	25.0	25.0	25.0	/	25.0
V4	20.0	20.0	20.0	20.0	20.0

perature of 60 °C with a drying distance of 30 cm from the fabric for two minutes. Based on product technical information [21] (Good Life Innovations Ltd (Special FX Creative), n.d.), this type of thermochromic dye is not resistant to heat. For this reason, curing at a high temperature was not performed in this experiment.

2.2.2 Fluid stability test

Sedimentation photography is the main method for studying sedimentation in fluids. A decrease in fluid stability can be caused by the distribution of particles that tend to agglomerate when stored for a certain period of time. In this method, a number of synthesized nanofluids containing silica gel were stored in a tube to take photos at regular intervals for seven days. Visual analysis was carried out to determine the stability. The observation was carried out at room temperature for seven days to see if there was any separation and phase change, following the method described in a previous study [22].

2.2.3 Visual colour-change response test

The colour change evaluation of each printed sample was performed 30 times to observe the temperature when changing colour. A Peltier cooler box, equipped with thermo-control as presented in Figure 4, was used as a container to observe changes in the colour response of the fabric that can be adjusted at a certain temperature. The colour changes of the fabric were observed.

2.2.4 Evaluation of colour fastness to rubbing and washing

The colour fastness to rubbing of the thermochromic cotton fabrics was tested according to SNI ISO 105-X12 (E): 2016 (Textiles – Tests for colour fastness – Part X12: Colour fastness to rubbing). Samples were separately rubbed to and from in a straight line at a rate of one cycle per second, 20 times, 10 times to and 10 times from, along a track (104 ± 3) mm, with dry and wet standard crocking clothes under vertical pressure (downward force of (9 ± 0,2) N by a manual crocking fastness tester with a rubbing finger appropriate for solid colour fabrics. Before testing, samples and rubbing clothes were conditioned for at least four hours in the standard atmosphere defined in ISO 139. The evaluation was carried out by assessing the staining of the cotton rubbing cloths with the grey scale for staining under suitable illumination, in accordance with ISO 105-A03. While evaluating, each tested rubbing cloth was backed by three layers of the identical rubbing cloth. The colour fastness to washing was tested according to SNI ISO 105-C06:2010 (Textiles – Tests for colour fastness – Part C06: Colour Fastness to domestic and commercial laundering). Two-single fabrics made of cotton and wool were attached to the different sides of the tested fabric, in accordance with relevant sections F01 to F08 of ISO 105-F:1985. The washing conditions followed the test number A1M in Table 2 in the standard: at 40 °C for 45 minutes in 150 ml washing

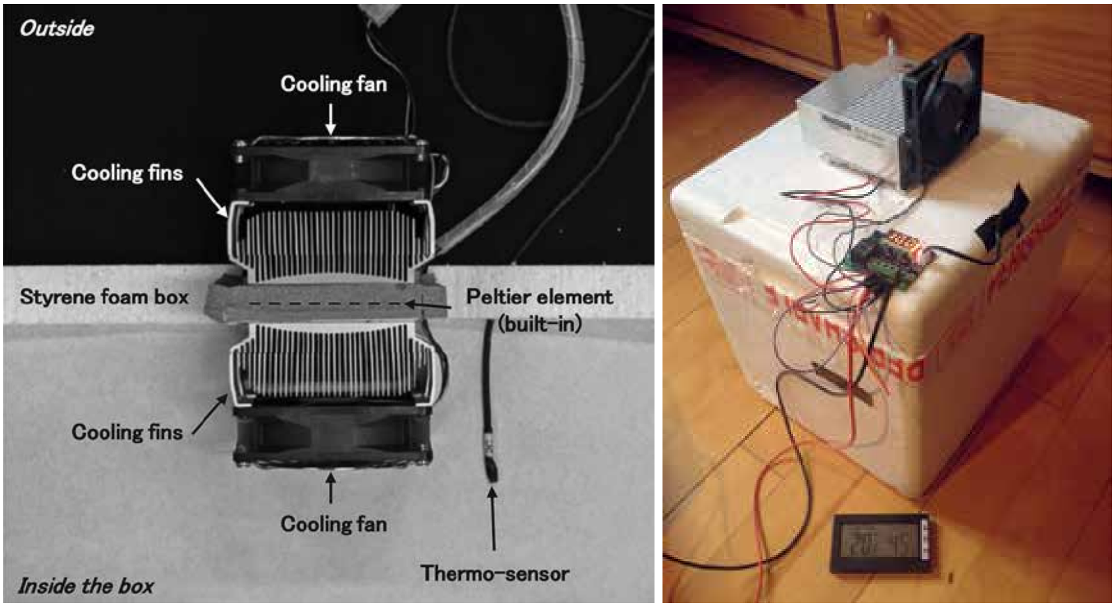

Figure 4: Temperature control design [23]

liquor containing 4 g/l ECE phosphate reference detergent, without an optical brightening agent, and 10 steel balls. The test number A1M is equivalent to five cycles of domestic washing. The evaluation was carried out by assessing the change in colour of the sample and the staining of the adjacent fabrics using the grey scale, according to ISO 105-A03. In order to verify that the thermochromic effect was still active, all the tested samples were re-evaluated in a Peltier cooler box according to the aforementioned procedures (2.2.3).

3 Results and discussion

The silica nanoparticles used in this study were a product of rice husk ash, which was extracted from the Baroma variety of rice using the sol-gel method. The result was in the form of a gel that was used as an additional material in the printing process on fabrics. Silica gel was an inorganic and amorphous polymer formed by the condensation of silicate tetrahedrons using oxygen as a binding site, giving rise to siloxane (Si-O-Si) bonds. The synthesis method of the silica gel will be reported separately, so it is not described in details in this study. The particle size of the silica from the rice husk analysed by PSA was distributed between 53.64–60.66 nm, while the original size of the thermochromic dyes (TLC) used in this study was 2.603 nm. The large size of the dye was caused by aggregation during the analysis process. In the process of mixing silica gel and dye, a stirring process was applied using a magnetic stirrer at a speed of 500 rpm to allow movement for the dye to fill the pores and stick to the silica surface as illustrated in Figure 5. This followed one of mechanisms described by Pilkington et al. [24] about immobilization techniques, which were divided into four major groups, i.e. based on the physical mechanisms of immobilization, adsorption to a pre-formed carrier, physical entrapment within a porous matrix, self-aggregation in floes and the containment of cells behind a barrier. The result of the particle size obtained after this process was 5.827 nm. The distribution of thermochromic dyes filling the pores of the nano silica gel and making a physical bonding with the silica surface could be the reason for an increase in the particle size during analysis.

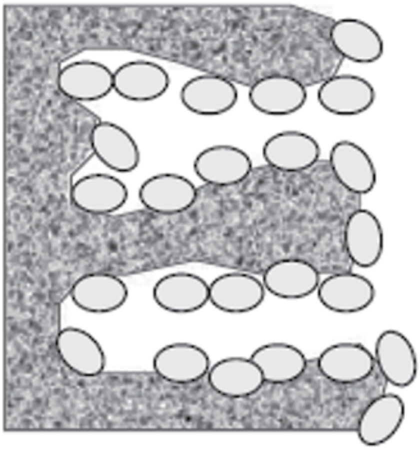

Figure 5: Illustration of immobilization of particles in substance pores [25]

The mixture stability for each variation provided, i.e. thermochromic liquid crystal dye (TLC) + binder, TLC + silica, TLC + binder + silica, and TLC + binder + silica + PDMS was observed as previously explained for seven days. The predetermined time interval was set to observe the stability of the mixtures. Sedimentation was not shown by all mixtures, as can be seen from the image in Figure 6. All mixtures kept showing agglomerations after being stored for seven days, which occurred because of the Van der Waals forces between very reactive nanoparticles. This agglomeration must be maintained until all the particles were dispersed in the entire fluid. Although agglomeration has become one of obstacles in the manufacture of mixed flow, stability was demonstrated in this case.

Five printed fabrics with different composition of chemicals were evaluated, in particular for their thermochromic effects and fastness. As previously mentioned, the five printed fabrics were treated differently, i.e. blank, V1), V2, V3 and V4. A Peltier cooler box, equipped with a thermo-control in a container, was used to observe the activation temperature of each sample. To determine the typical activation temperature (T) of the dye, the test was repeated 30 times. From the test, it was determined that the average temperatures to turn the dye coloured and colourless were 24.13 °C and 29.37 °C, respectively. These two activation temperatures were then used as a standard temperature to verify the thermochromic effect after each treatment. The black fabric used for the application of thermochromic dyes changed from colourless to red, green, and

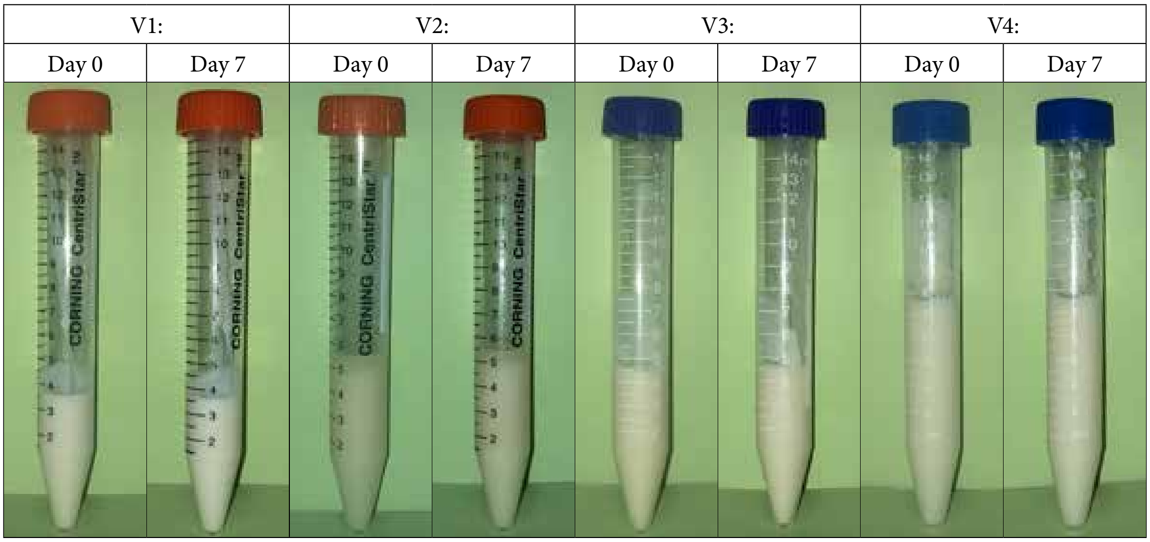

Figure 6: Visual appearances of fluid stability of various printing substance mixtures

blue and then turned colourless again at the optimal temperature (29 °C). Reversibility was demonstrated in this test due to the alternating changes of the dyestuff structure, depending on the ambient temperature. As previously mentioned, based on observations of the printed fabric, the colour change of the TLC started at an average of 24 °C, while the optimum temperature change was at 29 °C. This dye has the special feature of changing the colour spectrum due to temperature. Colour emerged from changes in the liquid crystal orientation structure with regard to temperature and the way light interacts with liquid crystals to produce coloured reflection by interference [26]. TLC is capable of rotating the plane of polarization of linearly polarized light and reflecting colours in the visible light spectrum from the red to the blue spectrum, depending on temperature [5]. This explains why TLC has an activation temperature range of 24–29 °C. Figure 7 shows the visual appearance of each printed fabric with all variations with different composition at ambient temperature (32 °C), as well as the colour changing at their activation temperature (24–29 °C).

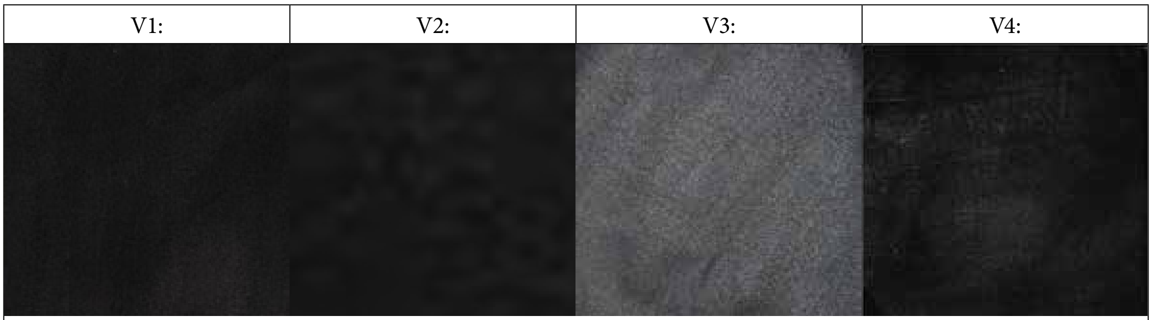

(a) ambient temperature

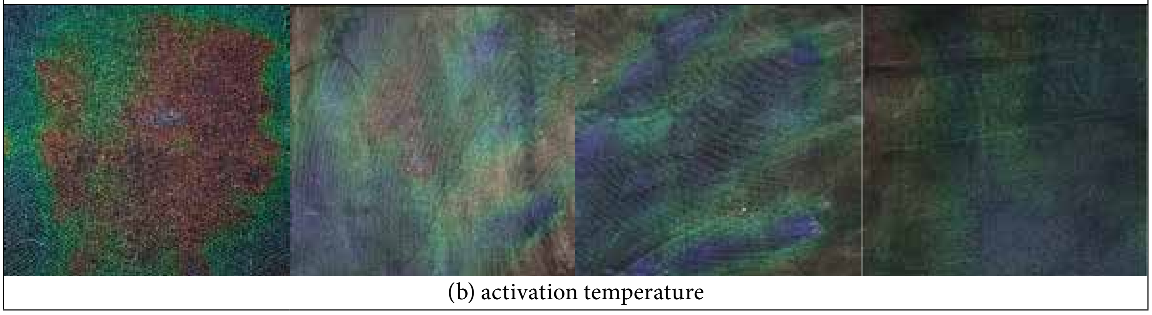

(b) activation temperature

Figure 7: Visual observation of the thermochromic effect of the printed fabrics

The evaluation of fastness to washing and rubbing was carried out for all printed fabrics. The thermochromic effect of each fabric after being washed and rubbed was also observed. The results of the fastness tests are presented in Table 1. It can be seen that the addition of silica to the commonly used composition of the TLC printing process (V3) improved its washing and rubbing fastnesses from 3 or 3–4 to 4. The addition of PDMS resulted in further improved, giving staining scales of 4–5 and 4 for washing and rubbing fastness, respectively. Moreover, the resulting thermochromic cotton fabrics presented good thermochromic performances after washing and rubbing. In other words, the washings did not change the thermochromic capability of the TLC applied to the fabrics. On the contrary, the washing fastness of each fabric printed with TLC + binder and TLC + silica alone (V1 and V2) did not show better results. It appears that the binder and silica resulted in similar effects with regard to the strength of the physical interaction between TLC and the fabric, which in turn affected their fastnesses to washing and rubbing. This is possible because the diffusion of dyes into the pores of silica provided protection to the dyes from direct interaction to washing and rubbing, but could not improve the interaction with the fabric. Likewise, the binding agent helped the dyes interact with the fabric. After washing or rubbing, however, the interactions were weakened, as there was no protection similar to the silica-dye combination. When combined, both effects were obtained.

As observed, the silica had an -OH group that was expected to help improve fastness properties against both washing and rubbing. Silica is a material that contains a large number of small 'nano-sized' pores, making it possible to be used as a matrix material to accommodate a variety of functional materials. A thermochromic dye interacted with the surface of the silica matrix. The tiny pores of silica provided free space for the dye molecules to fill. In the presence of -OH on the silica and -OH on the fabric, hydrogen bonds occurred together with the formation of a physical bond (Van der Waals). These bonds played a role by providing the effect of increasing the fastness of the dye.

The addition of a binder in the printing process can generally increase colour fastness. This is because the binder is a film-forming agent composed of long-chain macromolecules, which when applied to the textile together with the pigment, produce a three-dimensional network. However, this process requires several supportive conditions such as heat and change in pH value [27]. The TLC used in this study was very unstable to an increase in temperature. For this reason, heating to allow complete polymerization and thus the formation of the three-dimensional network was not applied. This explains why the addition of a binder to the mixture did not work optimally as expected. PDMS in this study was added as a long chain alkyl agent and has excellent water-repellent properties [28]. The addition of PDMS also had a good effect on the surface of the printed fabric because it removed the white effect of the added silica (see V4 in Figure 7). The addition of these chemicals also reduced the surface tension properties of the fabric. From the observations, it could be seen that printing only with dyes gave the worst fastness results, in both washing and rubbing, which was expected. The evaluation of the fabric with the addition of binder and silica successively gave better fastness results than before. The addition of PDMS to the mixture then gave the best results in colour resistance to both washing and rubbing. This is due to the long alkyl chain which has a water-repelling effect that reduces the solubility of the dye during washing, as seen in Figure 8.

Table 2: Colour fastnesses of the thermochromic print fabrics

Samples	Colour fastness to washing			Colour fastness to rubbing		Thermochromic effect	
	Grey scale for staining		Grey scale for colour change	Grey scale for staining		After washing	After rubbing
	on cotton	on wool		On dry rubbing cloth	On wet rubbing cloth		
Blank	3	3	3	3	2-3	√	-
V1	3-4	3-4	3	3-4	3	√	√
V2	3-4	3-4	3-4	3-4	3	√	√
V3	4	4	4	4	4	√	√
V4	4-5	4	4-5	4	4	√	√

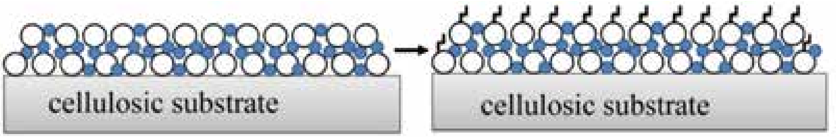

Figure 8: Illustration of fabric surface scheme after the printing process with and without PDMS [29]

4 Conclusion

Durable, reversible colour-changing cotton fabrics were successfully prepared using printing TLC with silica nanoparticles. Moreover, the thermochromic fabrics demonstrated improved colour fastness due to the silica nanoparticle hydrogen and physical bond structures among the fibres. Washing and rubbing fastnesses all exceeded 3–4. The evaluation of colour fastness to washing and rubbing gave better results with the addition of silica than without that addition, but variations of silica, binder, PDMS and dye (in a ratio of 1:1:1:1) gave the best results.

Acknowledgments

The authors are grateful for the material support and laboratory facilities of the Indonesian Agricultural Postharvest Research and Development at the Ministry of Agriculture. The authors would also like to thank Smartex funding under the Erasmus+ scheme of the European Union (project number: 610465-EPP-1-2019-1-EL-EPPKA2-CHBE-JP Smart textiles Modernisation of Curriculum of Textile Engineering and Textile Technology in Indonesia, Malaysia, and Pakistan 9SMARTEX)) for the support given to this study.

References

1. FERRARA, M., BENGISU, M. Intelligent design with chromogenic materials. *JAIC-Journal of the International Colour Association*, 2014, **13**, 54–66, https://aic-color.org/resources/Documents/jaic_v13_06_GdC2013.pdf.
2. CHOWDHURY, M.A., BUTOLA, B.S., JOSHI, M. Application of thermochromic colorants on textiles: temperature dependence of colorimetric properties. *Coloration Technology*, 2013, **129**(3), 232–237, doi: 10.1111/cote.12015.
3. JAKOVLJEVIĆ, M., KULČAR, R., PASANEC PREPROTIĆ, S., POLJIČAK, A., KLANJŠEK GUNDE, M. Dynamic colour changes of thermochromic leuco dye and liquid crystal based printing inks. In *International Joint Conference on Environmental and Light Industry Technologies, 20 – 22 November 2013, Budapest, Hungary*, doi: 10.13140/RG.2.2.34274.56005.
4. BAMFIELD, P., HUTCHINGS, M.G. *Chromic phenomena: technological applications of colour chemistry*. Cambridge : Royal Society of Chemistry, 2010, 9–20, doi: 10.1039/9781849731034-FP009.
5. LCR Hallcrest. *Handbook of thermochromic liquid crystal technology*. Glenview : Hallcrest, 2014.
6. AITKEN, D., BURKINSHAW, S.M., GRIFFITHS, J., TOWNS, A.D. Textile applications of thermochromic systems. *Review of Progress in Coloration and Related Topics*, 1996, **26**(1), 1–8.
7. GOBALAKRISHNAN, M., THANABAL, V., RAJESH KUMAR, S., ASHOK KUMAR, A. The effect of binders on the fastness properties of thermochromic dyes. *International Journal of Engineering Trends and Technology*, 2020, **68**(2), 61–63.
8. SOBKOVÁ, M. T*he application aspects of thermochromic textile coating : Master's Thesis*. [Brno : University of Technology, Faculty of Chemistry], 2018, https://www.vut.cz/www_base/zav_prace_soubor_verejne.php?file_id=170153.
9. RIBEIRO, L.S., PINTO, T., MONTEIRO, A., SOARES, O.S.G.P., PEREIRA, C., FREIRE, C., PEREIRA, M.F.R. Silica nanoparticles functionalized with a thermochromic dye for textile applications. *Journal of Materials Science*, 2013, **48**(14), 5085–5092, doi: 10.1007/s10853-013-7296-7.
10. MAHLTIG, B., HAUFE, H., BÖTTCHER, H. Functionalisation of textiles by inorganic sol-gel coatings. *Journal of Materials Chemistry*, 2005, **15**(41), 4385–4398, doi: 10.1039/b505177k.
11. Luas panen dan produksi padi di Indonesia 2021 [online]. Badan Pusat Statistik [accessed 10 November 2022]. Available on World Wide Web: <https://www.bps.go.id/publication/2022/07/12/c52d5cebe530c363d0ea4198/luas-panen-dan-produksi-padi-di-indonesia-2021.html#:~:text=Abstraksi,54%2C42%20juta%20ton%20GKG>.
12. SINGH, B. Rice husk ash. In *Waste and Supplementary Cementitious Materials in Concrete: Characterisation, Properties, and*

Applications. Edited by Rafat Siddique and Paulo Cachim. Elsevier, 2018, 417–460, doi: 10.1016/B978-0-08-102156-9.00013-4.

13. BAKAR, R.A., YAHYA, R., GAN, S.N. Production of high purity amorphous silica from rice husk. *Procedia Chemistry*, 2016, **19**, 189–195, doi: 10.1016/j.proche.2016.03.092.
14. RAHMAN, I.A., PADAVETTAN, V. Synthesis of silica nanoparticles by sol-gel: size-dependent properties, surface modification, and applications in silica-polymer nanocompositesa review. *Journal of Nanomaterials*, 2012, **2012**, doi: 10.1155/2012/132424.
15. DESSIE, A., ESHETU, B. The role of binders and its chemistry in textile pigment printing. *Journal of Textile Science & Engineering*, 2021, **11**(1), 1–6.
16. LIOU, T.H., YANG, C.C. Synthesis and surface characteristics of nanosilica produced from alkali-extracted rice husk ash. *Materials Science and Engineering B: Solid-State Materials for Advanced Technology*, 2011, **176**(7), 521–529, doi: 10.1016/j.mseb.2011.01.007.
17. SETYAWAN, N., HOERUDIN, WULANAWATI, A. Simple extraction of silica nanoparticles from rice husk using technical grade solvent: effect of volume and concentration. *IOP Conference Series: Earth and Environmental Science*, 2019, **309**(1), 1–8, doi: 10.1088/1755-1315/309/1/012032.
18. KUŚMIEREK, K., ŚWIĄTKOWSKI, A. The influence of different agitation techniques on the adsorption kinetics of 4-chlorophenol on granular activated carbon. *Reaction Kinetics, Mechanisms and Catalysis*, 2015, **116**(1), 261–271, doi: 10.1007/s11144-015-0889-1.
19. CHINDAPRASIRT, P., RATTANASAK, U. Eco-production of silica from sugarcane bagasse ash for use as a photochromic pigment filler. *Scientific Reports*, 2020, **10**(1), 1–8, doi: 10.1038/s41598-020-66885-y.
20. Temperature responsive liquid crystal sprayable ink [online]. SFXC [accessed 10 November 2022]. Available on World Wide Web: <https://www.sfxc.co.uk/products/sfxc-sprayable-liquid-crystal-ink>.
21. Instructions for liquid crystal ink [online]. Good Life Innovations Ltd (Special FX Creative) [accessed 10 November 2022]. Available on World Wide Web: <https://findmydata.cloud/uploads/pdf/liquid-crystal-ink-24c-to-29c-7.pdf>.
22. HARIYATNO, S.P., PARAMITA, V., AMALIA, R. The effect of surfactant, time, and speed of stirring in the emulsification process of soybeaan oil in water. *Journal of Vocational Studies on Applied Research*, 2021, **3**(1), 21–25.
23. Homemade Peltier cooler / fridge with temperature controller DIY [online]. DIY Electronics [accessed 10 November 2022]. Available on World Wide Web: <https://www.instructables.com/Homemade-Peltier-Cooler-W-Temperature-Control-DIY-/>.
24. PILKINGTON, P.H., MARGARITIS, A., MENSOUR, N.A., RUSSELL, I. Fundamentals of immobilised yeast cells for continuous beer fermentation: a review. *Journal of the Institute of Brewing*, 1998, **104**(1), 19–31, doi: 10.1002/j.2050-0416.1998.tb00970.x.
25. NEDOVIC, V.A., OBRADOVIC, B., LESKOSEK-CUKALOVIC, I., VUNJAK-NOVAKOVIC, G. Immobilized yeast bioreactor systems for brewing – recent achievements. In *Engineering and Manufacturing for Biotechnology*. Edited by Marcel Hofman and Philippe Thonart. (Focus on Biotechnology, vol 4). Dordrecht : Springer, 2001, 277–292, doi: 10.1007/0-306-46889-1_18.
26. CHRISTIE, R.M. Chromic materials for technical textile applications. In *Advances in the Dyeing and Finishing of Technical Textiles*. Edited by M.L. Gulrajani. Elsevier, 2013, 3–36, doi: 10.1533/9780857097613.1.3.
27. ASADUZZAMAN, M., HOSSAIN, F., KAMRUZZAMAN, M., MIAH, M.R. Effects of binder and thickeners of pigment printing paste on fastness properties of printed fabric. *International Journal of Scientific and Engineering Research*, 2016, **7**(9), 710–719.
28. Wacker Chemie AG [online]. WACKER [accessed 10 November 2022]. Available on World Wide Web: < https://www.wacker.com>.
29. AYAZI-YAZDI, S., KARIMI, L., MIRJALILI, M., KARIMNEJAD, M. Fabrication of photochromic, hydrophobic, antibacterial, and ultraviolet-blocking cotton fabric using silica nanoparticles functionalized with a photochromic dye. *The Journal of the Textile Institute*, 2017, **108**(5), 856–863, doi: 10.1080/00405000.2016.1195088.

Mahfuza Pervin, Sanjida Sultana, Fahmida Faiza Fahmi, Zinia Yasmin, Sushama Saha Swati
Primeasia University, Department of Textile Engineering, Banani, Dhaka, Bangladesh

---

Evaluation of the Stripping Performance of Monochlorotriazine/Vinyl Sulphone Reactive Dyes with a Reductive Stripping Agent

Ocena učinkovitosti razbarvanja monoklorotriazin/vinilsulfonskih reaktivnih barvil z redukcijskim razbarvalnim sredstvom

Original scientific article/*Izvirni znanstveni članek*
Received/*Prispelo* 8-2022 • Accepted/*Sprejeto* 11-2022

Corresponding author/*Korespondenčna avtorica:*
Fahmida Faiza Fahmi
E-mail: faizabutex@gmail.com
ORCID ID: 0000-0002-0486-4856

Abstract

The wet processing industry experiences various problems, such as the faulty and uneven shade of dyeing, colour patch formation on the surface of dyed fabric, etc. during the dyeing and subsequent processing of textile materials. Stripping is considered a process that helps to reuse faulty dyed fabrics by minimizing dyeing faults. The aim of this paper is to evaluate the effectiveness of stripping agents and the quality of stripped cotton knit fabrics that were coloured using bi-functional (monochlorotriazine/vinyl sulphone) reactive dyes. First, the trichromatic combination of Drimarene Yellow CL2R, Drimarene Red CL5B and Drimarene Blue HFRL dyes was used to dye fabrics in two different shade percentages, namely light shade (0.3% owf) and dark shade (3.0% owf). Consequently, stripping was carried out using varying concentrations of stripping chemicals (hydrose ($Na_2S_2O_4$) and caustic soda (NaOH)) and process temperatures. Stripped fabrics were assessed after measuring the weight loss percentage, strength loss percentage, whiteness index and stripping efficiency. The results of that assessment showed a relatively better stripping performance with the chemical concentration of 5 g/L hydrose and 5 g/L caustic soda at 100 °C. Under this condition, the value of the whiteness index and stripping efficiency were adequate, with a minimum weight loss percentage and strength loss percentage. The stripping performance for the light shade (0.3% owf) fabric was deemed to be better than that for the dark shade (3.0% owf) fabric.

Keywords: reactive dye, reductive stripping, temperature, whiteness index, stripping efficiency

Izvleček

Industrija mokre obdelave se srečuje z raznolikimi težavami, kot so napačni in neenakomerni barvni odtenki, barvni madeži na površini obarvanega blaga in težavami, ki nastanejo med barvanjem in poznejšo obdelavo tekstilnih materialov. Razbarvanje je postopek, ki zmanjša napako pri barvanju in s tem omogoči ponovno uporabo barvanega blaga. Namen tega članka je oceniti učinkovitost sredstev za razbarvanje in kakovost razbarvanih bombažnih pletiv z uporabo bifunkcionalnih (monoklorotriazinskih/vinil sulfonskih) reaktivnih barvil. Prvič je bila za barvanje pletiv v dveh različnih odtenkih uporabljena trikromatska kombinacija barvil Drimarene Yellow CL2R, Drimarene Red CL5B in

Drimarene Blue HFRL, in sicer za svetli odtenek 0,3 % barvila na maso pletiva in za temni odtenek 3,0 % barvila na maso pletiva. Zato je bilo razbarvanje izvedeno z različnimi koncentracijami sredstev za razbarvanje (natrijev hidrosulfit in natrijev hidroksid) in spreminjanjem temperature postopka. Razbarvana pletiva so bila ocenjena glede na odstotek zmanjšanja mase, odstotek znižanja trdnosti, indeksa beline in učinkovitosti razbarvanja. Ugotovljena je bila relativno boljša učinkovitost razbarvanja s koncentracijo 5 g/L natrijevega hidrosulfita in 5 g/L natrijevega hidroksida pri 100 °C. Pri teh pogojih sta bili vrednosti indeksa beline in učinkovitosti razbarvanja ustrezni ob minimalnem odstotku zmanjšanja mase in trdnosti. Učinkovitejše razbarvanje je bilo doseženo pri pletivu s svetlim odtenkom (0,3 % barvila na maso pletiva) kot pri pletivu s temnim odtenkom (3,0 % barvila na maso pletiva).

Ključne besede: reaktivno barvilo, reduktivno razbarvanje, temperatura, indeks beline, učinkovitost razbarvanja

1 Introduction

Reactive dyes are one of the versatile classes of dyes containing a reactive group that makes a covalent bond with the terminal hydroxyl group (-OH) of cellulosic fibres, and act as an integral part of the fibre [1–3]. Textile companies use over 10,000 different classes of synthetic dyes for colouring numerous materials with a production of over 7 × 10^5 metric tonnes every year [4–6, 8]. During the dyeing and finishing of textile products, certain common faults are typically found, including uneven dyeing, inappropriate dyeing and the formation of colour patches on the fabric surface [6–8]. During the colouration process of cellulosic fibres with reactive dyes, undesirable errors and accidents occur, such as colour dots, different colour hues, and off shades that decrease fabric quality and value significantly. Various methods such as direct levelling, lightening with auxiliaries, re-dyeing in deeper shades or colour stripping can be employed to rectify dyeing faults. These dyeing faults can be overcome using the chemical stripping process of reactive dyes. Though dyeing faults can be removed by the stripping process, this process is comparatively difficult due to the presence of the covalent bond formed between the fibre and reactive dyes. Stripping is thus one of the reduction processes that can be used to reduce the concentration of dye in dyed fabric. These processes are also known as “destructive stripping” or “back stripping”. In destructive stripping, colours are chemically reduced, while only the depth of shade is altered in back stripping. The stripping process aims to break the bonds between the chromophoric groups and the bridging groups of reactive dyes that are bonded with the cellulosic fibres through the reactive group, and thus creates discolouration [9]. For reduction purposes, strong reducing agents are used, which are electro-positive elements that can lose electrons in chemical reactions, known as electron donors. An atom with a relatively large atomic radius tends to be a better reductant or reducing agent. In such elements, the distance from the nucleus to the valence electrons is so long that these electrons are not strongly attracted. This type of element, such as hydrose, also tends to be a strong reducing agent for reductive stripping. The presence of caustic soda in a boiling solution under a suitable alkaline medium is created, and the alkaline aqueous solution helps hydrose to accelerate the release of nascent hydrogen. This nascent hydrogen attracts the covalent bond between the cotton fibre and reactive dyes, which is mainly responsible for the effective completion of the reducing reaction of the stripping process [8, 9]. Chemical reduction of an azo group (-N=N-) to an almost colourless amine derivative is possible in the case of destructive stripping [6, 8]. Chromophore groups of reactive dyes can be reduced, and an attempt is made to break chemical bonds to remove colours from fabric [10]. In order to increase the effectiveness of a reducing agent’s ability to remove dyes from fabric and reduce reactive dyes, a stripping assistant is incorporated in addition to reducing agents [8]. The purpose of using a reducing agent is to promote the reduction process for the removal of fixed dyes from fabric, while a stripping assistant helps to promote the reduction capacity. A variety of combinations of reducing agents and stripping assistants are used to strip the dye from fabric [8]. The type of dyes, fibres, reducing agents, auxiliaries, stripping assistants and significant processing parameters (time, temperature, and pH) basically regulate the mechanism of reductive stripping. For a proper reduction effect, the use of appropriate time and temperature is mandatory. Treating fabric in a boiling alkaline solution is necessary to ensure an effective stripping process. Without boiling an alkaline solution, stripping cannot be completed effectively. That is why a temperature of 100 °C is employed. By conducting the stripping process at 80 °C, an attempt was made to determine whether the stripping of fabric could be carried out properly at a lower temperature or not [10]. In this work, stripping is carried out at temperatures of 80 °C and at 100 °C separately. Reactive dyes cannot be adequately removed from cellulose base fabric because a covalent bond has formed between the dye and fibre [8, 9]. The quality of the fabric is impacted and occasionally produces a harsh handle when high temperatures are used in alkaline reductive stripping [6].

By adjusting the reducing agent, alkali level and temperature, the author of one study report demonstrated the impact of reductive stripping on the quality of cotton fabric that was coloured using reactive dyes [7]. Another author discussed in detail an analysis of the performance of stripping chemicals on bi-functional reactive dyes [6]. The chemical colour stripping of cellulosic fabric dyed using reactive dyes has been shown in certain other studies. In this research work, the identical nature of reactive dye was used to produce a combination shade, while different shade percentages were used for dyeing fabrics to establish stripping processes. In addition, the whiteness index of stripped fabrics was assessed in this work, which was not found in other related studies. The aim of this study was to develop more effective stripping processes and to investigate the optimum concentration of reducing agents and temperature, and to assess the impact of stripping on the quality of dyed cotton fabric [7].

2 Materials and methods

2.1 Materials

Single jersey cotton fabric of 152 g/m^2 was selected to carry out the assessment. The pre-treated (scoured and bleached) fabric samples were sourced from Epyllion Knittex Limited, Banglabazar, Gazipur. Three distinct reactive dyes – Drimarene Yellow CL2R, Drimarene Red CL5B, and Drimarene Blue HFRL – were used to produce trichromatic shades for the assessment process and gathered from Archroma (Bangladesh) Limited. Auxiliary chemicals for the dyeing and stripping process, such as Dekol 1097 (sequestering agent), Leonil EH (wetting agent), Glauber's salt ($Na_2SO_4 \cdot 10\ H_2O$), soda ash (Na_2CO_3), acetic acid (CH_3COOH), hydrose ($Na_2S_2O_4$), and caustic soda (NaOH), were also supplied by the same supplier for research purposes.

2.2 Dyeing process

The pre-treated fabric was dyed with a trichromatic combination to produce a light shade (0.3% owf) and a dark shade (3.0% owf), using the exhaust method in an IR sample dyeing machine for 40 minutes at a temperature of 60 °C. The liquor ratio of the sample was maintained at 1:30, while the pH value of the dye bath was 10.5 during dyeing process. The study continued using the hot wash method after the dyeing process, and the specimens went through the neutralization process with 1cc/L of acetic acid for five minutes and the soaping process with 1 g/L of Dekol SN for five minutes at a temperature of 80 °C. The dyeing of pre-treated fabric was carried out according to the recipe given in Table 1 and using the dyeing curve in Figure 1.

Table 1: Recipe of the dyeing process to produce light shade (0.3% owf) and dark shade (3.0% owf) fabric using reactive dyes

No.	Shades of the dyed fabric			Dyeing auxiliaries			
	Dyes	Combined shade (%owf)	Individual shade (%owf)	Glauber's salt(g/L)	Soda ash(g/L)	Wetting agent (cm^3/L)	Sequestering agent(cm^3/L)
1	Drimarene Red CL5B Drimarene Yellow CL2R Drimarene Blue HFRL	0.3	0.1	20	12	1	1
2	Drimarene Red CL5B Drimarene Yellow CL2R Drimarene Blue HFRL	3.0	1.0	60	18	1	1

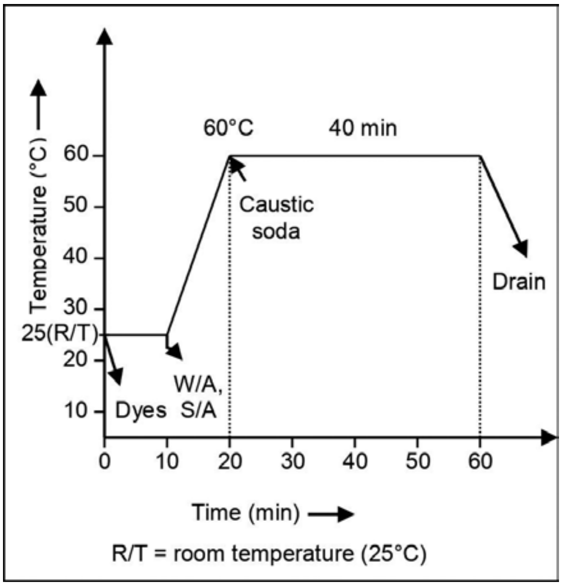

Figure 1: Time-temperature curve of dyeing

2.3 Stripping process

The assessment of the stripping performance of eight different variations of stripping recipes was performed for each shade percentageusingan IR exhaust sample dyeing machine with a material-to-liquor ratio of 1:40. The timeframe required for the stripping operation was 30 minutes. Details regarding the recipes used for the stripping process are given in Table 2, while the stripping curve is shown in Figures 2 and 3.

2.4 Assessment of fabric quality

Measurement of weight loss percentage

The reduction of fabric weight after stripping five-grams of fabric sample was calculated by examining the weight of the fabric before and after the stripping process. Weight reduction after the stripping process was measured using equation 1 [11].

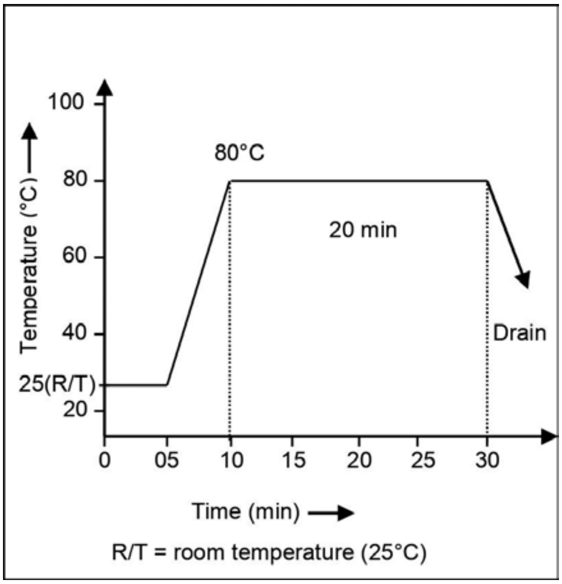

Figure 2: Time-temperature curve of stripping (80 °C)

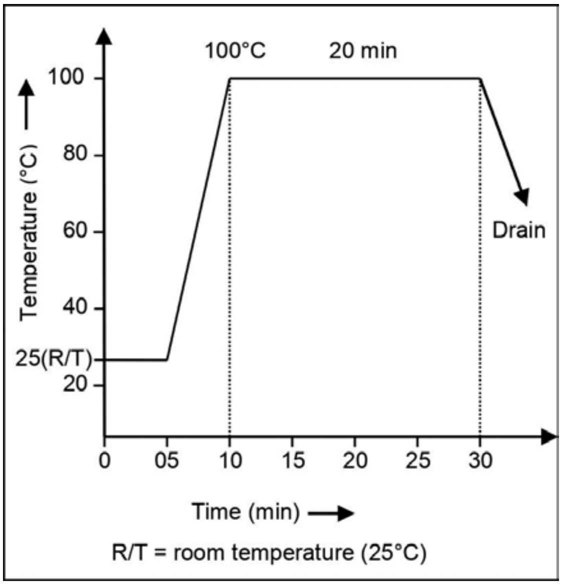

Figure 3: Time-temperature curve of stripping (100 °C)

$$\text{Weight loss} = \frac{\text{(Fabric weight before stripping - Fabric weight after stripping)}}{\text{Fabric weight before stripping}} \times 100\ (\%) \tag{1}$$

Measurement of fabric strength loss percentage

The strength loss of the stripped fabrics was evaluated by a bursting strength tester, which was an indicator of the effectiveness of the stripping process. The bursting strength of the dyed and striped fabric was evaluated using ISO 13938-1:1999. Calculation of the bursting strength loss of the stripped fabric was executed by the following mentioned equation 2 [11].

$$\text{Strength loss} = \frac{\text{(Fabric strength before stripping - Fabric strength after stripping)}}{\text{Fabric strength before stripping}} \times 100\ (\%) \tag{2}$$

Table 2: Recipe of the stripping process with reductive stripping chemicals

No.	Temperature used in process (°C)	Concentration of hydrose (g/L)	Concentration of caustic soda (g/L)
1	80	5	2.5
2		5	5
3		10	5
4		10	10
5	100	5	2.5
6		5	5
7		10	5
8		10	10

The consequence of strength loss due to stripping in the fibre surface was visualized using scanning electron microscope (SEM) images for the dyed and stripped fabrics of the light shade (0.3% owf) and the dark shade (3.0% owf) at a magnification of 500x.

The strength factor with respect to hydroxyl groups (-OH) was determined by Fourier transform infrared (FTIR) using PerkinElmer FTIR instrument model MB 3000 manufactured by ABB Canada.

Assessment of whiteness index

Whiteness is associated with the region in the colour space where objects are recognized as white. The whiteness index is measured by the degree of departure of the object from pure white [12]. It was measured using a Datacolor SF 600 dual-beam spectrophotometer in accordance with CIE (Commission internationale de l'éclairage) standards. The whiteness index of pre-treated fabric was 70.74 (WI-CIE) and whiteness index of stripped fabric was measured to assess the outcome of stripping.

Stripping efficiency

Stripping efficiency was assessed using the degree of colour removal from dyed samples. Lightness values (L^*) were measured using a Spectraflash SF600X machine in accordance with the method set out in the CIE standards, under a D-65 light source with the observer positioned at 10°. The stripping efficiency of dyed samples was calculated using equation 3 below [6].

$$\text{Stripping efficiency} = \frac{\text{Lightness value of stripped sample}}{\text{Lightness value of dyed sample}} \times 100\ (\%) \qquad (3)$$

3 Results and discussion

After the assessment of all parameters of pre-treated, dyed, and stripped fabrics, data were recorded in Table 3. Those data indicate various findings including variation in weight loss percentage, strength loss percentage, whiteness index and stripping efficiency for light shade (0.3% owf) and dark shade (3.0% owf) stripped at two different temperatures 80 °C and 100 °C.

The stripped dyed samples were assessed according to the weight loss percentage, strength loss percentage, whiteness index and stripping efficiency. Of those samples, 18 were developed after dyeing, stripping and the assessment of qualitative parameters, such as whiteness index and stripping efficiency. The images of dyed and best-stripped fabric areshown in Figure 4.

3.1 Weight loss percentage of fabric due to stripping

Figures 5 and 6 illustrate the weight loss percentage of the stripped fabric of light shade (0.3% owf) and dark shade (3.0% owf), respectively. For both light shade (0.3% owf) and dark shade (3.0% owf) fabrics, the weight loss percentage increased linearly with an increase in the stripping chemical's concentration and stripping temperature. The highest weight loss percentage of the light shade (Figure 5) was determined at 100 °C, with a concentration of 10 g/L hydrose and 10 g/L caustic soda. The calculated weight loss percentage due to stripping at a temperature of 100 °C with the maximum concentration was higher than the weight loss percentage at a temperature of 80 °C with the minimum concentration. This occurs because the use of a high concentration of chemicals accelerates the weight loss percentage due to

Table 3: indicates values of weight loss, strength loss of dyed and stripped fabrics, while thevalues of the whiteness index and stripping efficiency were given in Table by comparing the difference in the condition between pre-treated and stripped fabric

Combined shade	No.	Concentration of stripping chemicals (g/L)	Temperature (°C)	Weight loss (%)	Strength loss (%)	Whiteness index	Stripping efficiency (%)
0.3% owf Light shade	1	H-5, C- 2.5	80	0.0	0.4	4.29	91.33
	2		100	0.6	0.6	7.85	91.41
	3	H-5, C-5	80	0.6	0.8	4.32	93.23
	4		100	0.9	0.9	8.17	92.87
	5	H-10, C-5	80	0.8	1.25	4.57	92.61
	6		100	1.2	1.4	17.39	91.32
	7	H-10, C-10	80	0.9	1.3	5.12	94.53
	8		100	1.5	1.5	21.83	95.45
3.0% owf Dark shade	9	H-5, C- 2.5	80	0.6	4.5	-11.12	69.88
	10		100	0.8	5.2	-7.71	78.26
	11	H-5, C-5	80	0.9	5.66	-10.72	73.32
	12		100	1.1	6.5	-7.53	73.81
	13	H-10, C-5	80	1.2	6.66	-9.0	72.54
	14		100	1.4	7.5	-6.62	72.44
	15	H-10, C-10	80	1.3	7.2	-8.36	78.46
	16		100	1.6	7.7	-4.54	79.79

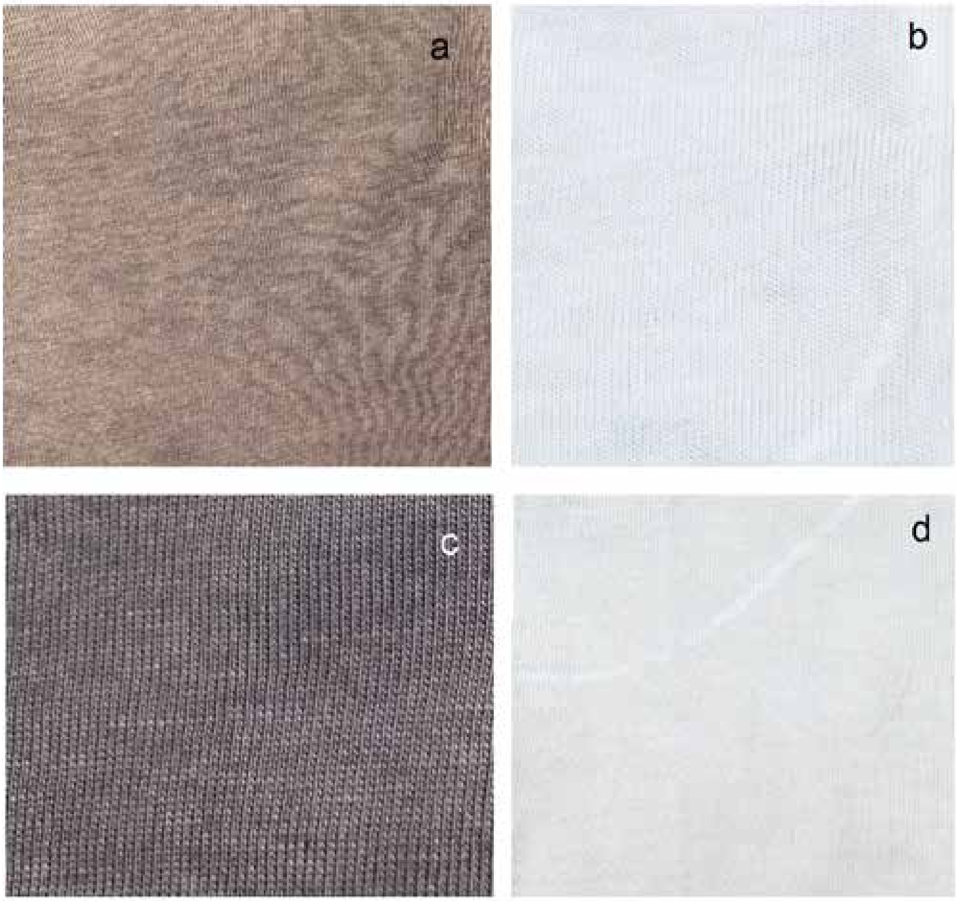

Figure 4: Images of (a) dyed light shade (0.3% owf) fabric, (b) best-stripped light shade (0.3% owf) fabric, (c) dyed dark shade (3.0% owf) fabric, and (d) best-stripped dark shade (3.0% owf) fabric

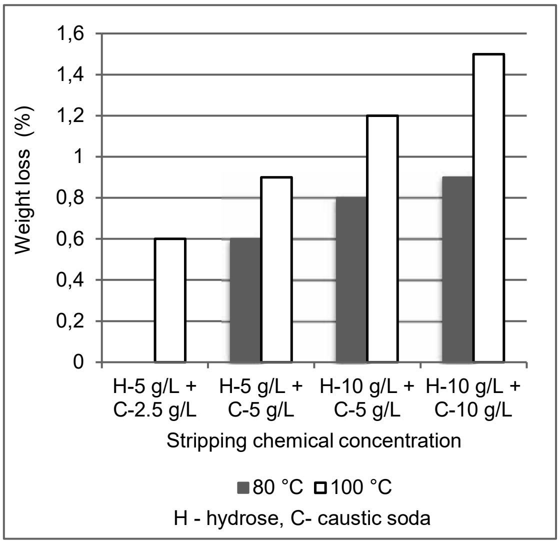

Figure 5: Percentage of fabric weight loss for stripped light shade (0.3% owf) fabric

chemical effectiveness and an increase in temperature, and vice versa [13, 14]. Cotton fibre loses weight because the alcohol group that contains the glucose unit of the cellobiose unit (a repeating unit of cellulose) functions as a weak acid [8]. The maximum weight loss percentage was 1.5% and 1.6% for the light and dark shade fabric, respectively, using the highest concentration of stripping chemicals (10 g/L hydrose and 10 g/L caustic soda) at 100 °C. For the light and dark shade fabrics, the lowest weight loss percentage was 0% and 0.6%, respectively, using the lowest concentration of stripping chemicals (5 g/L hydrose and 2.5 g/L caustic soda) at 80 °C.

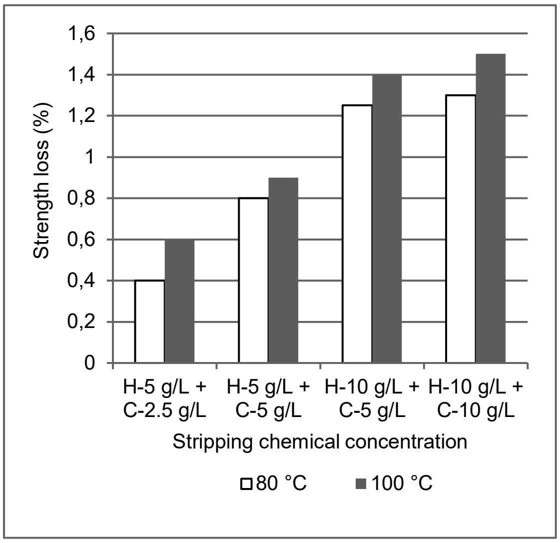

Figure 7: Percentage of fabric strength loss for stripped light shade (0.3% owf) fabric

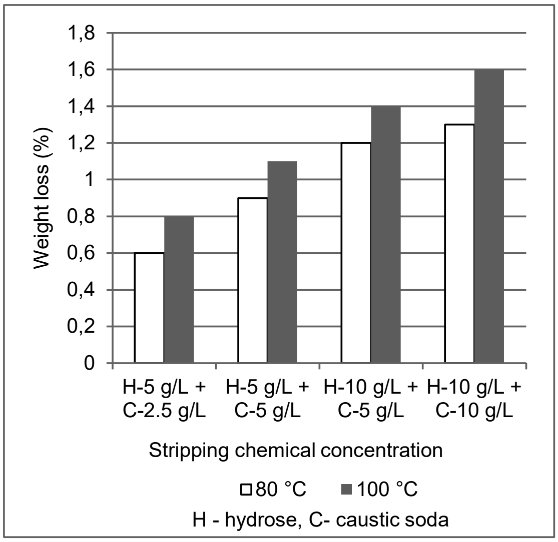

Figure 6: Percentage of fabric weight loss for stripped dark shade (3.0% owf) fabric

3.2 Strength loss of fabric due to stripping

Figures 7 and 8 illustrate the strength loss percentage of the stripped fabric of light shade (0.3% owf) and dark shade (3.0% owf), respectively. For both light shade (0.3% owf) and dark shade (3.0% owf) fabrics, the percentage of strength loss increased proportionally with an increase in the stripping chemical's concentration and stripping temperature. The highest strength loss percentage of the light shade (Figure 7) occurred with a concentration of 10 g/L hydrose and 10 g/L caustic soda at 100 °C temperature. The calculated strength loss percentage stripped at a temperature of 100 °C with

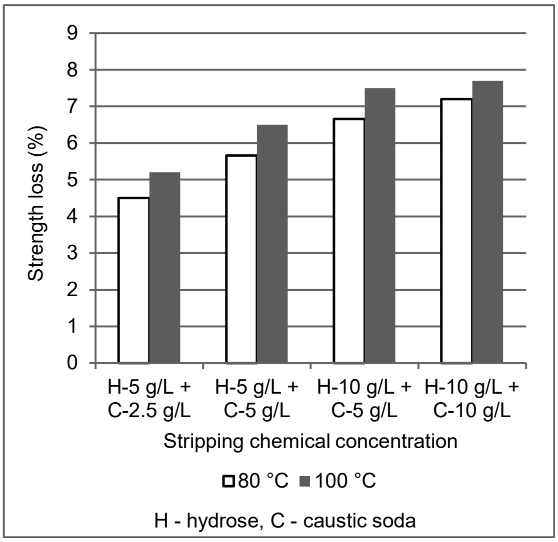

Figure 8: Percentage of fabric strength loss for stripped dark shade (3.0% owf) fabric

the maximum concentration was higher than the strength loss percentage at temperature of 80 °C with the minimum concentration. The use of a high concentration of chemicals reduces the bursting strength and damages the physical structure of fibre due to chemical effectiveness and an increase in temperature, and vice versa [13, 14].

SEM images were used to assess changes that occurred in the fibre surface after the stripping process. The SEM images presented in Figures 9a and 9b showed variations in the morphology of dyed (light shade 0.3% owf) and stripped fabric in which a magnification of 500× was used to examine the surface properties. The SEM images of light shade (0.3% owf) dyed fabric showed flat and smooth surface characteristics, spirally twisted ribbon-like fibre (Figure 9a), whereas the microfibril network of the stripped fabric remained disordered (Figure 9b). Stripped fabric showed a rougher surface than the dyed (light shade 0.3% owf) fabric. During the stripping process, the use of a reducing agent and sodium hydroxide (strong alkali) attacked the crystalline region of cotton. Consequently, swelling occurred due to increased amorphousness. This swelling effect caused the cotton fibre structure to open, while an untwisted condition was partially noticed (Figure 9b). Fibre damage occurred as a result.

Similar effects were visualized by comparing Figure 10a and Figure 10b, which consecutively examined the surface properties of dyed (dark shade 3.0% owf) and stripped fabric at a magnification of 500×.

Swelling occurs in cotton in the presence of an alkaline solution during stripping. The crystalline region of cotton is converted to an amorphous region as the alkali acts as an intracrystalline swelling agent, resulting in the strength loss of cotton fibre when hydroxyl groups are reduced after stripping. Moreover, loss of strength occurs when strongly covalent bonded dyes with cotton are stripped from fibre with an aqueous solution of strong alkali under high temperatures. As a result, the alcohol

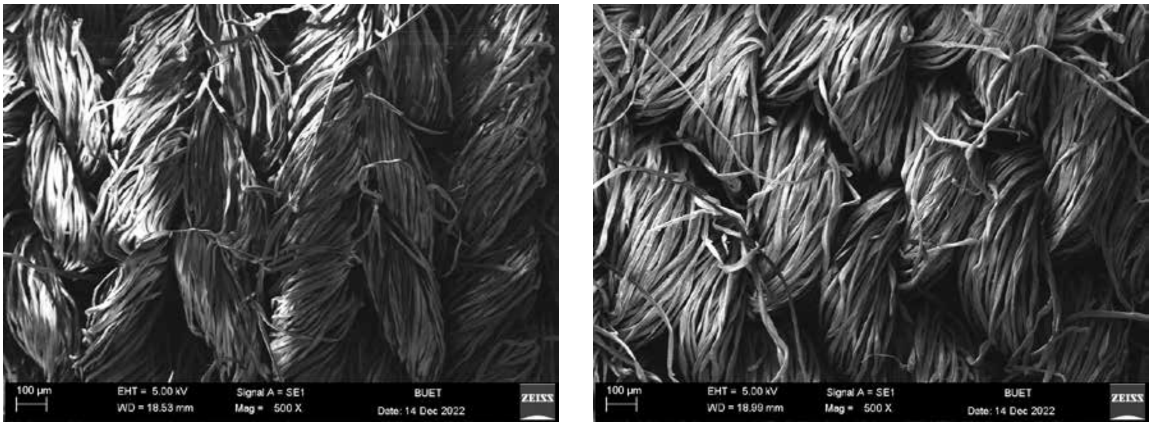

a) *b)*

Figure 9: SEM images for light shade (0.3% owf) a) dyed fabric, and b) stripped fabric

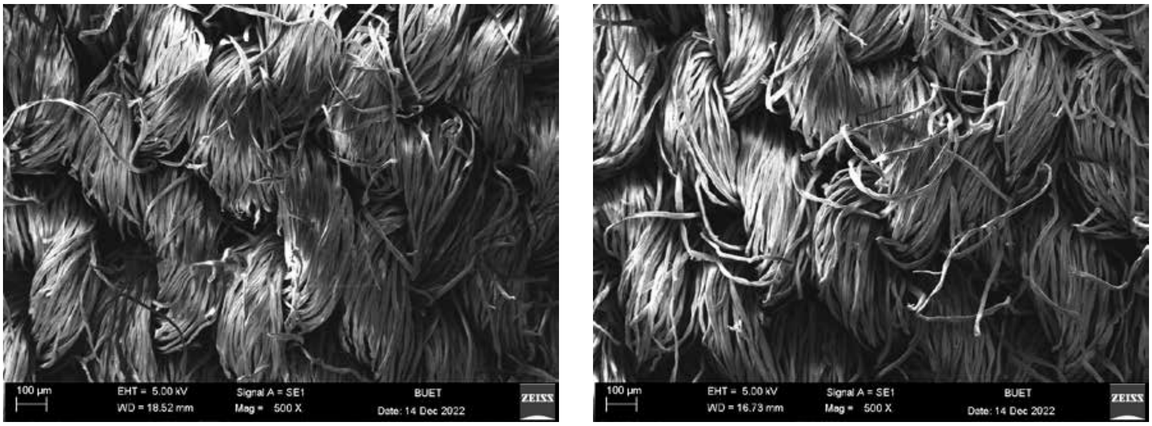

a) *b)*

Figure 10: SEM images for dark shade (3.0% owf) a) dyed fabric, and b) stripped fabric

group containing the glucose unit of the cellobiose unit (repeating unit of cellulose) acts as a weak acid. The strength of cotton fibre thus decreases [8].

FTIR analysis was performed for selected fabrics to analyze the presence of a hydroxyl group (-OH) in the dyed and stripped fabrics to justify the strength factor. The fabric with a higher stripping efficiency and whiteness index was chosen for FTIR stripped fabric analysis, where the chemical concentration of hydrose and caustic soda was 10 g/L each and the stripping temperature was 100 °C. The related light shade (0.3% owf) dyed fabric was chosen to perform the FTIR analysis of dyed fabric. The black line indicates the dyed fabric, and the additional coloured line indicates the stripped fabric in the FTIR spectrum in order to analyze absorbance.

Figures 11 represents the absorbance of IR radiation through the dyed fabric and stripped fabric for the analysis of the presence of an -OH group in the fabric. Here, the peak found in the range 3550–3200 cm^{-1} wave number of the frequency region indicates the presence of -OH groups in the fabric. The graph shows higher and lower absorbance of IR for dyed and stripped fabric, respectively. Higher absorption indicates a strongly covalent bonded -OH group, which in turn indicates a higher amount of -OH group in the dyed fabric. On the other hand, lower absorbance was found in stripped fabric, indicating a weakly bonded -OH group in the fabric as -OH group significantly reduced after stripping.

The highest strength loss percentage was 1.5% and 7.7% for the light and dark shade fabrics, respectively, using a higher concentration of stripping chemicals (10 g/L hydrose and 10 g/L caustic soda) at 100 °C. The lowest strength loss percentages for the light and dark shade fabrics were 0.4% and 4.5%, by using a lower concentration of stripping chemicals (5 g/L hydrose and 2.5 g/L caustic soda) at 80 °C.

3.3 Assessment of whiteness index

Figures 12 and 13 illustrate the whiteness index of the stripped fabric of light shade (0.3% owf) and dark shade (3.0% owf), respectively. For both light shade (0.3% owf) and dark shade (3.0% owf) fabrics, the whiteness index was raised by increasing the stripping chemical's concentration and stripping temperature. The highest whiteness index of the stripped light shade fabric (Figure 12) was 21.83, with a concentration of 10 g/L hydrose and 10 g/L caustic soda at 100 °C temperature. The whiteness index for stripping with the highest concentration was higher than the whiteness index with the lowest concentration of hydrose and caustic soda. A

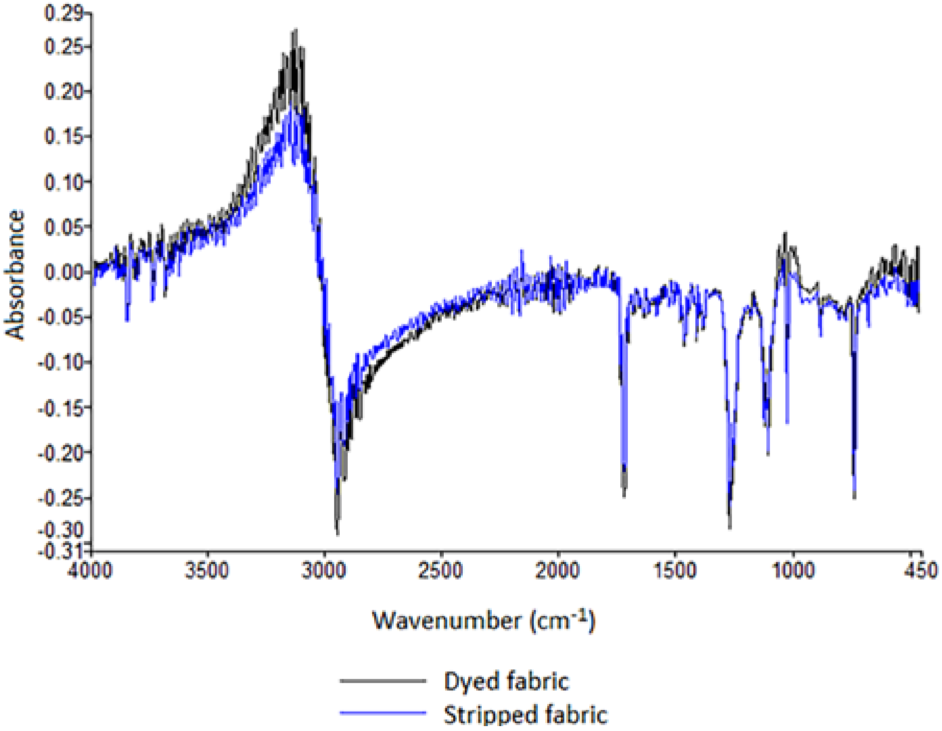

Figure 11: FTIR examination of dyed and stripped fabric for analysis of absorbency

change in temperature from low to high also affected the whiteness index slightly in the same manner. As the shade percentage of dyes in dark shade fabric was found to be higher, the whiteness index value for stripped dark shade fabric was lower than the stripped light shade fabric. Here, negative values of the whiteness index were seen for dark shade stripped fabric, where the values were lower at 80 °C than at 100 °C. The reason for this was the excessive reddish appearance of stripped fabrics at 80 °C relative to fabric at 100 °C, while stripping at 100 °C was found to be satisfactory. The highest whiteness index was 21.83 and -4.54 for the light and dark shade fabric, respectively, using a higher concentration of stripping chemicals (10 g/L hydrose and 10 g/L caustic soda) at 100 °C. The lowest whiteness index for the light and dark shade fabrics was 4.29 and -11.12, respectively, using a lower concentration of stripping chemicals (5 g/L hydrose and 2.5 g/L caustic soda) at 80 °C.

3.4 Assessment of stripping efficiency

Figures 14 and 15 illustrate the stripping efficiency of the stripped fabric of light shade (0.3% owf) and dark shade (3.0% owf), respectively. For both light shade (0.3% owf) and dark shade (3.0% owf) fabrics, stripping efficiency increased proportionally with an increase in the stripping chemical's concentration and stripping temperature. The highest stripping efficiency of the light shade (Figure 14) was 95.45%, with a concentration of 10g/L hydrose and 10 g/L caustic soda at 100 °C. The calculated stripping efficiency at 100 °C with the highest concentration of stripping chemicals was higher than the stripping efficiency at 80 °C with the lowest concentration of stripping chemicals. The use of a high concentration of chemicals increases the stripping efficiency due to chemical effectiveness and an increase in temperature, and vice versa [15]. For light-shade fabrics, the value of stripping efficiency was found to be higher because the light shade fabric absorbs less dyes than the darker shade of fabric. For this reason, the same concentration of stripping chemicals (hydrose and caustic soda) can easily strip out the colours from the light shade of fabric as it contains less dyes than the dark shade of fabric, and vice versa. From achieved values, it can be concluded that the stripping efficiency of the light shade (0.3% owf) stripped fabric was higher than the stripping efficiency of the dark shade (3.0% owf) stripped fabric. The highest stripping efficiency was 95.45% and 79.79% for the light and dark shade fabric, respectively, using the highest concentration of stripping chemicals (10 g/L hydrose and 10 g/L caustic soda) at 100 °C. The lowest stripping efficiency for the light and dark shade fabric was 91.33% and 69.88%, respectively, using the lowest concentration of stripping chemicals (5 g/L hydrose and 2.5 g/L caustic soda) at 80 °C.

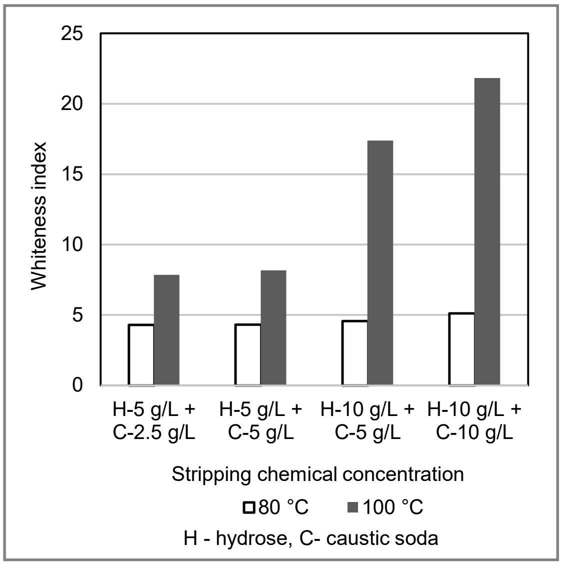

Figure 12: Whiteness index of stripped light shade (0.3% owf) fabric

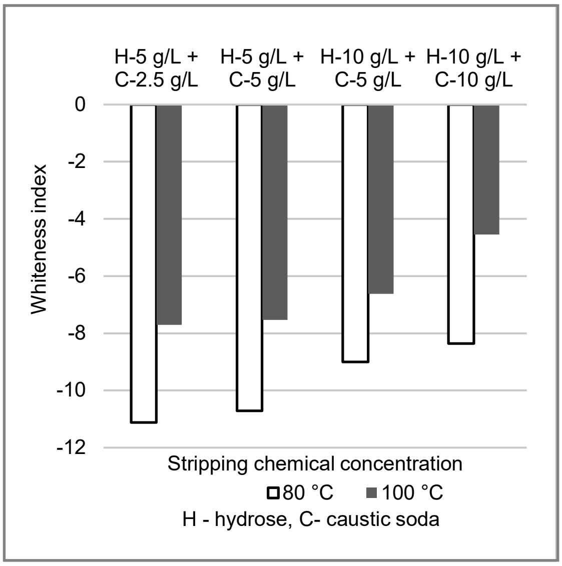

Figure 13: Whiteness index of stripped dark shade (3.0% owf) fabric

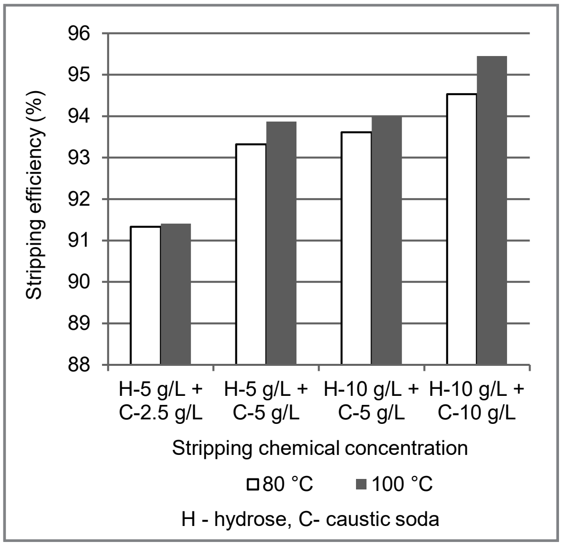

Figure 14: Stripping efficiency of stripped light shade (0.3% owf) fabric

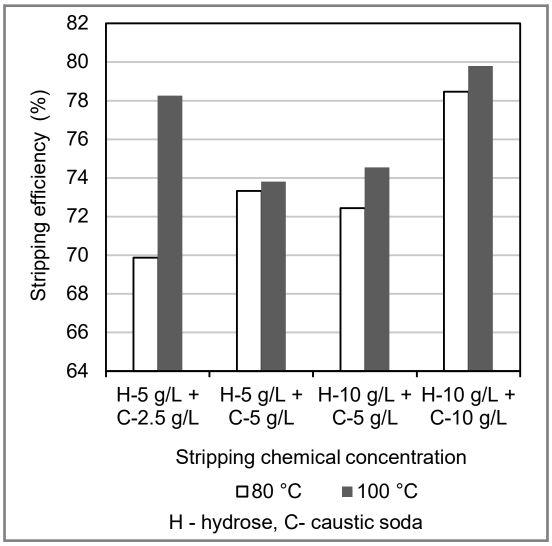

Figure 15: Stripping efficiency of stripped dark shade (3.0% owf) fabric

4 Conclusion

This work was carried out for the purpose of studying alkali reductive stripping in cotton knit fabric dyed with the Drimarene Yellow CL2R, Drimarene Red CL5B and Drimarene Blue HFRL reactive dyes, taking into account different concentrations of stripping chemicals (hydrose as reducing agent and caustic soda) and process temperatures as stripping parameters.

Increasing the stripping chemical concentration and process temperature resulted in a proportionate increase in the weight loss and strength loss percentage of the fabric. The dyed fabrics with shade percentages of 0.3% owf and 3.0% owf demonstrated maximum weight loss and strength loss percentage whenthey were treated with 10 g/L hydrose and 10 g/L caustic soda at 100 °C. The whiteness index values of light shade (0.3% owf) stripped fabrics were higher than that of dark shade (3.0% owf) stripped fabrics. Similarly, the stripping efficiency of the light shade (0.3% owf) stripped fabric was higher than that of dark shade (3.0% owf).

To maintain the good effects of stripping on fabric quality, it is recommended to use a lower concentration of stripping chemicals (5 g/L hydrose and 5 g/L caustic soda) at 100 °C. Stripping performances were improved by increasing the process temperature from 80 °C to 100 °C. The selection of standard process parameters can ensure an effective stripping process. As a result, the fabrics are readied for re-dyeing, which reduces the amount of waste and makes the textile and garment industry eco-friendlier and more sustainable.

References

1. BURKINSHAW, S.M., SALIHU, G. The role of auxiliaries in the immersion dyeing of textile fibres: Part 6 analysis of conventional models that describe the manner by which inorganic electrolytes promote reactive dye uptake on cellulosic fibres. *Dyes and Pigments*, 2019, **161**, 595–604, doi: 10.1016/j.dyepig.2017.09.028.
2. HANBING, W., HAASE, H., MAHLTIG, B. Cationic pretreatment for reactive dyeing of cotton and its simultaneous antibacterial functionalisation. *Tekstilec*, 2020, **63**(1), 27–37, doi: 10.14502/Tekstilec2020.63.27-37.
3. LEWIS, D.M. Developments in the chemistry of reactive dyes and their application processes. *Coloration Technology*, 2014, **130**(6), 382–412, doi: 10.1111/cote.12114.
4. SLAMA, H. B., CHENARI BOUKET, A., POURHASSAN, Z., ALENEZI, F. N., SILINI, A., CHERIF-SILINI, H., OSZAKO, T., LUPTAKOVA, L., GOLIŃSKA, P., BELBAHRI, L. Diversity of synthetic dyes from textile industries, discharge impacts and treatment methods. *Applied Sciences*, 2021, **11**(14), 1–21, doi: 10.3390/app11146255.

5. ISLAM, M.R., MOSTAFA, M.G. Textile dyeing effluents and environment concerns - a review. *Journal of Environmental Science and Natural Resources*, 2019, **11**(1–2), 131–144, doi: 10.3329/jesnr.v11i1-2.43380.
6. GHOSH, N.C., FATEMA, U.K., MUNNI, A. Performance evaluation of stripping agents on bi-functional reactive dyes. *American Journal of Engineering Research (AJER),* 2018, **7**(2), 250–258, https://www.ajer.org/papers/Vol-7-issue-2/ZF070201250258.pdf.
7. ISLAM, M.M. Identification of different types of dyeing fault, causes and controlling method for quality and productivity. *International Research Journal of Modernization in Engineering Technology and Science*, 2021, **3**(4), 1147–1157.
8. UDDIN, M.G., ISLAM, M.M., ISLAM, M.R. Effects of reductive stripping of reactive dyes on the quality of cotton fabric. *Fashion and Textiles*, 2015, **2**(1), 1–12, doi: 10.1186/s40691-015-0032-y.
9. TAYYABA, N., YOUNAS, T., ALI, S. Chemical color stripping of cellulose fabric dyed with reactive dyes. *International Journal of Science and Innovative Research (IJESIR)*, 2021, **2**(5), 4–16, https://ijesir.org/wp-content/uploads/2021/ppp0100044IJESIR.pdf.
10. UDDIN, M.G., ISLAM, M.R. Evaluating the performance of alkali reductive stripping process of reactive dyes. *Journal of Fashion Technology and Textile Engineering*, 2015, **3**(2), doi: 10.4172/2329-9568.1000122.
11. KHAN, M.I., HOSNE, N., YEASIN, M., TURABI, H.A., RAIHAN, M.A.H., BISWAS, H. Dyeing of cotton fabric with different shade% of reactive dyes and different stripping condition to find out the maximum – minimum percentage of strength loss, weight loss, and pilling resistance of stripped fabric. *North American Academic Research (NAAR) Journal*, 2021, **4**(12), 163–179, doi: 10.5281/zenodo.5822854.
12. BERNS, Roy S. Numerical color specification: colorimetry. In *Billmeyer and Saltzman's Principles of Color Technology*. Hoboken : Wiley, 2019, 51–84, doi: 10.1002/9781119367314.ch4.
13. ASGHER, M., MUZAMMIL, M., QAMAR, S.A., KHALID, N., BILAL, M. Environmentally friendly color stripping of solar golden yellow R dyed cotton fabric by ligninolytic consortia from *Ganoderma lucidum* IBL-05. *Case Studies in Chemical and Environmental Engineering*, 2020, **2**, doi: 10.1016/j.cscee.2020.100031.
14. CHATHA, S.A.S., ASGHER, M., ALI, S., HUSSAIN, A.I. Biological color stripping: a novel technology for removal of dye from cellulose fibers. *Carbohydrate Polymers*, 2012, **87**(2), 1476–1481, doi: 10.1016/j.carbpol.2011.09.041.
15. OĞULATA, R.T., BALCI, O. Investigation of the stripping process of the reactive dyes using organic sulphur reducing agents in alkali condition. *Fibers and Polymers*, 2007, **8**, 25–36, doi: 10.1007/BF02908156.

Mykola Riabchykov, Liudmyla Nazarchuk, Oksana Tkachuk
Lutsk National Technical University, Lvivska street, 75, Lutsk, Ukraine

Basic Parameters of Medical Textile Materials for Removal and Retention of Exudate from Wounds

Osnovni parametri medicinskih tekstilij za odvajanje in zadrževanje izcedka pri vnetju ran

Original scientific article/*Izvirni znanstveni članek*
Received/*Prispelo* 7-2022 • Accepted/*Sprejeto* 10-2022

Corresponding author/*Korespondenčni avtor:*
Prof dr. Mykola Riabchykov
E-mail: mriabchykov@gmail.com
Tel.: +30988404276
ORCID ID: 0000-0002-9382-7562

Abstract

The article focuses on predicting the properties of textile materials intended for the treatment of wounds. The main requirements for medical textile materials for liquid transportation were identified. Exudate from wounds and therapeutic fluids from a dressing must move through material with the necessary efficiency. This ensures that unwanted substances are removed from the wound and the necessary moisture is maintained. These requirements can be provided using a mathematical model of the process. Such a model can be substantiated by solving a non-linear differential diffusion equation. For this purpose, the function of changing the moisture content inside a textile material was approximated using a polynomial function that satisfies the boundary conditions. This approximation made it possible to reduce the problem to the solution of an ordinary differential equation with respect to time. The obtained analytical solution of the change in moisture content with respect to time and coordinate includes two diffusion constants. The results of macro-experiments, together with analytical results, made it possible to determine the diffusion coefficient and the nonlinearity coefficient in an explicit form. The results made it possible to predict the moisture content at a given point of textile material at any given time, the total amount of absorbed liquid and the intensity of absorption. The resulting function can recommend the geometric and physical parameters of medical textile materials for the treatment of wounds with a given intensity of exudate sorption.

Keywords: Textile medical materials, diffusion coefficient, nonlinear equation, removal of exudate

Izvleček

Članek se ukvarja z metodo predvidevanja lastnosti tekstilnih materialov za zdravljenje ran. Oblikovane so glavne zahteve za prenos tekočine skozi medicinske tekstilije. Izcedki iz ran in terapevtskih tekočin iz oblog se morajo učinkovito premikati skozi material, da zagotovijo odstranitev neželenih snovi iz rane in ohranitev potrebne vlažnosti. Te zahteve je možno določiti z matematičnim modelom, ki temelji na reševanju nelinearne diferencialne difuzijske enačbe. V ta namen je funkcija spreminjanja vsebnosti vlage v tekstilnem materialu predpostavljena s pomočjo polinoma, ki izpolnjuje robne pogoje. Ta predpostavka je omogočila rešitev problema s pomočjo navadne diferencialne enačbe v odvisnosti od časa. Dobljena analitična rešitev spremembe vsebnosti vlage v odvisnosti od časa usklajuje tudi vključitev dveh difuzijskih konstant. Rezultati makroeksperimentov skupaj z rezultati analize omogočajo določitev koeficienta difuzije in koeficienta nelinearnosti v eksplicitni obliki. Rezultati omogočajo napovedovanje vsebnosti vlage v določeni *točki tekstilije v danem trenutku, skupne količine absorbirane tekočine in intenzivnosti absorpcije. S pomočjo dobljene funkcije se lahko priporoči geometrijske in fizikalne parametre medicinskih tekstilij za zdravljenje ran z dano intenzivnostjo sorpcije izcedka.*

Ključne besede: tekstilni medicinski materiali, difuzijski koeficient, nelinearna enačba, odstranitev izcedka

1 Introduction

Military actions in Ukraine have led to a significant increase in the number of wounded people with open wounds. This results in the need for research related to their treatment. Traditionally, there are two main processes in the treatment of gunshot wounds. The first determines the emergency treatment of a wound on the battlefield. This article discusses the conditions for the second stage of treatment in hospitals.

Together with the predominantly medical aspects, this process requires research in technical fields, in particular textiles. Wound dressings remain the primary treatment for wounds [1]. Indeed, in recent years, the design of such bandages has developed significantly, which has increased the effectiveness of their use [2]. It should be noted that such bandages are special textiles. In many cases, they act as active multifunctional devices that remove harmful substances from the wound and deliver medical liquids in the opposite direction. Despite the large number of publications on predicting the kinetics of the passage of liquids through textile materials [3, 4], their results are difficult to use in practice for the design of real textile medical devices.

The main requirements for textile materials for wound healing relate to the need to regulate the movement of fluids removed from a wound on the one hand, and the healing fluids supplied to the wound on the other. In particular, article [5] defines the need for the permanent removal of exudate from purulent wounds [6]. The condition of healing is not merely the removal of exudate. This process must be regulated. It is necessary to maintain the necessary humidity, which can be provided by the parameters of the bandage. Article [7] shows the actual humidity parameters in the area of the bandage when removing exudate. It has been noted that, in some cases, modern bandages do not provide the necessary parameters for the removal of exudate. There is also a need for the subjective control of wound moisture.

It was noted [1] that wound dressings should support the local environment in the wound area. The main process is fluid sorption. These processes can be passive or active.

Research [8] focused on the development of materials that can effectively remove excess exudate from wounds. It was noted that the cavities in such materials should occupy 60–70%. Materials should provide sorption of exudate in the parameters of 1700–1800 g/m^2/day.

Article [9] states that an ideal dressing should effectively remove exudate from wounds. This is a necessary condition for treatment. The structures of nanofiber materials that can provide this process are given.

Study [10] noted the difficulty of measuring the effectiveness of wound dressings in the treatment of complex wounds. Measurements of moisture content and time, as well as treatment processes were determined. The importance of preserving the parameters of the environment at the site of wound healing was noted.

Modern bandages and foams do not always work effectively for wound healing. Article [2] proposes ways to create smart tools that can independently regulate the healing process, in particular the process of removing exudate.

The basic theoretical principles of wound healing consist of several areas [11]. The first determines the creation of the necessary moist environment for the wound. Advances in the creation of special materials have allowed us to focus on creating medical liquids that can help heal wounds. All these processes determine the need for fluid movement through textile medical materials.

Study [12] identified methods for the parameters of the passage of liquids through textile materials, in particular with the help of coloured liquids and real-time moisture content control. The desired structural characteristics to ensure the required parameters of fluid flow were also noted. Article [13] focuses on to the creation of materials that provide the necessary filtering parameters.

Article [14] defines the parameters of the passage of different liquids through fabrics and textiles for different times. The parameters of the moisture content of solutions are also determined.

Nanoparticles of metal oxides improve the performance of medical textiles [15]. These nanoparticles can be located on the surface of such materials [16], or be part of antibacterial liquids that need to be transported with a given efficiency [15].

The creation of effective textile materials, for the treatment of wounds in particular, depends on the presence of a theoretical basis that describes the movement of fluid through the material.

Article [17] focuses on the creation of a mass transfer model through textile materials taking into account various parameters. Study [18] considered comfortable conditions for the use of textiles in terms of heat and liquid distribution.

Processes of filtration of liquid in technical textile materials of water and various mixes are considered in article [19]. Structures for control of filtration process are offered.

The passage of high viscosity liquids through textiles is also described in the study [20].

It should be noted that all theoretical models of medical textiles must use diffusion parameters that in general are not absolute constants. They are determined by the parameters of fluid saturation inside the material.

For these purposes, the values of diffusion coefficients of textile materials are estimated in Article [21]. Hygroscopic experiments are presented. At the same time, the real values of diffusion coefficients raise some doubts. This is especially relevant for the additional accumulation factor.

In study [22], the diffusion coefficient was determined based on the use of the finite element method in conjunction with computed tomography. It is stated that comparisons were made using macro experiments. In general, methods for determining diffusion coefficients are not very developed. It is thus unclear which macro experiments are in question.

Deviations of diffusion parameters from the constant value determine the transformation of differential equations of fluid propagation through textile materials into nonlinear equations. The general means of solving such equations are unknown.

In [23], attempts were made to solve nonlinear diffusion equations using exponential and trigonometric series. Study [24] presents numerical methods of finite differences, and study [25] proposes iterative methods.

Analysis of research proves the relevance of determining the parameters of the passage of fluid through medical textiles. The proposed models of the passage of fluid through such materials are not general in nature and are very difficult to use in practice. Existing methods for determining diffusion coefficients are very complex and do not guarantee real results.

The purpose of this study was to develop practical methods for determining the parameters of the passage of liquid through textile materials for medical purposes, while ensuring the determination of diffusion coefficients based on macro experiments for these materials.

2 Methodology

The essence of the accumulation of fluid in the middle of medical materials is its moisture content in the system of cavities of such materials. Such materials can be a textile weave of threads, or a system of pores for foamed materials. Methods for adjusting the pore parameters for such materials are shown in [26]. The structure of materials with pores for fluid retention is shown in Figure 1.

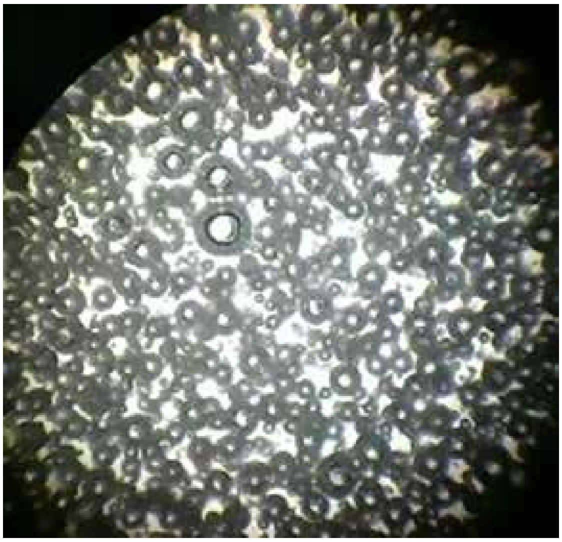

Figure 1: Porous material for medical purposes

The proposed methodology involves the use of generalized material characteristics that are used in the treatment of wounds. Such characteristics allow the data to be averaged and the methods to be applied to various structures such as textiles, foams, and nonwovens.

There are several approaches to determining the parameters of the passage of fluid through medical textiles. The first involves considering the material

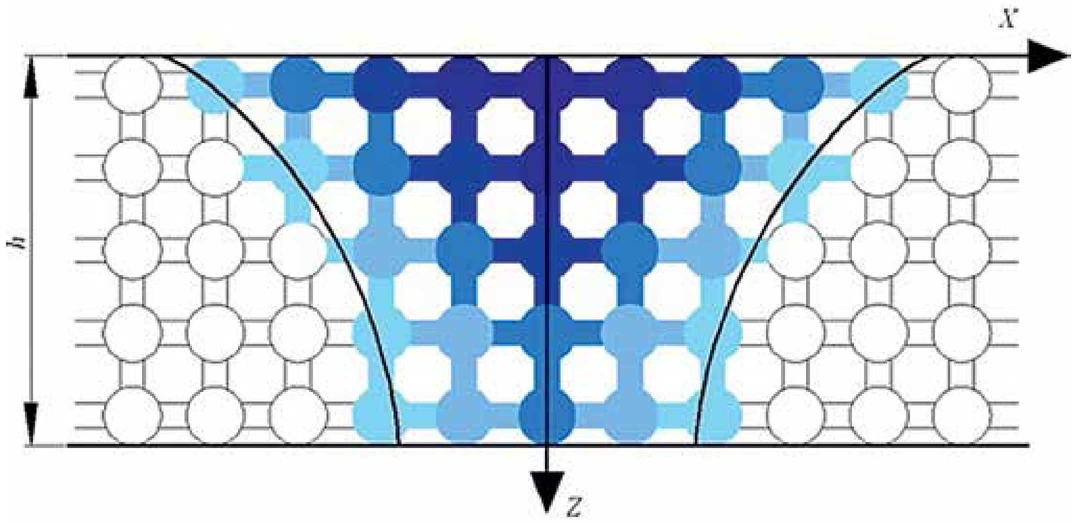

Figure 2: Discrete model of fluid passage through material

in the discrete environment model [4]. Such methods are able to solve complex spatial problems. For example, Figure 2 shows the fluid moisture content profile based on the solution of a discrete problem. As already determined, each individual task requires very large resources and is not suitable for practical use. At the same time, its solution leads to the conclusion that the dependence for fluid moisture content can be approximated using a fairly simple dependence.

Figure 2 shows an X coordinate, which is directed along the surface of the material from the point of penetration of the liquid, a Z coordinate, which is directed from the surface of penetration of the liquid deep into the material, and h indicating material thickness.

Despite the fact that the mechanics of fluid accumulation in the material has a discrete nature, it is more convenient to describe the diffusion process in continuous functions using a differential equation.

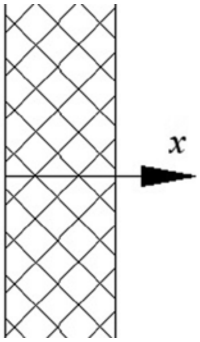

Figure 3: Estimated scheme of fluid movement through material

The passage of liquid through textile materials can be described using the differential diffusion equation. Consider the calculation scheme in the form of a uniaxial model. In this case, the propagation axis is denoted by x, the propagation time t, and the liquid moisture content U at the point.

The differential diffusion equation for such a scheme takes the form [3]

$$\frac{\partial U}{\partial t} = \frac{\partial}{\partial x}\left(D\frac{\partial U}{\partial x}\right) \tag{1}$$

where ∂ is the partial derivative.

The diffusion coefficient D in most sources is considered to depend on the liquid moisture content. In particular, the dependence in the form is proposed in [4] $D = D_0(1+\sigma \cdot U)$, where σ - is the coefficient of influence.

In this case, the differential diffusion equation will be rewritten as

$$\frac{\partial U}{\partial t} = D_0\sigma\left(\frac{\partial U}{\partial x}\right)^2 + D_0\frac{\partial^2 U}{\partial x^2} + D_0\sigma U\frac{\partial^2 U}{\partial x^2} \tag{2}$$

The following facts should be noted for this equation

The equation is nonlinear, while the general methods for solving such equations are unknown. The coefficients characterizing the diffusion properties of a textile material are generally quite difficult to determine. You can use additional experiments to determine them, which then require the use of solutions of the equation. This means the desirability of analytically solving the diffusion equation. It should be noted that the numerical solutions [24, 25] are insufficient because they require the numerical values of the coefficients.

At the same time, attempts to determine diffusion coefficients on the basis of numerical modelling of the structure of textile material [23] require a very large amount of preparatory work separately for each material.

It would be desirable to develop approximate analytical methods for solving the diffusion equation, which can simultaneously help determine the diffusion coefficients and control the parameters of fluid flow through textile materials.

Let's move on to dimensionless coordinates: dimensionless moisture content $u = \frac{U}{U_0}$, where U_0 is determined by the liquid coming from the outside to the material (the moisture content of the liquid at zero moment of the absorption process); dimensionless coordinate $z = \frac{x}{h}$, where h is the thickness of the material; dimensionless time $\tau = \frac{t}{t_{\max}}$, where t_{max} is the saturation time of the material.

Then functions and derivatives can be written as:

$$U = u \cdot U_0; \qquad \frac{\partial U}{\partial t} = t_{\max} U_0 \frac{\partial u}{\partial t};$$

$$\frac{\partial U}{\partial x} = \frac{U_0}{h}\frac{\partial u}{\partial z}; \qquad \frac{\partial U^2}{\partial x^2} = \frac{U_0}{h^2}\frac{\partial^2 u}{\partial z^2}.$$

In view of the above, equation (2) should be rewritten as:

$$\frac{\partial u}{\partial \tau} = \frac{D_0 \sigma U_0}{t_{\max} h^2}\left(\frac{\partial u}{\partial z}\right)^2 + \frac{D_0}{t_{\max} h^2}\frac{\partial^2 u}{\partial z^2} + \frac{D_0 \sigma U_0}{t_{\max} h^2} u \frac{\partial^2 u}{\partial z^2} \quad (3)$$

Let's introduce additional definitions:

$$K_1 = \frac{D_0}{t_{\max} h^2}; \qquad K_2 = \frac{D_0 \sigma U_0}{t_{\max} h^2}$$

The equation can be obtained in the form:

$$\frac{\partial u}{\partial \tau} = K_1 \frac{\partial^2 u}{\partial z^2} + K_2 u \frac{\partial^2 u}{\partial z^2} + K_2 \left(\frac{\partial u}{\partial z}\right)^2 \quad (4)$$

Note that the diffusion coefficients in the equation are still unknown. Therefore, it is desirable to solve the equation analytically. Given the small thicknesses of the materials under consideration, we will solve the equation for the centre point. Given the results of discrete modelling, a change in fluid moisture content in the thickness of the material will be determined as a power function of the second order $u = w_0 - w_1 \cdot z + w_2 \cdot z^2$, where the coefficients can be time-dependent only.

To analyse the parameters of the passage of liquids through textile medical materials, an experiment, shown in Figure 4 was also built.

Liquid was fed to the surface of material 1, from dispenser 2. A sample of the material was located on mobile device 4. The presence and moisture content of liquid on the upper and lower surfaces was monitored by determining the brightness of the two cameras 4 and 5.

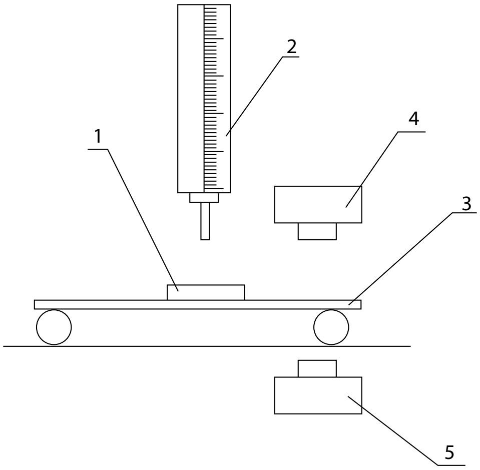

Figure 4: Research device

The parameters of the sample under study are shown in Figure 5.

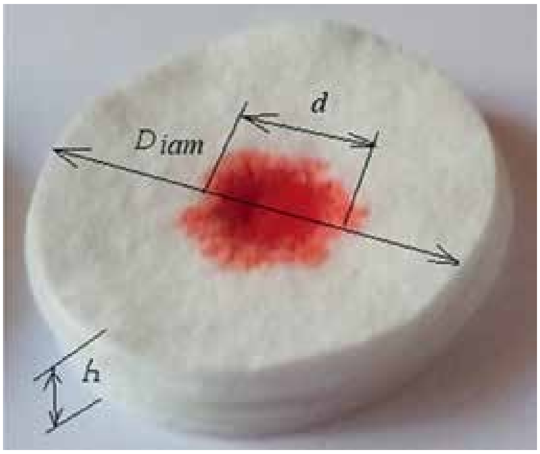

Figure 5: Prototype

The experimental technique facilitates the determination of the time of appearance of liquid on the lower surface of the material, as well as the intensity of the brightness to determine the moisture content of liquid on the upper and lower surface of the material.

3 Results and discussion

When searching for a solution to the equation, the initial and boundary conditions must be taken into account. For the zero-coordinate $x = 0$, the dimensionless moisture content on the surface at any time is equal to one. For the opposite boundary, the moisture content derivative in the coordinate is zero.

Given the relatively small thickness of the textile material, the dependence of a change in moisture content on the thickness in the form of a polynomial of the second order is proposed.

$$u = w_0 - w_1 \cdot z + w_2 \cdot z^2$$

Given the first boundary condition, it is possible to rewrite

$$u = 1 - w_1 \cdot z + w_2 \cdot z^2$$

In the following we will consider two stages of liquid passage through material. The first stage involves the moisture content of liquid inside the material without going outside.

Let us denote the coordinate of the point s to which the liquid inside the material has reached.

Then the equation for this stage will be rewritten in the form

$$u = 1 - 2 \cdot \frac{z}{s} + \frac{z^2}{s^2} \cdot$$

in the centre of the layer at $z=s/2$ moisture content

$$uc = \frac{1}{4}$$

For this central point, the equation can be written as

$$\frac{ds}{dt} = 5 \cdot K_2 \left(\frac{1.2\frac{K_1}{K_2} + s}{s} \right)$$

Once marked $\beta = 1.2\frac{K_1}{K_2}$, the solution can be found in the form

$$s + \ln\left(\frac{\beta}{\beta + s}\right)^{\beta} = 5K_2 \cdot t$$

Given the real values of the parameter β, it is possible to write approximately

$$s \approx 5K_2 \cdot t$$

The moisture content inside the material can be written as dependence

$$u = \begin{cases} 1 - 2 \cdot \dfrac{z}{5K_2 \cdot t} + \dfrac{z^2}{(5K_2 \cdot t)^2}, z < 5K_2 \cdot t \\ 0, z > 5K_2 \cdot t \end{cases}.$$

The time the liquid reaches the opposite surface is

$$t_0 = \frac{1}{5K_2}$$

This dependence implies the possibility of determining at least one of the two diffusion constants, since the time of appearance of the liquid can be recorded, for example, according to the scheme of Figure 2.

The second stage of fluid distribution determines the appearance of fluid on the outer surface.

Taking into account the second boundary condition transforms the dependence for moisture content in the form

$$u = 1 - w_1 \cdot z + \frac{w_1}{2} \cdot z^2$$

In the centre of the layer at z=1/2

$$uc = 1 - w_1 \cdot z + \frac{w_1}{2} \cdot z^2 = 1 - \frac{3}{8} w_1$$

For the central point of the diffusion, the equation can be rewritten as

$$\frac{dw_1}{dt} = -\frac{2}{3} K_2 \cdot \left[4 \cdot w_1 \left(1 + \frac{K_1}{K_2} \right) - \frac{5}{3} w_1^2 \right]$$

Denoting $\alpha = \frac{12}{5}\left(\frac{\sigma \cdot U_0 + 1}{\sigma \cdot U_0}\right)$, we can find the solution of this equation in the form $\frac{1}{\alpha} \ln \frac{C \cdot w_1}{\alpha - w_1} = -\frac{10}{9} K_2 \cdot t$, where C is the integration constant.

This equation facilitates the explicit expression of unknown function

$$w_1 = \frac{\alpha \cdot \exp\left(-\frac{10\cdot\alpha}{9}K_2 \cdot t\right)}{C + \exp\left(-\frac{10\cdot\alpha}{9}K_2 \cdot t\right)}$$

It can be rewritten as

$$u = 1 - \frac{\alpha \cdot \exp\left(-\frac{10\cdot\alpha}{9}K_2 \cdot t\right)}{C + \exp\left(-\frac{10\cdot\alpha}{9}K_2 \cdot t\right)}\left(z - \frac{z^2}{2}\right)$$

An unknown constant can be found from the condition of equality of moisture content at the end of the first stage and the beginning of the first stage.

$$u = 1 - \frac{\alpha \cdot \exp\left(-\frac{10\cdot\alpha}{9}K_2 \cdot t\right)}{\frac{1}{2}\alpha \cdot \exp\left(-\frac{2\cdot\alpha}{9}\right) - \exp\left(-\frac{2\cdot\alpha}{9}\right) + \exp\left(-\frac{10\cdot\alpha}{9}K_2 \cdot t\right)}\left(z - \frac{z^2}{2}\right)$$

We note two diffusion constants $K2$ and α, which are clearly related to the diffusion coefficients D_0 and σ.
If time is chosen as a constant, one can write for the first stage

$$u = \begin{cases} 1 - 2 \cdot \frac{z}{t/t_0} + \frac{z^2}{\left(t/t_0\right)^2}, z < t/t_0 \\ 0, z > t/t_0 \end{cases}.$$

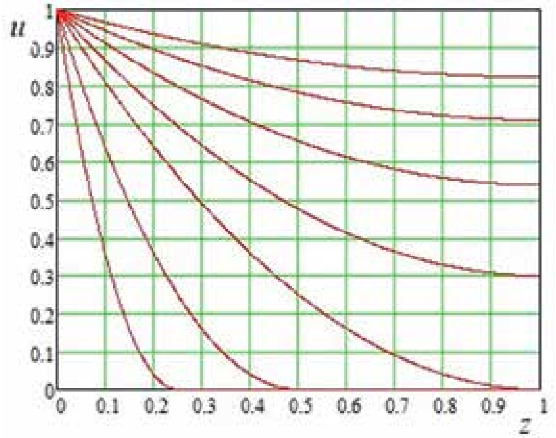

Figure 6: Change in thickness moisture content for different points in time

For the second stage

$$u = 1 - \frac{\alpha \cdot \exp\left(-\frac{2\cdot\alpha}{9}\frac{t}{t_0}\right)}{\frac{1}{2}\alpha \cdot \exp\left(-\frac{2\cdot\alpha}{9}\right) - \exp\left(-\frac{2\cdot\alpha}{9}\right) + \exp\left(-\frac{2\cdot\alpha}{9}\frac{t}{t_0}\right)}\left(z - \frac{z^2}{2}\right)$$

The dependence of a change in moisture content on the thickness of the material for different moments of time is shown in Figure 6.

The total amount of liquid inside the material can be found as an integral of the moisture content (Figure 7).

$$W(t) = \int_0^1 u(z,t)dz$$

The intensity of the increase in moisture content can be found as a derivative (Figure 8).
Moisture content on the outer surface of the material

$$u = 1 - \frac{\alpha \cdot \exp\left(-\frac{2\cdot\alpha}{9}\frac{t}{t_0}\right)}{\alpha \cdot \exp\left(-\frac{2\cdot\alpha}{9}\right) - 2\cdot\exp\left(-\frac{2\cdot\alpha}{9}\right) + 2\cdot\exp\left(-\frac{2\cdot\alpha}{9}\frac{t}{t_0}\right)}$$

Record the time that is twice the time of passage of the liquid through the material. Then the moisture content at this point on the surface of the material

$$u1 = 1 - \frac{\alpha \cdot \exp\left(-\frac{4\cdot\alpha}{9}\right)}{\alpha \cdot \exp\left(-\frac{2\cdot\alpha}{9}\right) - 2\cdot\exp\left(-\frac{2\cdot\alpha}{9}\right) + 2\cdot\exp\left(-\frac{4\cdot\alpha}{9}\right)}$$

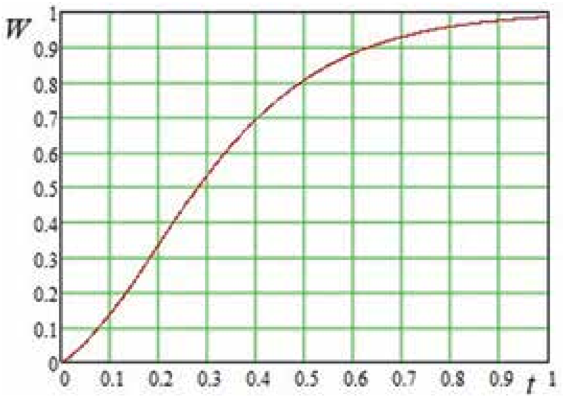

Figure 7: Placement of liquid in material

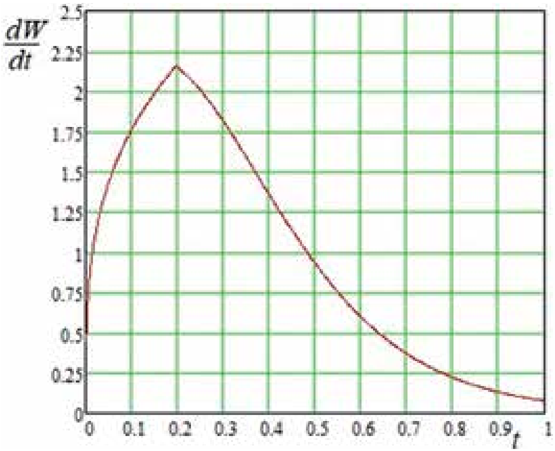

Figure 8: Intensity of the increase in fluid moisture content

Figure 9: Determination of the nonlinearity coefficient

The obtained dependence is approximated using the expression

$$u1 = 1 - e^{-0.26(\alpha - 2)}$$

Where it is possible to find

$$\alpha = 2 - \frac{\ln(1 - u1)}{0.26}$$

Where the nonlinearity coefficient is

$$\sigma \cdot U_0 = \frac{12}{5\alpha - 12} = \frac{12}{19.23 \cdot |\ln(1 - u1)| - 2}$$

Thus, the expressions obtained in the solution, facilitate the determination of the diffusion coefficients for medical material on the basis of macro-experiments.

After that, it is possible to predict the amount and intensity of exudate removal from a wound using medical material of arbitrary size. The resulting function includes both time parameters and penetration depth parameters. It is therefore possible to determine the liquid content at any point along the depth at any time.

Experimental studies of liquid for the material medical cotton wool with a density of 15–17 kg/m^3 (Figure 10) were conducted, which confirmed the performance of the constructed mathematical model.

In further studies, real experimental studies are planned to determine the diffusion coefficients of various materials and the use of the above methods for the design and functioning of real materials.

The difference in the determination of experimental and theoretical data over time is graphically shown in Figure 11. The deviation for a number of experiments varies over time, but the average value of *D* over all time does not exceed 3.4%.

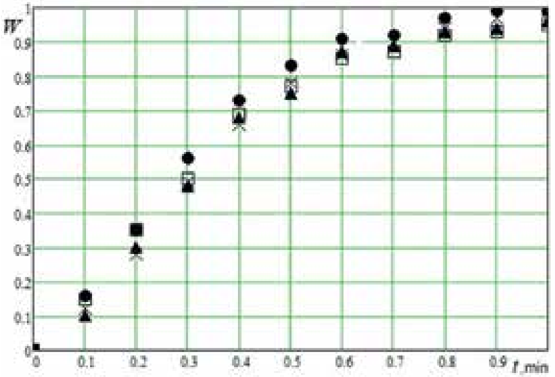

Figure 10: Experimental data of moisture content in medical cotton wool

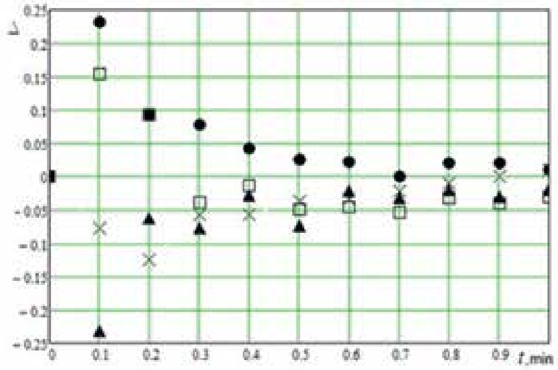

Figure 11: Deviation of experimental data

4 Conclusion

A function that facilitates the determination of the amount of exudate removed from a wound using textile medical materials is obtained on the basis of the approximate analytical solution of the diffusion equation.

These results facilitate the prediction of the condition of a dressing at any time. These mathematical equations take into account the geometric parameters of the bandage. One can predict the process of exudate movement for a dressing of any size or determine the geometric and structural parameters of the material to achieve a given intensity of exudate movement.

The solution is obtained in general form. Indicators of the porosity and hydrophilicity of the substrate, and the density and viscosity of the liquid affect the values of the diffusion coefficients, but not the form of the equation. The solution has been experimentally verified for one type of material (medical cotton wool). Additional studies will focus on the dependences of these coefficients on the characteristics of the material and liquid.

The obtained methods facilitate the determination of the diffusion coefficients and nonlinearity coefficients on the basis of macroexperiments.

These results can have a positive effect on the effectiveness of medical textiles.

References

1. HOLLOWAY, S., HARDING, G.K. Wound dressings. *Surgery,* 2022, **40**(1), 25–32, doi: 10.1016/j.mpsur.2021.11.002.
2. RUONAN, D., BAOLIN, G. Smart wound dressings for wound healing. *Nanotoday*, 2021, **40**, 1–22, doi: 10.1016/j.nantod.2021.101290.
3. RIABCHYKOV, N., VLASENKO, V., ARABULI, S. Linear mathematical model of water uptake perpendicular to fabric plane. *Vlakna a textile*, 2011, **18**(2), 24–30.
4. SCHUTSKAYA, G., SUPRUN, N. Discrete three-dimensional model of moisture spreading in textile materials. *Vlákna a textil*, 2016, **23**(2), 31–36.
5. LUO, B., XIAO, Y., JIANG, M., WANG, L., GE, Y., ZHENG, M. Successful management of exudate and odor using a pouch system in a patient with malignant facial wound: a case report. *Asia-Pacific Journal of Oncology Nursing*, 2022, **9**(4), 236–241, doi: 10.1016/j.apjon.2022.02.006.
6. LI, Y., ZHANG, Y., WANG, Y., YU, K., HU, E., LU, F., SHANG, S., XIE, R., LAN, G. Regulating wound moisture for accelerated healing: A strategy for the continuous drainage of wound exudates by mimicking plant transpiration. *Chemical Engineering Journal*, 2022, **429**, 1–13, doi: 10.1016/j.cej.2021.131964.
7. PICKLES, S., McALLISTER, E., McCULLAGH, G., NIEROBA, T. J. Quality improvement evaluation of postoperative wound dressings in orthopaedic patients. *International Journal of Orthopaedic and Trauma Nursing*, 2022, **45**, 1–8, doi: 10.1016/j.ijotn.2022.100922.
8. WOJCIK, M., KAZIMIERCZAK, P., BENKO, A., PALKA, K., VIVCHARENKO, V., PRZEKORA, A. Superabsorbent curdlan-based foam dressings with typical hydrocolloids properties for highly exuding wound management. *Materials Science and Engineering: C*, 2021, **124**, 1–16, doi: 10.1016/j.msec.2021.112068.
9. QI, L., OU, K., HOU, Y., YUAN, P., YU, W., LI, X., WANG, B., HE, J., CUI, S., CHEN, X. Unidirectional water-transport antibacterial trilayered nanofiber-based wound dressings induced by hydrophilic-hydrophobic gradient and self-pumping effects. *Materials & Design*, 2021, **201**, 1–12, doi: 10.1016/j.matdes.2021.109461.
10. RAEPSAET, C., ALVES, P., CULLEN, B., GEFEN, A., LÁZARO-MARTÍNEZ, J.L., LEV-TOV, H., NAJAFI, B., SA,NTAMARIA, N., SHARPE, A., SWANSON, T., WOO, K., BEECKMAN, D. Clinical research on the use of bordered foam dressings in the treatment of complex wounds: a systematic review of reported outcomes and applied measurement instruments. *Journal of Tissue Viability*, 2022, **31**(3), 514–522, doi: 10.1016/j.jtv.2022.05.005.
11. LAURANO, R., BOFFITO, M., CIARDELLI, G., CHIONO, V. Wound dressing products: a translational investigation from the bench to the market. *Engineered Regeneration*, 2022, **3**(2), 182–200, doi: 10.1016/j.engreg.2022.04.002.
12. SINHA, A., STAVRAKIS, K.A, STOJANOVIĆ, G.M. Textile-based electrochemical sensors and their applications. *Talanta*, 2022, **244**, 1–16, doi: 10.1016/j.talanta.2022.123425.
13. JIANG, C., WANG, K., LIU, Y., ZHANG, C., WANG, B. Textile-based sandwich scaffold using wet electrospun yarns for skin tissue en-

gineering. *Journal of the Mechanical Behavior of Biomedical Materials*, 2021, **119**, 1–9, doi: 10.1016/j.jmbbm.2021.104499.

14. PIRONTI, C., MOTTA, O., PROTO, A. Development of a new vapour phase methodology for textiles disinfection. *Cleaner Engineering and Technology*, 2021, **4**, 1–7, doi: 10.1016/j.clet.2021.100170.
15. BENGALLI, R., COLANTUONI, A., PERELSHTEIN, I., GEDANKEN, A., COLLINI, M., MANTECCA, P., FIANDRA, L. In vitro skin toxicity of CuO and ZnO nanoparticles: Application in the safety assessment of antimicrobial coated textiles. *NanoImpact*, 2021, **2021**, 1–11, doi: 10.1016/j.impact.2020.100282.
16. RIABCHYKOV, M., SYCHOV, Y., ALEKSZNDROV, O., NIKULINA, A. Bacteriostatic properties of medical textiles treated with nanomaterials based on Fe_2O_3. *IOP Conference Series: Materials Science and Engineering*, 2021, **1031**(1), 1–6, doi: 10.1088/1757-899X/1031/1/012036.
17. DAI, J., DIAO, Y. Numerical analysis of transient coupled heat and moisture transfer in textile drying with porous relative impact jet. *Applied Thermal Engineering*, 2022, **212**, 1–12, doi: 10.1016/j.applthermaleng.2022.118613.
18. LAN, X., WANG, Y., PENG, J., SI, Y., REN, J., DING, B., LI, B. Designing heat transfer pathways for advanced thermoregulatory textiles. *Materials Today Physics*, 2021, **17**, 1–28, doi: 10.1016/j.mtphys.2021.100342.
19. LIN, J., CHEN, Q., HUANG, X., YAN, Z., LIN, X., YE, W., ARCADIO, S., LUIS, P., BI, J., VAN DER BRUGGEN, B., ZHAO, S. Integrated loose nanofiltration-electrodialysis process for sustainable resource extraction from high-salinity textile wastewater. *Journal of Hazardous Materials*, 2021, **419**, 1–9, doi: 10.1016/j.jhazmat.2021.126505.
20. TIAN, Y., HUANG, X., CHENG, Y., NIU, Y., MA, J., ZHAO, Y., KOU, X., KE, Q. Applications of adhesives in textiles: a review. *European Polymer Journal*, 2022, **167**, 1–15, doi: 10.1016/j.eurpolymj.2022.111089.
21. KESSENTINI, R., KLINKOVA, O., TAWFIQ, I., HADDAR, M. Modeling the moisture diffusion and hygroscopic swelling of a textile reinforced conveyor belt. *Polymer Testing*, 2019, **75**, 159–166, doi: 10.1016/j.polymertesting.2019.01.013.
22. SINCHUK, Y., PANNIER, Y., ANTORANZ-GONZALEZ, R., GIGLIOTTI, M. Analysis of moisture diffusion induced stress in carbon/epoxy 3D textile composite materials with voids by μ-CT based Finite Element Models. *Composite Structures*, 2019, **212**, 561–570, doi: 10.1016/j.compstruct.2018.12.041.
23. ABDELRAHMAN, M.A.E., MUSTAFAINC, ABDO, N., MOBARAK, M. New exact solutions for the reaction-diffusion equation in mathematical physics. *Journal of Ocean Engineering and Science*, 2022, in press, doi: 10.1016/j.joes.2022.05.006.
24. ZHANG, Q., ZHANG, J., SUN, Z. Optimal convergence rate of the explicit Euler method for convection–diffusion equations. *Applied Mathematics Letters*, 2022, **131**, 1–10, doi: 10.1016/j.aml.2022.108048.
25. LIU, T. Parameter estimation with the multigrid-homotopy method for a nonlinear diffusion equation. *Journal of Computational and Applied Mathematics*, 2022, **413**, 1–14, doi: 10.1016/j.cam.2022.114393.
26. RIABCHYKOV, M., ALEXANDROV, A., SYCHOV, Y., POPOVA, T., NECHIPOR, S. Magnetic nanotechnology in the production of foamed textile materials for medical purposes. Fibres and Textiles, 2021, **28**(3), 66–71, http://vat.ft.tul.cz/2021/3/VaT_2021_3_7.pdf.

Ferdausee Rahman Anannya[1]*, Farhana Afroz*[1]*, Golam Kibria*[1]*, Md. Lutfor Rahman*[2]*, Nasrin Jamine*[1]*,*
Md. Arif Mahmud[3]
[1] *BGMEA University of Fashion and Technology, Nishatnagar, Dhour, Dhaka 1230, Bangladesh*
[2] *Primeasia University, 12-Kemal Ataturk Avenue, Banani, Dhaka 1213, Bangladesh*
[3] *Ahsanullah University of Science and Technology, 141, 142 Love Road, Tejgaon Industrial Area, Dhaka 1208 , Bangladesh*

Use of Banana Peel in the Development of a Less Flammable Polyester Composite

Uporaba bananinega olupka pri razvoju manj vnetljivega poliestrskega kompozita

Original scientific article/*Izvirni znanstveni članek*

Received/*Prispelo* 9-2022 • Accepted/*Sprejeto* 12-2022

Corresponding author/*Korespondenčni avtor:*
Md. Arif Mahmud, MSc
E-mail: arif.shawon@hotmail.com
ORCID ID: 0000-0002-7879-0175

Abstract

This study attempted to produce a cheap polyester composite material using an agricultural waste banana peel in the structure. Banana fibre has been used in composites as reinforcements, but banana peel has never been used with polyester before. The possibility of improved thermal and flammability properties of a composite due to increased moisture in the structure, and the char-forming ability of the cellulosic part of banana peel or the production of highly flammable material due to the presence of carbohydrates in the structure were the assumptions. To tackle the second assumption, aluminium trihydrate (ATH) was added. The handmade composites showed a drastic drop in tensile strength from 38.02 MPa to 16.72 MPa due to a lack of chemical bonding between the constituents. The impact and flexural strength showed some improvement with the addition of banana peel, along with ATH, to record results of 10.92 kg/cm and 49 MPa, respectively, after the initial drop that occurred when only ATH was added. However, these results were still inferior to the properties of pure polyester. The results of flammability and thermal resistance matched the second assumption, as flame retardancy was kept under control by the presence of ATH. The absorbency properties remained almost unaffected.

Keywords: tensile strength, viscosity, hydrophobicity, flame retardancy, char

Izvleček

V tej raziskavi je predstavljen poskus izdelati poceni poliestrski kompozit z uporabo bananinega olupka kot kmetijskega odpadka. Bananina vlakna so že bila uporabljena v kompozitih kot ojačitev, bananin olupek pa do zdaj še ni bil uporabljen skupaj s poliestrom. Predvidena je bila možnost za izboljšanje toplotnih lastnosti in vnetljivosti kompozita zaradi povečane vlage v strukturi in sposobnosti pooglenitve celuloznega dela bananinega olupka ali izdelava lahko vnetljivega materiala zaradi prisotnosti ogljikovih hidratov v strukturi. V zvezi z drugo predpostavko je bil dodan aluminijev trihidrat (ATH). Ročno izdelani kompoziti so, ker ni kemičnih vezi med sestavinami, pokazali drastičen padec natezne trdnosti z 38,02 MPa na 16,72 MPa. Udarna in upogibna trdnost sta se nekoliko izboljšali z dodatkom bananinega olupka in ATH skupaj, kjer so bile izmerjene vrednosti 10,92 kg/cm oziroma 49 MPa višje kot na vzorcih, kjer je bil dodan samo ATH. Vendar so bili ti rezultati še vedno slabši od lastnosti čistega poliestra. Rezultati vnetljivosti in toplotnega upora so potrdili drugo predpostavko, saj je bila odpornost proti gorenju pod nadzorom zaradi prisotnosti ATH. Vpojnost je ostala skoraj nespremenjena.

Ključne besede: natezna trdnost, viskoznost, hidrofobnost, negorljivost, zoglenelost

1 Introduction

Bio-composites have recently gained significant popularity because of advantages, such as biodegradability, the reduction of carbon dioxide released into the atmosphere and cost reduction due to the use of cheaper bio-fibres [1]. Natural fibres or fibrous materials from similar sources are the most commonly used component for producing fully or partially biodegradable composite materials. Natural fibre composites are used as a more or less compatible alternative for replacing environmentally harmful synthetic materials, which can be beneficial in terms of controlling pollution problems. In addition, these materials have the advantages of low cost and reasonable mechanical properties. Most importantly, these composites require low-production energy consumption [2–4]. These natural bio-fibres are collected from agro-waste, plants and trees [3]. They also have some significant problems that can affect the properties of final products when used as a reinforcement in composite materials. Bio-fibres are hydrophilic in nature and always tend to absorb water or moisture. This can cause fibre swelling and improper bonding between the fibre and matrix molecules. The different nature of the synthetic matrix and hydrophilic fibres are also responsible for the poor properties of composite materials. In addition, the irregular size, shape, and density of fibres often lead to the poor mechanical properties of the resultant bio-composites [5]. In addition to the above-described drawbacks, the poor flame retardancy or high flammability of bio-fibres can be considered a more significant problem of composites produced using bio-fibres due to the high flammability of those fibres, especially cellulosic fibres.

The main advantage of bio-composites is that, even though these materials can only undergo biodegradation when dumped into the environment, only direct exposure to environmental contents can cause the biodegradation of these materials. For this reason, bio-composites have often been used in various cars in door panels and body parts since 2000 [3]. However, the poor resistance of bio-fibres to ultraviolet (UV) rays limits their uses in the materials that come under less exposure to UV rays. However, the effect of UV rays on degradability is not that significant on cellulosic materials compared with lignin and hemicellulose [6]. The strength of bio-composites is not affected that much, as the strength mainly depends on the crystallinity of cellulose. From that point of view, the choice of fibre is key for producing bio-composites of better strength and durability. Considering all the advantages and disadvantages, bio-fibres and other natural materials are often used only to reduce cost, making the composites lighter and more environment friendly, rather than concentrating on improving any other properties of the composite. According to recent research results, surface modification and the use of additional filler materials to improve or retain the performance of composites are common ways of developing bio-composites [6].

Considering all the facts above, this study aimed to develop a cheap bio-composite (partially degradable) using cellulosic agricultural waste material. Among common agricultural waste, banana peels are produced in large quantities around the world. About 1,200 million tonnes of bananas were produced in 2020 [7], and one-tenth of production was determined to be the waste of bananas in the form of the peel or skin [8]. The huge production of banana peels around the world needs to be utilized more efficiently than the current trend. Banana peels consist of various materials, including a very high proportion of moisture (57–60%), a considerable quantity of cellulosic fibre content (15–25%), carbohydrates (23–35%), some amount of ash (6–9%), different types of sugars (1–3%), etc [9]. The fibre contents in banana peels can be extracted [8] and used in different applications, which can be the subject of future studies. They have not, however, been used in developing composite structures due to the very low amount of fibre in banana peels and the inferior mechanical properties of the fibres compared to other natural fibres [2, 8]. The aim of this study was to use banana peels in a different application, focusing on its contents rather than its properties. Since banana peels are waste products, not much cost is expected for utilizing them in any structure. Expensive polymers such as epoxy, polyester, etc. are used daily in various applications. Using banana peels along with these materials can be a good option for utilizing a waste product that is produced in massive quantities worldwide and reduce the cost of final products. However, the tensile properties of composites are expected to be negatively affected by adding banana peels to the structure. This is because natural hygroscopic contents are known for making no chemical bonds with synthetic resin materials, apart from mechanical bonds [10, 11]. The only way to improve this condition is to use surface modifying agents, which would increase the cost of the material.

In addition to the last problem, the cellulosic and carbohydrate materials of banana peels are also highly flammable when favourable conditions exist, but this only helps to catch the fire at the beginning relatively quickly and easily. Later, the formed char from the cellulosic material is expected to help reduce flames by absorbing the heat from them [10]. This issue can be solved by using a very small amount flame-retardant filler powder (to keep the cost of the material in check), which can also improve the tensile properties of polyester. Because the addition of powder can increase the viscosity of the resin, which may improve tensile properties to a small degree when used in small amounts [12], it would also reduce the flammability of the composite at the same time. Even though the increased viscosity of the resin is expected to result in a more rigid and less flexible material, adding banana peels is also expected to add pliability to the structure and reduce the rigidity of the material. This would neutralize the adverse effect of the increased viscosity of the resin. On the other hand, the high moisture content of banana peels might be useful in keeping flammability in check and neutralizing the highly flammable nature of the carbohydrate and cellulosic content. The flammability may not be adversely affected at all because cellulosic materials that are known to be easily flammable are expected to produce char that can stop the spread of flames [10, 13]. The effect of banana peels on tensile and especially the flame-retardant properties have not been studied previously, but will be studied in this article.

The resin selected for this study was unsaturated polyester. There were reasons to select polyester as the resin, even though there were other synthetic polymers available on the market that are cheaper than polyester. The superior tensile properties and thermoset characteristics are the reasons why polyester was chosen. Since the addition of banana peel was expected to have a negative effect on tensile properties, a resin of superior tensile properties was required. Polyester is one of the cheapest thermoset resins. For example, a kg of unsaturated polyester resin was available at one-fifth of the price of epoxy resin. Although epoxy has superior tensile and flexural properties, and its thermal properties are also quite good [10, 14, 15], polyester was chosen instead due to the high price of epoxy.

In addition, a flame-retardant filler was intended for the composite in small quantities to avoid or neutralize the banana peels' negative effect on the polyester composite's flammability. Fillers are generally small particles that can be used for almost any function, but these mainly add special specific properties according to requirements [12]. Using a thermoset resin actually helps the cause of using filler in the composite structure because the polyester resin can be cured using an agent at room temperature [10], and it helps the filler to keep its original chemical structure, which is essential for performing its specific role in the structure. A flame-retardant filler was intended to be used in this study. There are many flame-retardant filler materials available on the market. For example, metal hydroxides work by absorbing heat, boron-based materials form an insulating layer, halogen-based materials produce gases that help to reduce flames, and phosphorus-based materials produce a high percentage of char [10, 14, 16–19]. The most commonly used flame-retardant filler materials are boric acid, ammonium chloride, zinc chloride, borate, phosphoric acid, aluminium trihydrate, etc. [10, 14, 20, 21]. Among these, many researchers have suggested that metallic hydroxides, such as aluminium trihydrate and magnesium hydroxide, are the most environment-friendly filler materials [10, 14, 16, 22]. These are also not so costly. These chemicals absorb heat in an endothermic type of reaction and produce water when decomposed as a by-product [17]. Among these, aluminium trihydrate, also known as ATH, was preferred for this study over magnesium hydroxide because it is the cheaper of the two, and ATH starts to decompose at about 180°C, which is important when used with polyester, which offers the least resistance to high temperature. ATH can produce a reasonable amount of char, which can help prevent flames from spreading too quickly [23]. A flame retardant material such ATH works at a relatively lower temperature than other commonly used flame-retardant filler materials. This might help banana peels keep their limitations hidden if used in small quantities by keeping the cost of the material in mind.

Thus, this study used dried and ground banana peels in unsaturated polyester resin to produce a composite structure. An additional filler material, ATH, was also used to control the flammable nature of the composite or, more specifically, to control the possibility of increased flammability of the composite due to the addition of banana peels in the structure. The aim of this study was to find an industrial application of banana peels in composite materials. For that purpose, the mechanical properties of the composite were also checked, together with absorbency and flammability, to determine the suitability of the produced material for any real-life application.

2 Materials and methods

This study did not require too many chemicals. Only unsaturated polyester resin, crystalizing or hardening agents, and filler materials were required as chemicals. Other required materials were used for making the composite, such as a mould, beakers, weights, non-sticky paper, and a stirrer. The final products were subject to several tests.

2.1 Materials

Unsaturated polyester resin (density: 1.12 g/cm^3, gel time: 8–11 minutes at 25°C (use of a 2% hardener)) of the Polynt brand, methyl ethyl ketone peroxide (MEKP: active oxygen: 8–9%, density: 1.17 g/cm^3) of a local brand, and ATH in powder form (density: 2.42 g/cm^3, molar mass: 78 gm/mol) of the Qualikems brand was used. Banana peels were collected from the local market, and then dried and ground using a domestic grinder. The banana peels were used in a small particle form where the particle sizes were about 1 mm in length. All the chemicals were bought from the local market. All other materials were also collected from the local market.

2.2 Methods

Composite samples were made using varying percentages of ATH and banana peels (in terms of weight). One sample of pure polyester was made as the standard for comparison. The prepared samples were conditioned at 25°C and 65% relative humidity for several days, and all tests were performed under the same conditions. Average values were recorded for all the tests.

2.2.1 Composite preparation

Banana peels and polyester were mixed by vigorous stirring for about 30 minutes in different combinations, as shown below. Composite boards of 8 mm in thickness were made. The prepared mixtures were poured into the mould by hand. A 2.0% hardener was added to the mixtures for curing action, just before the mixture was poured into the mould. Non-sticky plastic paper was used to cover the mixtures in the mould, and a glass rod was used to roll the mixture softly to remove any air bubbles. A 10 kg or 98 N load was applied to the mould during the curing process. The curing took place at room temperature for two hours afterwards. When ATH was added, the same process was followed while the ATH was added to the mixture along with banana peels and polyester resin. The combinations were calculated according to equations 1, 2 and 3 [24].

The weight fraction of ATH:

$$W_{\mathrm{ATH}} = \frac{Wa}{Wa + Wb + Wm} \times 100 \tag{1}$$

The weight fraction of banana peels:

$$W_{\mathrm{BP}} = \frac{Wf}{Wa + Wb + Wm} \times 100 \tag{2}$$

The weight fraction of polyester:

$$W_{\mathrm{POL}} = \frac{Wm}{Wa + Wb + Wm} \times 100 \tag{3}$$

where W_a represents the weight of ATH, W_b represents the weight of banana peels and W_m represents the weight of the polyester matrix

A list of samples is presented in Table 1.

Table 1: List of samples

Sample no.	Weight fraction			Actual weight of components for 300 g of composite		
	ATH (%)	Banana peel (%)	Polyester (%)	W_a (g)	W_b (g)	W_m (g)
1	0	0	100	0	0	300
2	4	0	96	12	0	288
3	6	0	94	18	0	282
4	4	2	94	12	6	282
5	4	5	91	12	15	273
6	4	10	86	12	30	258

2.2.2 FTIR analysis

Fourier transform infrared spectroscopy (FTIR) was used to determine the presence of different functional groups using an infrared spectrum of absorption, emission and photoconductivity [25]. FTIR spectrum analysis was performed within the range of 4,000 cm^{-1} and 400 cm^{-1}. This range is generally known as the mid-range of the FTIR spectrum. A Shimadzu FTIR Spectrometer (Shimadzu, Japan) was used for this study. The machine works by passing infrared rays through a specimen to a detector screen. Different functional groups absorb the infrared rays at different points of the wavenumber. The detector screen detects the percentage of absorbance of the infrared rays by a specimen. The degree of absorbance and the wave number at which the absorption occurs is analysed to determine the specimen's chemical specification. In this study, FTIR was used to determine if any newly created bonds were in the composite containing polyester, ATH and banana peel.

2.2.3 Tensile strength test

The tensile strength of a material can be defined as a material's ability to resist forces that are applied to pull it apart and its ability to stretch when put under stress. It is determined by measuring the required force to break a sample, and the modulus and elongation percentage of a material before it is broken. The calculation is performed based on the relation between the required force to break a samples with respect to the thickness and width thereof. For this study, the tensile strength was measured using a universal testing machine (UTM, Hounsfield, England) according to the ASTM D638 standard method.

2.2.4 Impact strength test

The impact strength of a material its resistance to any specific impact. This test was performed using the Izod impact testing method according to the ASTM D256 test standard. A universal impact tester (Qualitest, USA) was used for the test. The specimens were placed against a pendulum weighing 634 kg. The initial angle of the pendulum was 150°. The degree to which the specimen breaks when hit by the pendulum was calculated. Impact strength was then calculated from the resistance of the specimen. The lower the degree to which the pendulum breaks the specimen, the better the impact strength. The pendulum hits the specimen and then tries to reach the opposite end through the force (torque) created by movement of the pendulum itself. If the specimen offers high resistance, the pendulum fails to reach the opposite end; instead, it reaches a mark on the other end. That point is checked, and the angle at which the pendulum reaches the mark indicates the specimen's impact strength.

2.2.5 Flexural strength test

Flexural strength is defined as the stress in a material just before it breaks when being bent [26]. This test was performed according to ASTM D790 method using a UTM (Hounsfield, England). A three-point bending system was used for this study. The distance between the lower two points was set to 100 mm. In this method, the two ends of the specimen were bent upwards by applying pressure at the middle of the specimen using the third point that forced the midpoint to go down and eventually break the specimen [27].

2.2.6 Flame retardancy test

Flame retardancy or resistance is the measure of a material's burning rate or its behaviour when exposed to fire. This property was tested using three methods: two burning behaviour tests and an oxygen index test. The burn tests were performed according to the ASTM D3801 and ASTM D635 standards using vertical and horizontal burning method instruments. The oxygen index measurement test was performed according to the ASTM D2863-19 standard.

Vertical burning method

The burning rates of the materials and dripping tendency were checked based on this test, which was performed using a Horizontal and Vertical Flame Test Apparatus (Testech, China). For the vertical test, the sample size to be chosen was 13 mm × 125 mm, with 6 mm of the sample clamped inside the clamp that held the sample vertically. A cotton layer measuring 50 mm × 50 mm was placed 300 mm below the sample to detect any dripping of the sample during burning. The specimen was initially exposed to a 20 mm high blue flame from a gas burner for a maximum of 10 seconds. The specimen was then removed from the flame and the self-extinguishing time of the specimen was measured, if self-extinguishing occurred. In the case of self-extinguishing, the specimen was re-exposed to flames according to the previous step and the duration of

Table 2: Classification of materials in terms of flame retardancy in the vertical burning test

Criteria	Rating			
	V-0	V-1	V-2	V-HB
Required time for burning of each individual test specimen (In seconds after first and second application of flames)	≤ 10	≤ 30	≤ 30	N/A
Total required time for burning (In seconds)	≤ 50	≤ 250	≤ 250	N/A
Time of burning and afterglow after second flame application (In seconds)	≤ 30	≤ 60	≤ 60	N/A
Dripping from burning specimens (Ignition of the cotton layer)	No	No	Yes	N/A
Combustion up to the holding clamp (In case of the specimens being completely burned)	No	No	No	Yes

self-extinguishing was again calculated. If self-extinguishing did not occur again, the material was put subject to the recommended horizontal burning test. The cotton layer placed below the specimen was checked to detect dripping. All of the results were then compared with the material rating Table 2 to categorize the specimen. The test was performed inside a closed box.

Horizontal burning method

The burning rate of the material in mm per minute was calculated based on this test. The higher burning rate of a specimen means higher material flammability and vice versa. The sample size for this test was 125 mm × 12.5 mm. The samples needed to be marked at 25mm and 100mm from one end. The specimen was clamped horizontally at an unmarked end. A 100 mm square wire gauze screen was placed beside the specimen to check burning behaviour. The marked end of a specimen was exposed to a 20 mm high blue flame from a gas burner for a maximum of 30 seconds or until the flame reached the 25 mm mark of the specimen, whichever occurred first. The time required for the flame to travel from one end to the opposite end where a mark was made at a distance of 100 mm was measured [13]. The behaviour of specimens was then compared with the following ratings shown in Table 3 for the purpose of categorization. A Horizontal and Vertical Flame Test Apparatus (Testech, China) was used for this test.

Limited oxygen index test

A limited oxygen index test (LOI) was performed to determine the required minimum oxygen level to burn a material [28]. There is about 21% of oxygen on average in the earth's atmosphere. Thus, if a material requires more than 21% of oxygen to burn continuously, that material will not catch fire or extinguish a fire itself, and can be labelled self-extinguishable. Moreover, a material can be labelled as non-ignitable if it requires more than 21% of oxygen to ignite [10, 28]. A higher LOI value is therefore better [29]. The materials were exposed to vertical flames under the combined flow of oxygen and nitrogen. The required concentration of oxygen to burn the material was then calculated as a volume percentage. A Testech Limited Oxygen Index Tester (Testech, China) was used for the test. The specimen size was 100 mm × 10 mm. The specimen was ignited manually after being placed in a specimen holder. The burning took place using a nitrogen and oxygen gas flow. The fractional value of required oxygen was calculated from the machine reading.

Table 3: Rating of flame retardancy in the horizontal burning test

Rating	Criteria
1	No signs of combustion were visible after removing the ignition source.
2	The flame did not go beyond the 25 mm reference mark.
3	The flame went beyond the 25 mm reference mark but did not reach the 100 mm reference mark.
4	The flame reached the 100 mm reference mark, but the calculated linear burning rate did not exceed 40 mm/min for specimens having a thickness of 3–13 mm or 75 mm/min for specimens having a thickness of less than 3 mm.

2.2.7 Thermal degradation test

Thermogravimetric (TG) analysis is a technique used monitor the mass of a substance as a function of temperature or time. In this method, the specimen is subjected to a controlled temperature regime in a controlled atmosphere to check mass loss as the result of an increase in temperature. For this study, this test was performed using a SII Exstar 6000 TG/DTA instrument (Seiko Instruments Inc., Japan). The maximum temperature range was set to 600°C at increments of 20°C/min. The temperature was applied using a nitrogen gas flow. Aluminium was used as reference material. Another thermal property tested in this study was differential thermal analysis (DTA), which is the ratio of the temperature difference of the specimen and reference material relative to time or temperature. This test is an indicator of heat or energy absorption (endothermic) or production (exothermic) during a specimen's heat treatment. A flame-retardant material will always need to show an endothermic or heat-absorbing ability, which was checked using this test method. Derivative thermogravimetric (DTG) analysis is another measurement technique that determines a material's weight change rate relative to temperature [30]. The rate of weight change increases at a brisk rate when the decomposition of the main components takes place. This measure also indicates the rate of decomposition and the range of temperatures at which the materials decompose under heat.

3 Results and discussion

The samples were subjected to several tests. The main concern was a composite's mechanical properties after incorporating in the polyester resin two foreign materials that do not match the polyester polymer. First, a composite containing both ATH and banana peels, together with polyester, was compared with a pure polyester board to determine if any new bonds were created during the curing process of polyester using the FTIR method. The materials were then subjected to mechanical tests to determine the possible ratios used without deteriorating the material's mechanical properties too much. Lastly, the materials were subjected to a flame retardancy test to determine if the combinations chosen from the previous test could maintain the flame-retardant property within an acceptable range. The final composite sample's thermal properties were also compared to the pure polyester sample to see if the incorporation made any changes to the two new materials.

3.1 FTIR analysis

Sample 1 (100% polyester) and Sample 6 (85% polyester, 4% ATH and 8% banana peels) underwent FTIR analysis in this test. The FTIR spectrum from the tests is shown in Figure 1.

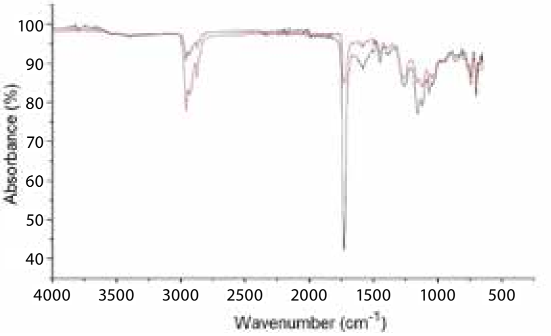

Figure 1: Spectrum of FTIR analysis

Here, the black line in the the FTIR spectrum refers to Sample 1 and the red line refers to Sample 6. The spectrum of Sample 6 showed no new bonds formed between the polyester, ATH and banana peels. The peaks were almost the same in the two graphs. The peaks around 3000 cm^{-1} indicate the presence of hydrogen bonds or, more specifically, the presence of -H and -OH functional groups. The presence of both cellulose and aluminium trihydrate affected this peak's rise, as both contain a high percentage of -OH in the structure. A peak in the range of 1700–1750 cm^{-1} indicates the presence of ester bonds or groups. The few peaks in the fingerprint range (below 1500 cm^{-1}) are also almost the same in the two graphs. The main differences between the two samples are the intensity of peaks, especially the ester bond's peak. The significant reduction of the peak in Sample 6 was because the newly included ATH and banana peel materials resisted polyester molecules to form bonds in between them. Some other peaks were also identified at a lesser intensity, reducing the bonds between the polyester molecules. This means the resulting materials are expected to show deteriorated mechanical properties. Another point can be made: there are no new bonds in the new material. This means that the ATH and banana peels have remained more or less unaffected in terms of chemical properties. As a rule, this will allow both the ATH and banana peels to resist flames.

3.2 Effect of ATH loading on the tensile properties of composites

ATH and banana peels were mixed in the polyester in powder form and ground matter form, respectively. Neither of the materials were dissolved in polyester. Instead, they helped to produce a dispersion-like mixture. The viscosity of the solution was increased with the increasing amount of ATH powder. The tensile test results are shown below in Figures 2, 3 and 4.

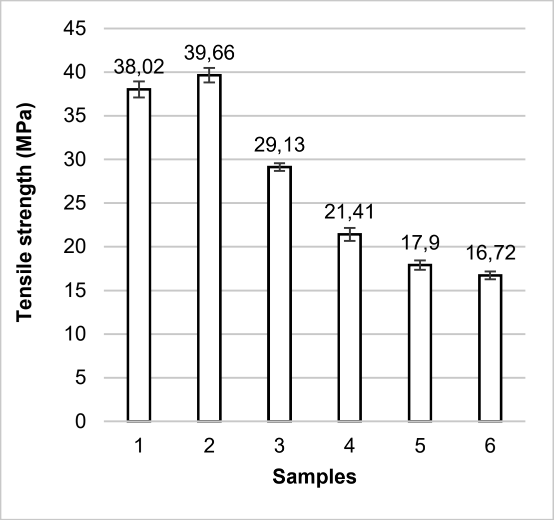

Figure 2: Effect of the addition of ATH and banana peels on tensile strength

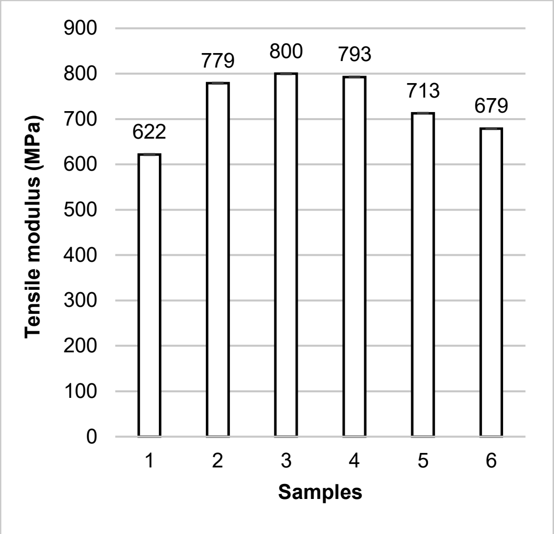

Figure 3: Effect of addition of ATH and banana peels on tensile modulus

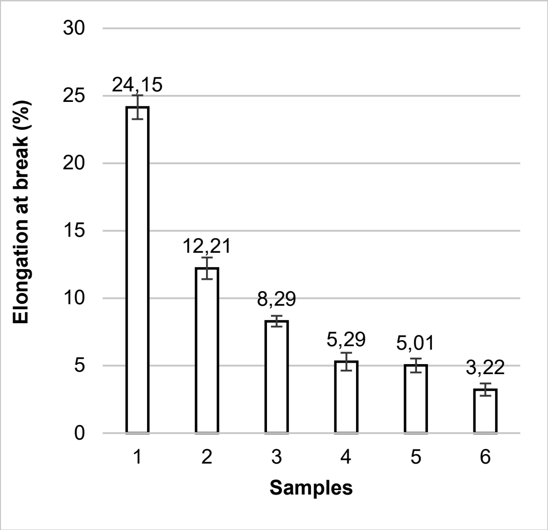

Figure 4: Effect of the addition of ATH and banana peels on elongation property

The results in Figure 2 show that using ATH with polyester improved the tensile properties of the samples at the beginning, only to see a deterioration with the further addition of ATH. At the same time, the introduction of ground dry banana peels reduced the tensile strength further. Polyester resin became viscous with the addition of ATH. The formation of a homogenous dispersion of polyester and ATH made the material viscous and presented a more uniform and compact structure at the beginning, which helped increase the tensile strength. The dispersion was able to be cured quickly into a hard and brittle material [21, 31]. The improved rigidity can also be confirmed by the tensile modulus results of Figure 3, where Sample 2 (containing 4% ATH) and Sample 3 (containing 6% ATH) showed superior tensile modulus. The material's hardness also improved the tensile strength of the composite at the beginning with the addition of 4% ATH. Later, however, the too-high brittleness and reduced extensibility of the material caused quicker breakage under stress because in the test of tensile properties, stress is applied uniformly onto the whole cross-section of the structure, and every pore or impurity within the cross-section affects the tensile properties of the material. As a result, the tensile modulus increased. The same trend can also be seen in the elongation property of the material in Figure 4, where a gradual decrement of elongation property can be seen due to the addition of ATH. However, when the granules of banana peels were introduced, the tensile strength fell further due to the presence of more impurities within the cross-section. The banana peels actually worked more like a filler than a reinforcing fibre. However, the banana peels were not expected to improve mechanical properties because fibres with a high lignin content in their structure generally struggle to make mechanically bonds with hydrophobic polyester, which cannot impregnate fibres or fillers containing lignin [32]. Although banana peels do not contain that much lignin, dried banana peels presented a surface that was difficult to be impregnated with polyester. Moreover, when there were no chemical bonds (as found in the FTIR analysis) and strong mechanical bonds between the filler and resin, the increased number of pores within the structure due to the presence of banana peel instead reduced the close bonds between polyester molecules. As a result, the composite gradually became fragile. However, nature of the materials did not help the tensile strength thereof. For this reason, the tensile strength decreased with the addition of banana peels to the structure.

Tensile modulus and elongation properties followed the same trend as tensile strength. Tensile modulus depends on the stress and strain on a material. Stress mainly depends on the required load to break a material, while strain is an indicator of a material's extensibility or elongation property. The strength of the samples increased with the addition of ATH, while the elongation property deteriorated from the beginning to the end due to increased hardness when ATH was added and then due to a lack of bonds between polyester molecules when banana peels were added together with ATH. As mentioned earlier, the addition of banana peels made the polyester a bit fragile due to a lack of bonding action between the polyester molecules. It caused the early breakage of materials when put under stress. The modulus decreased gradually as a result. On the other hand, the elongation property also deteriorated gradually and at a higher rate than tensile strength.

3.3 Impact strength test

The impact strength of a composite depends heavily on the aspect ratio of the reinforcing fibre and filler. The bonding between the additional materials and the resin is also essential. The results of the impact strength test of the samples are shown in Figure 5 below.

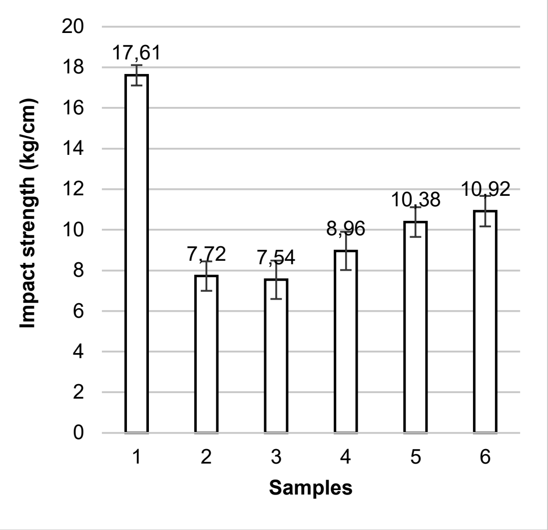

Figure 5: Effect of addition of ATH and banana peels on the impact strength of composites

The impact strength of the composites was affected significantly by the addition of ATH and banana peels. Results show that the impact strength decreased with the addition of ATH and improved again when banana peels were added. Impact strength is greatly affected by the bonding between matrix molecules and a matrix's fracture property [33]. The addition of ATH and banana peels reduced the bonds between the polyester molecules, but ATH had the most negative effect. When ATH was mixed with polyester at the beginning, it formed a homogenous dispersion with increased polyester viscosity, making the resulting composite material harder and slightly brittle. It also affected the fracture property of the composite negatively and resulted in a gradual decrease in the impact strength of the composites. When banana peels were added, however, the strength improved. Both ATH and banana peels worked more like filler materials in the composites. The fibrous materials helped reduce the impact of ATH powder on the structure. The impact strength test does not cover the full cross section of the material, but instead depends more on the specific positions of the composite that comes under the impact. The addition of rough fibrous materials of various lengths resisted the production of homogeneous dispersion similar to the samples that contained only ATH. The tendency of the powder to adhere to the rough fibrous surfaces also helped keep the ATH powder around the fibrous materials more than powder uniformly throughout the polyester [34]. It allowed the polyester molecules to come closer to form stronger bonds. Moreover, an impact test generally focuses on the surface of a material where the initial impact is made, where the presence of fibrous materials allows the polyester molecules to cover the full surface. Since the entire test does not depend on the whole cross-section of the material, the number of possible pores per unit area on average created by the presence of ATH fell. Instead, the adherence of ATH powder to the surface of the fibrous materials allowed the formation of typical bonds between the polyester molecules that would be suffice to increase the impact strength of the materials. The gradual increase in fibrous materials helped increase impact strength for the above-stated reasons. The addition of banana peels improved the impact strength of the composites. The same trend was recorded for the addition of 10% fibre, where the impact strength increased slightly. The ability of the filler or fibre to absorb impact also helps the process, as the low-density banana peel materials covered more spaces and were able to absorb the impact better than the brittle polyester resin. The soft nature achieved by the addition of banana peels was also played a role in this regard.

3.4 Flexural strength test

The flexural strengths of composites are shown in Figure 6.

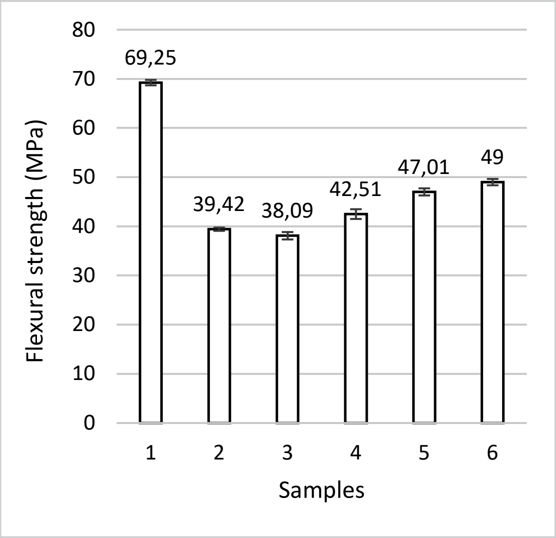

Figure 6: Effect of the addition of ATH and banana peels on the flexural strength of composites

The results show that flexural properties were very significantly affected by the addition of ATH and banana peels. The flexural strength was reduced drastically by the addition of ATH. On the other hand, flexural strength improved a bit gradually when the banana peels were added, together with the ATH. The ATH and banana peels both acted as foreign materials in polyester resin, which could not impregnate the materials; both acted as filler materials instead. These materials thus reduced some bonds between polyester molecules. To improve the flexural property, the composite had to become softer rather than hard and brittle. The addition of the ATH, however, resulted in the formation of a more homogeneous dispersion, where the disruption in bonds of polyester molecules took place uniformly. On the other hand, adding banana peels made the ATH adhere to its surfaces more than in a uniform dispersion in the mixture. It also resulted in an increase in uninterrupted bonds between polyester molecules in places, especially at the surface. The high density of banana peels actually made the materials remain inside the structure rather than at the surface of the composite [35]. A three-point flexural test initially puts the stress onto the surface of a material, and then the stress spreads within the structure. It allows the structure to withstand initial stress due to the presence of intra-bonded polyester molecules, resulting in better flexural resistance and better elastic properties. When the stress spreads within the whole structure gradually, and because the presence of the fillers actually makes the material softer due to a lack of bonds within the structure between polyester, the softness of the banana peels helps to absorb stress put forth in the flexural test better than pure polyester. The percentage of banana peels in this study is quite low, which is also the reason for this type of material characteristic. As a result, the addition of banana peels gradually increased the material's flexural strength, which could not surpass the flexural strength of pure polyester, but showed better results than materials containing only the ATH. The further addition of banana peels could have reduced the flexural strength due to the extension of the molecular bonds of polyester beyond the limit, but this concept was not tested in this study.

3.5 Flame retardancy tests

The results of these tests are shown in four parts. In the first part, the vertical burning behaviour of the materials was checked. The materials that failed the vertical test were then subjected to the horizontal burning test. The first step of this part was to determine if the materials could be considered flame retardant, even after the modifications made by adding ATH and banana peels. These results are shown in Tables 4 and 5, and in Figure 7. The LOI was then tested for Samples 1, 5 and 6, and the results of that test are given in Table 6.

Since all the samples failed the vertical burning test, the samples had to undergo the horizontal burning test. Table 5 below illustrates the horizontal burning test results.

All the samples self-extinguished within 10 seconds when first exposed to flames. The second time, however, the samples could not self-extinguish, and the entire samples were burned as a result. No dripping occurred, but ashes were produced. Since the materials fell only into the UL 94 HB rating category, all of these materials have the least flame-retardant property, i.e. they were not very flame-retardant. Instead, they burned slowly for quite a long period. The degree of horizontal burn rate varied with the specifications of the composite materials. The horizontal burning rates of the materials during the test are shown in Figure 7.

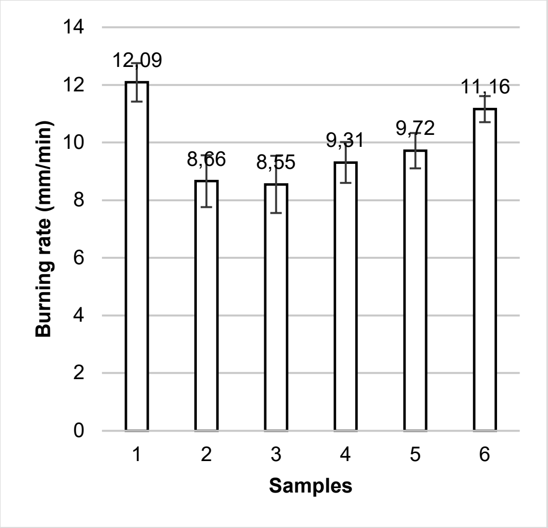

Figure 7: Effect of the addition of ATH and banana peels on the burning rate of composites

The results presented in Table 4 show that all the materials fell into the 4th or last category of flame-retardant materials (because they had a linear burn rate below 40 mm/min). The results in Figure 7

Table 4: Vertical burning behaviour of composites

Sample no.	UL 94 Rating				
	Burning stops within 10 seconds with no dripping	Burning stops within 30 seconds with no dripping	Burning stops within 30 seconds with dripping	Rating of samples	
				Vertical burning rating	Recommended for horizontal burn test
	UL 94 V-0	UL 94 V-1	UL 94 V-2	UL 94-V	UL 94 HB
1	No	No	No	No	Yes
2	No	No	No	No	Yes
3	No	No	No	No	Yes
4	No	No	No	No	Yes
5	No	No	No	No	Yes
6	No	No	No	No	Yes

Table 5: Horizontal burning behaviour of composites

Sample no.	Continuous burning of samples (Yes/No)	Flame reached 25 mm mark (Yes/No)	Flame reached 100 mm mark (Yes/No)	Linear burn rate exceeded 40 mm/min mark (Yes/No)	Rating of samples	UL 94 rating
1	Yes	Yes	Yes	No	4	HB
2	Yes	Yes	Yes	No	4	HB
3	Yes	Yes	Yes	No	4	HB
4	Yes	Yes	Yes	No	4	HB
5	Yes	Yes	Yes	No	4	HB
6	Yes	Yes	Yes	No	4	HB

Table 6: Limiting oxygen index (LOI) of composites

Sample no.	ATH (%)	Banana peels (%)	Polyester (%)	LOI (%)
1	0	0	100	19.1
5	4	5	91	19.5
6	4	10	86	19.2

show that the addition of the ATH improved flame-retardant properties, as flame spreading was reduced by the action of the ATH, which resulted in a reduction in the burning speed. However, the addition of banana peels increased the burning rate again gradually. The ATH was expected to improve flame retardancy, as it releases water during combustion and reacts endothermically during the reaction [10]. The samples containing the ATH absorbed the fire's heat and became hot, which resulted in the release of water molecules that delayed the burning rate, as seen in Figure 7. When the banana peels were added, however, the burning rate rose as expected. Even though the presence of cellulose could be useful for producing char and reducing the burning rate, the easily flammable small amount of cellulosic material could not produce a sufficient amount of char to improve the flame retardancy of the materials. The small amount of banana peels caught fire more easily and burned very quickly, as cellulosic materials are expected to be burn easily and quickly by nature. It could only help flame retardancy by producing a high amount of char, which did not happen. At the same time, the presence of moisture in the structure could have helped, but the moisture was dried during the drying of the banana peels and the heat produced during the curing of polyester. Instead, highly flammable carbohydrate parts made the materials more flammable. The percentage of ATH could have been increased to improve flame retardancy, but to do so, the mechanical properties and the composite price had to be sacrificed.

The expected results were thus achieved, as the addition of the ATH reduced flammability slightly, as evident in Figure 7, where the burn rate was found to be a bit lower for Samples 2 and 3. However, the addition of banana peels increased flammability as expected. If the banana peels had been added alone, flammability would have increased more significantly, but the presence of the ATH kept the flammability of the composite below the original rate of pure polyester. The LOI test results shown in Table 6 also support this concept. The increase in the LOI value indicated the improved flame retardancy of the material. The values are almost identical here for Samples 1, 5 and 6. The LOI increased slightly after the addition of the ATH and 5% banana peel, and it decreased further by increasing the amount of banana peels. Nevertheless, the results were slightly better than pure polyester, but the difference was too small. It can be said instead that the flammability of polyester did not change due to the addition of banana peels in the structure since cellulose and similar materials (such as starch, carbohydrates, hemicellulose, etc.) are generally very flammable and have LOI values of around 18 [10]. This LOI is lower than the polyester used in this study. This means the newly formed composite would become more flammable due to the addition of banana peels in the structure. To stop that trend, a small proportion of ATH was added to the structure, and it successfully maintained flammability within a similar range for the composite.

3.6 Thermal properties test

The thermal properties of TG and DTA were tested for Samples 1 and Sample 3 to compare the results. The TG and DTA analysis results are shown in Table 7 and Figures 8–10.

The results are almost the same in thermogravimetric analysis (TG), as shown in Table 7. The onset and endset temperatures of all the samples were almost same, while the peaks followed the same

Table 7: Thermogravimetric analysis results of the composites

Sample no.	T_{onnset} (°C)	$T_{endnset}$ (°C)	T_{max} (°C)	Residue at 600°C (%)
1	390.6	430.1	418.4	0
2	388.2	429.5	408.2	0
6	387.2	436.6	415.8	4.19

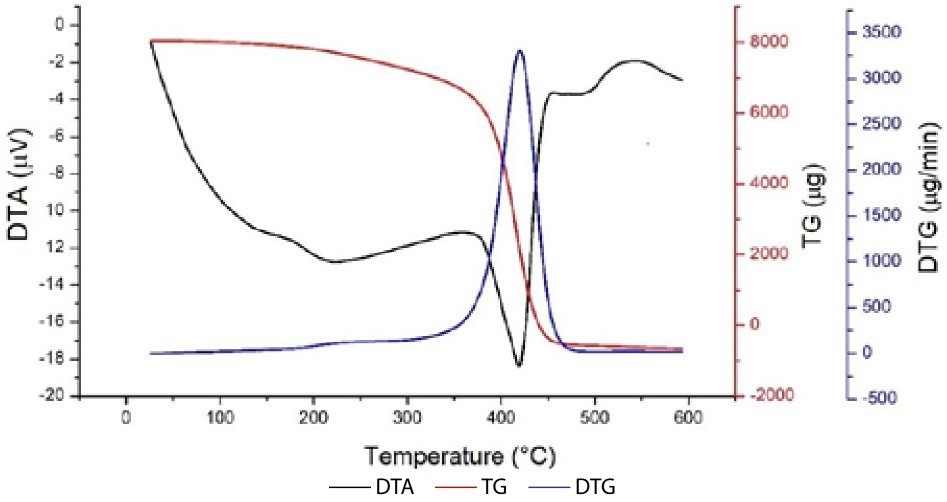

Figure 8: TG-DTA-DTG analysis curves for Sample 1

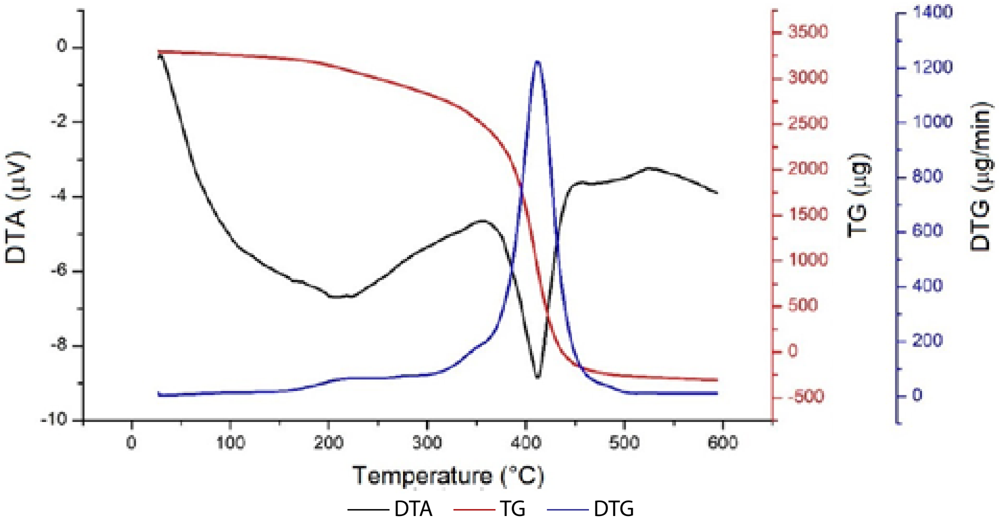

Figure 9: TG-DTA-DTG analysis curves for Sample 5

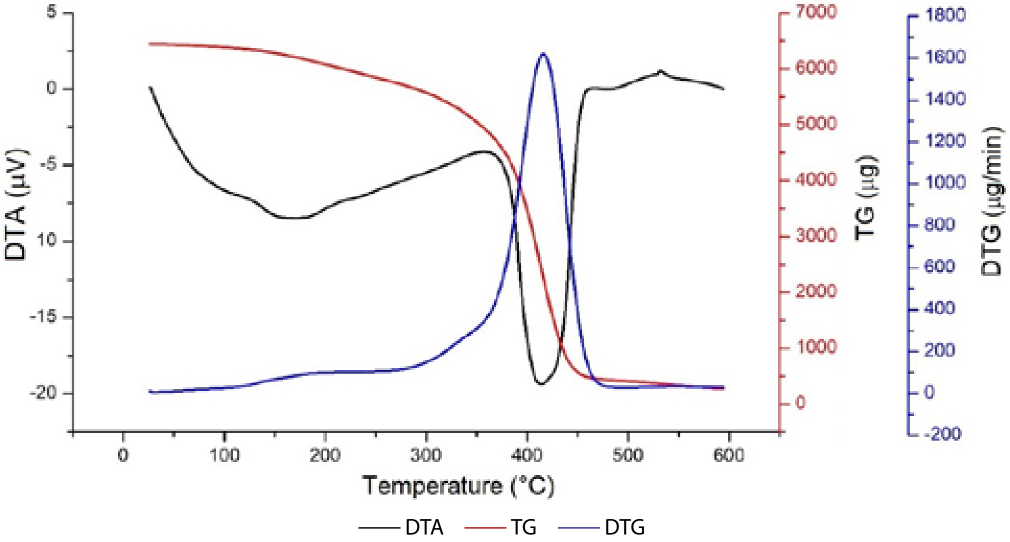

Figure 10: TG-DTA-DTG analysis curves for Sample 6

trend. However, there were a few differences as the onset mark had only about 70% weight of the material for Sample 1, containing polyester only, while Sample 2 and Sample 6, containing polyester, ATH and banana peels, recorded a material weight loss of around 35–38%. The percentage of weight loss increased due to the presence of moisture in the banana peels, which evaporated during heating and resulted in a loss of weight in the samples. In the beginning, moisture drying took place. The thermal degradation of polyester then started at around 390°C for all the samples. The addition of the ATH or banana peels did not affect the onset temperature much, but the weight loss percentage decreased in Sample 2 and Sample 6, as both samples had a smaller amount of filler materials. The ATH was also expected to evaporate by the time the onset temperature was reached because the ATH decomposed at about 180–200°C, resulting in a further decrease in the weight of the composites in Sample 2 and Sample 6. In that sense, both materials should record the same time and range of temperature during decomposition, as both contain a same amount of ATH. In reality, the weight loss in TG curves showed similar trends in all the materials. The onset and endset temperature, and the peak temperature all remained around same. This occurred because the filler percentages were too low to have any significant effect, but the difference between the samples can be assessed by looking closer look at the TG curve. Sample 1 is pure polyester, which showed minimal decomposition until a temperature of around 390°C, while the other two samples contained the ATH and banana peels. Both these materials are expected to decompose before 350°C. If the weight loss is assessed, it can be seen that Sample 1 has undergone very few changes in terms of weight until 350°C, with a weight loss percentage of around just 12%. In the case of Sample 2, however, the weight loss percentage rose to around 20% due to the evaporation of the ATH from the structure. Sample 6 contained banana peels, which increased weight loss to about 22%, indicating the decomposition of the cellulosic contents within the structure. However, the difference between Sample 2 and Sample 6 is less than the percentage of banana peels being added to the structure because of the formation of char, which is also evident in the end of the cycle, as Sample 6 produced about 4% of char. The results of TG thus confirm the presence of all the materials as expected. The DTA curves of Sample 2 and Sample 6 showed an endothermic reaction in the curve at around 200°C. Interestingly, pure polyester also showed an endothermic curve at the same temperature also later, while the second dip is also an indicator of a more endothermic than exothermic reaction. This means that polyester itself can absorb some heat and may not be too flammable.

Meanwhile, the DTG showed a significant increase in the rate of weight loss within the onset and endset temperatures, as expected, but there was a slight increase in the rate of weight loss near 200°C for Samples 2 and 6 relative to Sample 1 due to the presence of ATH in Samples 2 and 6. The banana peels did not have a significant impact, while the rise in the curve was lost with an increase in the weight loss percentage during the subsequent degradation of the polyester. However, the addition of the ATH and banana peels reduced the rate of weight loss in both samples drastically relative to Sample 1, where the rate of weight loss in terms of time was relatively high (more than 3000 μg/min), while it was around 1200–1500 μg/min in Sample 2 and Sample 6. Thus, the addition of the ATH and banana peels did not significantly affect the final properties of the composite material relative to the pure polyester. At the same time, there was no adverse effect. Instead, the thermal resistance was slightly better in Samples 2 and 6 than in pure polyester. The main aim of this study, which was to maintain unchanged properties of polyester due to the addition of foreign materials in the structure, was successfully achieved in terms of thermal properties.

3.7 Comparative analysis of results

The results of this study indicate that success was achieved to some degree, but there were also some deficiencies. The mechanical properties began to deteriorate drastically when fillers were added to the structure. To maintain the considerable strength of mechanical properties, the amounts of filler materials were compromised. The aim of the study was to use banana peels in a composite with polyester, without not affecting the properties of the polyester. The resulting material of this study showed a significant change in mechanical properties due to the addition of banana peels. However, the thermal and flammability properties of the composites were maintained almost unchanged through the addition of the ATH, together with banana peels. The absorbency property showed a slight but not significant improvement because the polyester was an absolutely non-absorbent material. The mechanical properties could not be maintained unchanged because of the inability of the process to form any chemical bond between the resin polyester and banana peels. The different natures of the two materials also played a part in this trend. The only way to retain or improve the tensile properties of the composite was the surface modification of the banana peels to make them compatible with polyester. Since this was not done, the results in terms of mechanical properties were more or less expected. However, success was achieved in terms of maintaining the thermal and flammability properties of the composite unchanged relative to the pure polyester. If the results are compared with some previous studies, it is possible to say that this study was successful.

Many researchers have proven that it is very difficult to improve the tensile properties of a natural fibre-reinforced synthetic resin composite because of the lack of chemical bonding between fibre and matrix molecules. Surface treatment, however, has very often produced positive results [6, 36, 37]. On the other hand, the use of flame-retardant type filler materials also affected the tensile properties of composites according to previous reports. A small comparison has been made in the two Tables (Table 8) below to determine the reliability of these claims. Table 8 compares the mechanical and flame-retardant properties of a few composites. Many researchers have not used banana peels. For this reason, only one similar type of composite by Luthra et al. but made of polypropylene was selected in this comparison part [38]. Another study was done by Sain et al. using a similar product, sawdust powder, and metallic hydroxide magnesium hydroxide as the filler, was used in the comparison [13].

Two other studies were also selected for the effect of flame-retardant filler materials only. He et al. produced unsaturated polyester composites using organic magnesium hydroxide as flame-retardant

Table 8: Comparison of mechanical and flame-retardant properties with other researches

Researches	Sample composition							Properties			
	Type of resin	Resin (%)	Filler or reinforcement (F/R)				Tensile strength (MPa)	Flexural strength (MPa)	UL 94-V rating	LOI
			F/R 1 (%)	F/R 2 (%)	F/R 3 (%)	F/R 4 (%)				
This study	Unsaturated Polyester	100	---	---	---	---	38.02	69.25	HB	19.1
		96	4	---	---	---	39.66	39.42	---	---
		91	4	5	---	---	17.9	47.01	HB	19.5
		86	4	10	---	---	16.72	49	HB	19.2
Sain et al. [12]	Polypropylene	97.5	---	---	---	---	22.6	39.5	---	25
		47.5	25	25	---	---	28.8	56	---	35
		47.5	25	20	5	---	26.4	53.1	---	26
		47.5	25	20	---	5	28.2	55	---	30
Luthra et al. [38]	Polypropylene	100	---	---	---	---	33	37.9	---	---
		90	10	---	---	---	27.8	36	---	---
		80	20	---	---	---	26.3	38.8	---	---
		70	30	---	---	---	24	38.2	---	---
Chen et al. [39]	Unsaturated polyester	100	---	---	---	---	31.9	52.1	HB	19.2
		90	10	---	---	---	27.6	48.6	V-1	22.3
		70	30	---	---	---	20.5	40.4	V-0	27.8
		70	---	7.5	15	7.5	18.7	35.1	V-0	25.7
He et al. [37]	Unsaturated polyester	100	---	---	---	---	---	35	---	20.5
		96	4	---	---	---	---	35	---	20.5
		93	1	6	---	---	---	21	---	26.4
		91	1	8	---	---	---	20	---	28.5

filler and expandable graphite for comparison [37]. Chen et al. produced microencapsulated flame-retardant filler to improve the flame retardancy of unsaturated polyester composites [39]. They used Ammonium polyphosphate (APP), Diatomite (Dia), and Triphenyl phosphate (TPP) as flame retardant fillers. They also produced a microcapsule of TPP filled with APP and Dia, and used that as a flame-retardant filler material with good effect.

The results vary significantly in the studies mentioned above for various reasons. All the researchers used different combinations and contents. The general points that can be made after reviewing the above comparison in Table 8 are as follows:

i) Mechanical properties are generally affected negatively by the addition of flame-retardant filler materials, except when surface modification of the filler material is performed.
ii) The percentage of filler must be much higher to significantly impact the flame-retarding property of the composites.
iii) The type of flame-retardant filler changes the impact on flame retardancy, as not all fillers have a similar flame-retarding or resisting ability.

The addition of both reinforcements and filler materials has a significant impact on the mechanical properties of the composites. Generally, that impact is negative. Associating any material with polyester is always difficult because it does not allow other materials to create chemical bonding with its molecules. This is due to the thermoset nature of the material. Creating any chemical bond requires the application of heat and pressure to a much higher degree. Instead, the thermoset polyester is cured at room temperature or at a maximum of around 80–100°C [39, 40]. This temperature is insufficient to initiate any chemical reaction that can create new bonds with other materials. Moreover, its hydrophobic nature does not allow any materials to enter its structure, while other materials are difficult to associate with it. For this reason, mechanical properties always deteriorate with the addition of reinforcing or filler materials, which are always foreign materials to the polyester molecules. These materials cause a resistance between polyester molecules, which results in the de-bonding of the polyester molecules in the structure. This was the case in this study and in other studies that were discussed earlier [37, 39]. The only way to improve or retain the mechanical properties of polyester, even after the addition of other materials, is through surface modification or the use of coupling agents, which helps to make the additional materials more similar in terms of surface characteristics [12, 40].

Compared to the other studies, adding a small amount of filler generally found in powder or nanoparticle forms does not have a significant effect on mechanical properties. When higher percentages are introduced, however, mechanical properties deteriorate drastically. The addition of fibrous materials, which are generally more hygroscopic, i.e. the opposite of the characteristics of polyester, has a greater effect on mechanical properties than fillers [32, 41]. It also depends on the size of the fibrous materials, if they are used without being converted into nanomaterials like in this study, where the banana peels were ground but still took the form of large particles because banana peels are not finer materials (particle size varied from 150 to 400 μm), while the aluminium trihydrate particles were much finer (around 5 μm). For this reason, the negative effect was more drastic than the filler materials, while aluminium trihydrate did not have any adverse impact. According to some researchers, particle size is also an essential issue in terms of the flame retardancy of a composite, as some reports suggest that smaller filler particles fared better than larger particles. This was mainly due to the cover effect of smaller particles, which could cover more area in the structure than larger particles and helped to reduce flame resistance [42]. Moreover, the smaller particles could produce a layer within the polyester structure that served as a heat barrier. For this reason, smaller particles are preferred as flame retarding agents for maintaining a composite's mechanical properties.

Another reason for poor mechanical properties is the curing agent used in this study, i.e. methyl ethyl ketone peroxide, which is a powerful agent and performs curing at room temperature within a minimal duration. It helps to create more uniform and stronger bonds between polyester molecules. At the same time, however, this type of curing agent gives very little time to form proper mechanical bonds when foreign materials are inserted between the polyester molecules. On the other hand, benzoyl peroxide is another curing agent used in several studies that require around 80°C. It also requires more than an hour to cure. It gives more time for the foreign materials to settle in the structure. This problem can still be avoided by using proper pressure during curing. Since the materials were produced using a hand lay-up process, the parameters could not be maintained as well as required, which caused a drastic deterioration in tensile properties when fibrous materials were added to the composites. Nevertheless, due to the use of a small amount of filler and fibrous materials, the mechanical properties remained similar to another research that was within the relevant range.

The LOI obtained in this study was too low, and the composites in this study cannot be deemed flame retardant at all. This is due to the use of a very small amount of flame-retardant filler, while one of the few possible outcomes of the enhanced flame-retarding property of the composite due to the high percentage of moisture trapped in the banana peels or the possible char forming ability of banana peels did not materialize. Instead, the other expected outcome of increased flammability materialized in the composites in this study. However, the presence of ATH as filler resulted in almost unchanged flammability, but did not have any further effect, either. For this reason, the composites in this study could not reach the level of a flame-retardant composite. The studies reduced the polyester percentage by a considerable amount to achieve the best results. Chen et al. used only about 70% resin and introduced about 30% flame-retardant filler materials in the structure of the composites [40]. The resulting materials fared considerably better when higher percentages of flame-retardant fillers were introduced. The composites in this study showed the least flame-retardant property, as all the materials fell into the horizontal burning category in the UL 94-V test. In contrast, other studies recorded a significantly better property, as V-0 and V-1 ratings were achieved by Chen et al. in their respective studies [40]. The minimum amount of filler required to attain a V-1 rating was 10% [39]. For further improvement, about 30% of fillers were required by both Jiang et al. and Chen et al. [40]. They introduced different combinations to achieve that level. Also worth of note is that they showed that combinations of different fillers were required for the best results instead of a single filler. A combination of several fillers can give a synergistic effect and enhance the power of the fillers. Otherwise, more than 30% would have been required to achieve a similar effect if the fillers were used alone, as different studies showed that more than 30% of fillers were required to have any significant effect on flame-retarding properties [43, 44]. On the other hand, char-forming ability could also significantly improve the flame-retardant property of a material, as shown by Sain et al. [13]. The formation of a non-flammable layer by the char can disrupt the flow of flame and can readily reduce the flame. However, the banana peels used in this study could not produce the amount of char required, possibly due to the low percentage. Sain et al. used surface modification to use a higher percentage of fibre without damaging the mechanical properties of the composites. In this study, however, the fibre percentage could not be increased up to the required level due to the drastic drop in the tensile strength of the composites, which was not a surprise. There was no other option due to the aim of this study to keep the cost of the final material down.

Another critical point to be discussed is the type of filler used in the discussed composites. The ability of the fillers differs from each other. The mechanisms of different fillers likewise differ from each other, as previously mentioned above. The main designated flame-retardant filler used in this study was aluminium trihydrate (ATH), which can be classified as a medium-strength filler. Studies have shown that quite a high percentage of aluminium trihydrate is required (equal to or above 30%) to have a better impact on the flame-retardant properties of a composite [43–46]. The thermal stability of aluminium trihydrate is also on the lower side as the 1st step of decomposition takes place at around 200°C when the water molecules are released [47]. Even though the 2nd step of degradation or the full degree of disintegration takes place much later, at around 500°C, the main flame-resisting process takes place during the 1st step of degradation when aluminium trihydrate absorbs heat and releases water molecules [10, 47]. Similar results in the composites were obtained when another metallic hydroxide, magnesium hydroxide, was used as the filler. It also follows a similar mechanism and gives more or less similar results as aluminium trihydrate [13, 39].

From the above comparisons, it is possible to come to some conclusions regarding this study. First, the objective was to produce a cheap material containing banana peels and ATH. The results achieved in the mechanical properties test showed a significant loss of strength due to these modifications, while in the flame retardancy test, the results were not of a very high standard. However, the flame-resisting property was still improved to a lesser degree. The reason for this was the use of a very small amount of flame-retardant filler material, and because the lignocellulosic banana peels used in this study did not have the desired effect of a high percentage of char formation, as expected. To improve the property further, the use of a higher percentage of flame-retardant filler material than in this study, or the use of cellulosic material containing a higher percentage of lignin than banana peels, or increasing the amount of the cellulosic material or replacing the filler material with a more effective filler material or materials, is recommended for future research. The true aim of this study was not to produce a flame-retardant composite, but rather to produce a cheap material using banana peels, and to keep the thermal and flammability property of the final material in check, even after modification. The tensile properties were damaged more than expected, but the thermal and flammability properties were kept within the desired range. This study can thus be deemed successful.

4 Conclusion

This study was an attempt to use banana peels to develop a polyester composite. Polyester was accompanied by ATH in different combinations. Due to the absence of newly formed chemical bonds between banana peels and polyester, the mechanical properties deteriorated drastically with the addition of ATH and banana peels. The tensile properties suffered the most with a reduction in strength of more than 50%, while flexural strength was also affected significantly for the same reason. However, the addition of fibre improved the impact and flexural properties to some extent after a drastic deterioration when the composites were made using only ATH and polyester. However, the results were still inferior to the properties of pure polyester. In terms of flame retardancy, the ATH did improve the property to a small degree when added. The small amount of banana peels proved insufficient to improve the flame-retardant properties of the materials because they produced some char. In contrast, they did not worsen flammability significantly because small quantities were used. More banana peels could not be added because of the deteriorating mechanical properties. The thermal properties proved the impact of both fillers on the composite, but no significant changes were identified with the addition of banana peels or the filler, again due to the presence of a very small quantity. In summary, the addition of banana peels and filler materials caused a deterioration in mechanical properties relative to pure polyester, but flammability was kept in check by incorporating filler material. The cost of the final product has definitely reduced, but that came at the cost of deteriorated mechanical properties. However, the banana peels were added in a small particle form, which acted more like a filler in this study. They can be altered in future studies to determine whether banana peels in the form of a reinforcing fibre can stop the deterioration of mechanical properties or if they can improve any of the mechanical properties instead.

References

1. RAMESH, M., DEEPA, C., KUMAR, L.R., SANJAY, M.R., SIENGCHIN, S. Life-cycle and environmental impact assessments on processing of plant fibres and its bio-composites: a critical review. *Journal of Industrial Textiles*, in press, doi: 10.1177/1528083720924730.
2. SANJAY, M.R., MADHU, P., JAWAID, M., SENTHAMARAIKANNAN, P., SENTHIL, S., PRADEEP, S. Characterization and properties of natural fiber polymer composites: a comprehensive review. *Journal of Cleaner Production*, 2018, **172**, 566–581, doi: 10.1016/j.jclepro.2017.10.101.
3. VINOD, A., SANJAY, M.R., SUCHART, S., JYOTISHKUMAR, P. Renewable and sustainable biobased materials: an assessment on biofibers, biofilms, biopolymers and biocomposites. *Journal of Cleaner Production*, 2020, **258**, 1–27, doi: 10.1016/j.jclepro.2020.120978.
4. MAACHE, M., BEZAZI, A., AMROUNE, S., SCARPA, F., DUFRESNE, A. Characterization of a novel natural cellulosic fiber from *Juncus effusus* L. *Carbohydrate Polymers*, 2017, 171, 163–172, doi: 10.1016/j.carbpol.2017.04.096.
5. TEKLU, T., WANGATIA, L.M., ALEMAYEHU, E. Effect of surface modification of sisal fibers on water absorption and mechanical properties of polyaniline composite. *Polymer Composites*, 2019, **40**(S1), E46–E52, doi: 10.1002/pc.24462.
6. CHANG, B.P., MOHANTY, A. K., MISRA, M. Studies on durability of sustainable biobased composites: a review. *RSC Advances*, 2020, **10**(31), 17955–17999, doi: 10.1039/C9RA09554C.

7. Crops and livestock products in 2020 [online]. FAO [accessed 4 December 2022]. Available on World Wide Web: <https://www.fao.org/faostat/en/#data/QCL>.
8. FERRANTE, A., SANTULLI, C., SUMMERSCALES, J. Evaluation of tensile strength of fibers extracted from banana peels. *Journal of Natural Fibers*, 2020, **17**(10), 1519–1531, doi: 10.1080/15440478.2019.1582000.
9. KHAWAS, P., DEKA, S. C. Comparative nutritional, functional, morphological, and diffractogram study on culinary banana (*Musa* ABB) peel at various stages of development. *International Journal of Food Properties*, 2016, **19**(12), 2832–2853, doi: 10.1080/10942912.2016.1141296.
10. ANANNYA, F.R., MAHMUD, M.A. Developments in flame-retardant bio-composite material production. *Advances in Civil Engineering Materials*, 2019, **8**(1), 9–22, doi: 10.1520/acem20180025.
11. MAHMUD, M.A., ANANNYA, F.R. Sugarcane bagasse – a source of cellulosic fiber for diverse applications. *Heliyon*, 2021, **7**(8), e07771, doi: 10.1016/j.heliyon.2021.e07771.
12. ŠTĚPEK, J., DAOUST, H. Reinforcing fillers, reinforcing agents, and coupling agents. In *Additives for Plastics*. New York : Springer, 1983, 70–98, doi: 10.1007/978-1-4419-8481-4_5.
13. SAIN, M., PARK, S.H., SUHARA, F., LAW, S. Flame retardant and mechanical properties of natural fibre–PP composites containing magnesium hydroxide. *Polymer Degradation and Stability*, **83**(2), 363–367, doi: 10.1016/S0141-3910(03)00280-5.
14. BAR, M., ALAGIRUSAMY, R., DAS, A. Flame retardant polymer composites. *Fibers and Polymers*, 2015, **16**(4), 705–717, doi: 10.1007/s12221-015-0705-6.
15. REIS, J.M.L.D. Effect of temperature on the mechanical properties of polymer mortars. *Materials Research*, 2012, **15**(4), 645–649, doi: 10.1590/S1516-14392012005000091.
16. ROTHON, R.N., HORNSBY, P.R. Flame retardant effects of magnesium hydroxide. *Polymer Degradation and Stability*, 1996, **54**(2–3), 383–385, doi: 10.1016/s0141-3910(96)00067-5.
17. HORNSBY, P.R. The application of fire-retardant fillers for use in textile barrier materials. In *Multifunctional Barriers for Flexible Structure*. Edited by Sophie Duquesne, Carole Magniez and Giovanni Camino. Berlin : Springer, 2007, 3–22, 10.1007/978-3-540-71920-5_1.
18. CAMINO, G., COSTA, L., DI CORTEMIGLIA, M.L. Overview of fire retardant mechanisms. *Polymer Degradation and Stability*, 1991, **33**(2), 131–154, doi: 10.1016/0141-3910(91)90014-I.
19. SCHINDLER, W.D., HAUSER, P.J. *Chemical FInishing of Textiles*. Cambridge : Woodhead, 2004.
20. RIGOLO, M., WOODHAMS, R.T. Basic magnesium carbonate flame retardants for polypropylene. *Polymer Engineering & Science*, 1992, **32**(5), 327–334, doi: 10.1002/pen.760320505.
21. *Fire Retardancy of Polymeric Materials*. Edited by C.A. Wilkie and A.B. Morgan. Boca Raton: CRC Press, 2000.
22. HORNSBY, P.R., WATSON, C.L. A study of the mechanism of flame retardance and smoke suppression in polymers filled with magnesium hydroxide. *Polymer Degradation and Stability*, 1990, **30**(1), 73–87, doi: 10.1016/0141-3910(90)90118-Q.
23. NAM, T.H., OGIHARA, S., TUNG, N.H., KOBAYASHI, S. Effect of alkali treatment on interfacial and mechanical properties of coir fiber reinforced poly (butylene succinate) biodegradable composites. *Composites Part B: Engineering*, 2011, **42**(6), 1648–1656, doi: 10.1016/j.compositesb.2011.04.001.
24. SANJAY, M.R., YOGESHA, B. Studies on hybridization effect of jute/kenaf/E-glass woven fabric epoxy composites for potential applications: effect of laminate stacking sequences. *Journal of Industrial Textiles*, 2018, **47**(7), 1830–1848, doi: 10.1177/1528083717710713.
25. SINDHU, R., BINOD, P., PANDEY, A. Microbial poly-3-hydroxybutyrate and related copolymers. In *Industrial Biorefineries & White Biotechnology*. Edited by Ashok Pandey, Rainer Höfer and Christian Larroche. Elsevier, 2015, 575–605.
26. *Mechanical testing of advanced fibre composites*. Edited by J. M. Hodgkinson. Cambridge : Woodhead, 2000.
27. PAWELEC, K.M., WHITE, A.A., BEST, S.M. Properties and characterization of bone repair materials. In *Bone Repair Biomaterials*. Edited by Kendell M. Pawelec and Josep A. Planell. Cambridge : Woodhead Publishing, 2019, 65–102.
28. HILADO, C.J. *Flammability Handbook for Plastics*, 5th ed. Boca Raton : CRC Press, 1998.
29. KOURTIDES, D.A., GILWEE JR, W.J., PARKER, J.A. Thermochemical characterization of some thermally stable thermoplastic and thermoset

polymers. *Polymer Engineering & Science*, 1979, **19**(1), 24–29, doi: 10.1002/pen.760190105.

30. KARAK, N. Vegetable oil-based polymer composites. Oxford : Woodhead Publishing, 2012, 247–270.
31. CHIU, S.H., WANG, W.K. The dynamic flammability and toxicity of magnesium hydroxide filled intumescent fire retardant polypropylene. *Journal of Applied Polymer Science*, 1989, **67**(6), 989–995, doi: 10.1002/(SICI)1097-4628(19980207)67:6<989::AID-APP4>3.0.CO;2-I.
32. MONTEIRO, S.N., TERRONES, L.A.H., D'ALMEIDA, J.R.M. Mechanical performance of coir fiber/polyester composites. *Polymer Testing*, 2008, **27**(5), 591–595, doi: 10.1016/j.polymertesting.2008.03.003.
33. RAY, D., SARKAR, B.K., BOSE, N.R. Impact fatigue behaviour of vinylester resin matrix composites reinforced with alkali treated jute fibres. *Composites Part A: applied Science and Manufacturing*, 2002, **33**(2), 233–241, doi: 10.1016/S1359-835X(01)00096-3.
34. WILSON, R., DINI, D., VAN WACHEM, B. The influence of surface roughness and adhesion on particle rolling. *Powder Technology*, **312**, 321–333, doi: 10.1016/j.powtec.2017.01.080.
35. MOHD DOM, Z., MUJIANTO, L., AZHAR, A., MASAUDIN, S., SAMSUDIN, R. Physicochemical properties of banana peel powder in functional food products. *Food Research*, 2021, **5**(1), 209–215, doi: 10.26656/fr.2017.5(S1).037.
36. GAÑÁN, P., MONDRAGON, I. Fique fiber-reinforced polyester composites: Effects of fiber surface treatments on mechanical behavior. *Journal of Materials Science*, 2004, **39**(9), 3121–3128, doi: 10.1023/B:JMSC.0000025841.67124.c3.
37. HE, J., ZENG, W., SHI, M., LV, X., FAN, H., LEI, Z. Influence of expandable graphite on flame retardancy and thermal stability property of unsaturated polyester resins/organic magnesium hydroxide composites. *Journal of Applied Polymer Science*, 2020, **137**(1), 47881, doi: 10.1002/app.47881.
38. LUTHRA, P., SINGH, R., KAPUR, G. S. Development of polypropylene/banana peel (treated and untreated) composites with and without compatibilizer and their studies. *Materials Research Express*, 2019, **6**(9), 095313, doi: 10.1088/2053-1591/ab2eea.
39. CHEN, Z., JIANG, M., CHEN, Z., CHEN, T., YU, Y., JIANG, J. Preparation and characterization of a microencapsulated flame retardant and its flame-retardant mechanism in unsaturated polyester resins. *Powder Technology*, **354**, 71–81, doi: 10.1016/j.powtec.2019.05.077.
40. JIANG, M., ZHANG, Y., YU, Y., ZHANG, Q., HUANG, B., CHEN, Z., JIANG, J. Flame retardancy of unsaturated polyester composites with modified ammonium polyphosphate, montmorillonite, and zinc borate. *Journal of Applied Polymer Science*, 2019, **136**(11), 47180, doi: 10.1002/app.47180.
41. HILL, C.A.S., ABDUL KHALIL, H.P.S. Effect of fiber treatments on mechanical properties of coir or oil palm fiber reinforced polyester composites. *Journal of Applied Polymer Science*, 2000, **78**(9), 1685–1697, doi: 10.1002/1097-4628(20001128)78:9<1685::AID-APP150>3.0.CO;2-U.
42. CHEN, H., WEN, X., GUAN, Y., MIN, J., WEN, Y., YANG, H., TANG, T. Effect of particle size on the flame retardancy of poly (butylene succinate)/$Mg(OH)_2$ composites. *Fire and Materials*, 2016, **40**(8), 1090–1096, doi: 10.1002/fam.
43. AI, L., CHEN, S., YANG, L., LIU, P. Synergistic flame retardant effect of organic boron flame retardant and aluminum hydroxide on polyethylene. *Fibers and Polymers*, 2021, **22**(2), 354–365, doi: 10.1007/s12221-021-9385-6.
44. LIU, L., ZHANG, H., SUN, L., KONG, Q., ZHANG, J. Flame-retardant effect of montmorillonite intercalation iron compounds in polypropylene/aluminum hydroxide composites system. *Journal of Thermal Analysis and Calorimetry*, 2016, **124**(2), 807–814, doi: 10.1007/s10973-015-5213-9.
45. IQBAL, M.A., IQBAL, M.A., FEDEL, M. Fire retardancy of aluminum hydroxide reinforced flame retardant modified epoxy resin composite. *Russian Journal of Applied Chemistry*, 2018, **91**(4), 680–686, doi: 10.1134/S1070427218040225.
46. PAN, Y., HAN, L., GUO, Z., FANG, Z. Improving the flame-retardant efficiency of aluminum hydroxide with fullerene for high-density polyethylene. *Journal of Applied Polymer Science*, 2017, **134**(9), doi: 10.1002/app.44551.
47. PÉREZ, N., QI, X.-L., NIE, S., ACUÑA, P., CHEN, M.-J., WANG, D.-Y. Flame retardant polypropylene composites with low densities. *Materials (Basel)*, 2019, **12**(1), 1–11, doi: 10.3390/ma12010152.

Marius Dotter[1], Lion Lukas Placke[1], Jan Lukas Storck[1], Uwe Güth[2]
[1] Faculty of Engineering and Mathematics, Bielefeld University of Applied Sciences, 33619 Bielefeld, Germany
[2] Department of Physical and Biophysical Chemistry (PC III), Faculty of Chemistry, Bielefeld University, 33615 Bielefeld, Germany

Characterization of PAN-TiO_2 Nanofiber Mats and their Application as Front Electrodes for Dye-sensitized Solar Cells

Karakterizacija PAN-TiO_2 nanovlaknatih kopren in njihova uporaba kot sprednjih elektrod za elektrokemijske sončne celice

Original scientific article/*Izvirni znanstveni članek*

Received/*Prispelo* 10-2022 • Accepted/*Sprejeto* 12-2022

Corresponding author/*Korespondenčni avtor:*
Marius Dotter, MSc
E-mail: marius.dotter@fh-bielefeld.de
Tel.: +4952110670934
ORCID ID: 0000-0001-8398-1809

Abstract

In the context of the energy transition to renewables, the spotlight is on large systems connected to the power grid, but this also offers room for smaller, more specialized applications. Photovoltaics, in particular, offer the possibility of the self-sufficient supply of smaller electrical appliances on smaller scales. The idea of making previously unused surfaces usable is by no means new, and textiles such as backpacks, tent tarpaulins and other covers are particularly suitable for this purpose. In order to create a non-toxic and easily recyclable product, dye-sensitized solar cells (DSSC), which can be manufactured through electrospinning with a textile feel, are an attractive option here. Therefore, this paper investigates a needle electrospun nanofiber mat, whose spin solution contains polyacrylonitrile (PAN) dissolved in dimethyl sulfoxide (DMSO) as well es TiO_2 nanoparticles. In addition to characterization, the nanofiber mat was dyed in a solution containing anthocyanins to later serve as a front electrode for a dye-sensitized solar cell. Although of lower efficiency, the DSSC provides stable results over two months of measurement.

Keywords: dye-sensitized solar cells (DSSC), long-term stability, electrospinning, polyacrylonitrile (PAN), TiO_2 nanoparticles

Izvleček

V okviru energetskega prehoda na obnovljive vire so v središču pozornosti veliki sistemi, povezani z električnim omrežjem, vendar pa je tu tudi prostor tudi za manjše, specializirane aplikacije. Predvsem fotovoltaika ponuja možnosti za samozadostno oskrbo manjših električnih naprav z manjšim obsegom. Zamisel o uporabi prej neizkoriščenih površin ni nova, za ta namen pa so še zlasti primerni izdelki iz tekstilij, kot so nahrbtniki, ponjave za šotore in druga pregrinjala. Za razvoj nestrupenega izdelka, ki ga je mogoče zlahka reciklirati, so tukaj privlačna možnost elektrokemijske sončne celice, ki jih je mogoče izdelati z elektropredenjem in ki imajo tekstilni otip. Zato je v tem članku raziskana nanovlaknata koprena, izdelana v enoigelnem postopku elektropredenja iz raztopine poliakrilonitrila (PAN), raztopljenega v dimetilsulfoksidu (DMSO), z dodatkom nanodelcev TiO_2. Poleg karakterizacije je bila nanovlaknata koprena tudi barvana v raztopini antocianov, da bi bila pozneje uporabljena kot sprednja elektroda za elektrokemijsko sončno celico. Čeprav je manj učinkovita, pa je elektrokemijska elektroda pri dvomesečnem merjenju zagotovila stabilne rezultate.

Ključne besede: elektrokemijske sončne celice, dolgotrajna stabilnost, elektropredenje, poliakrilonitril (PAN), nanodelci TiO_2

1 Introduction

Although the negative effects of conventional, primary methods of energy production such as coal and nuclear energy are well known, the development and expansion of renewable energy sources are not progressing fast enough [1]. New energy sources are not only suitable for replacing currently used sources by large-scale installations with power grid feed-in, but also offer further, special application areas for buildings or private use [2], for example existing tablet-sized photovoltaic systems for mobile use. Of course, the latter application will not cover broader energy demand, but small, decentralized devices for energy harvesting provide energy where otherwise previously charged accumulators or batteries would be used or it is otherwise difficult to install larger systems. This concept will be addressed here with an attempt to make textiles usable for energy production in everyday life. Here, tent/pavilion tarpaulins, backpacks and sunshades can serve as carriers for a dye-sensitized solar cell (DSSC) with textile haptics [3].

In a DSSC, a dye with a suitable orbital structure serves as a light absorber. The dye is classically bonded to a semiconductor, which slightly shifts the energetic structure and thus the colour of the dye. The dye releases electrons through light absorption, whereby the dye becomes positive and no longer active until its regeneration. Similar to normal silicon cells, this absorber layer is located on a light-transmissive, conductive layer in order to transport the current away. Usually, indium tin oxide (ITO) on glass is used for the latter. Through an external circuit, the electrons reach the back side of the DSSC. There is a catalyst layer, usually graphite or platinum, and an electrolyte matched to the dye. Through a Redox reaction, the dye is regenerated again and is once more available for energy absorption [4, 5].

As a further difference and advantage over conventional silicon-based cells, these DSSCs should be simple and inexpensive to manufacture and non-toxic in order to simplify their recycling [6]. At the same time, refined textiles should provide stability and contacting. A gel electrolyte with long-term stability ensures the good regeneration of the dye and hardly evaporates, which avoids the sealing and possible negation of the textile properties of the cell [3, 7-10]. However, the main focus here is on the simple production of the front electrode. As an alternative to conventional layers, we want to use nanofiber mats for this purpose, since they have the desired textile feel, are stable and flexible, can be customized with the appropriate materials and have a large surface area [11]. Several approaches already exist for producing a functioning front electrode for a DSSC from a nanofiber mat. Kohn et al. describe a multilayer needleless electrospinning process based on polyacrylonitrile (PAN), starting with a catalyst graphite layer, then a buffer layer on top, and finally a nanofiber mat with titanium dioxide (TiO_2) and dye already in the spin solution. The multilayer mat is subsequently impregnated with a conductive polymer, dried and then used as a DSSC [3]. However, for simplicity in the development process, usually only one component of the cell is spun, as in Mamun et al. [12]. They first spun a PAN nanofiber mat with TiO_2 content using needleless electrospinning, carbonized it for conductivity and then dip-coated it in dissolved anthocyanins. It should be noted that carbonization requires similar temperatures as sintering, and therefore entails similar problems, such as damage to the other layers.

Therefore, the electrospinning of the front electrode was further investigated and its long-term performance measured. In this work, PAN dissolved in dimethyl sulfoxide (DMSO) with suspended TiO_2 nanoparticles was spun using a needle electrospinning system, in contrast to previous studies. For this purpose, a previously mixed solution of polymer, solvent and additive was filled into a syringe pump and forced through a small nozzle under a fixed pressure. A high voltage was applied between the nozzle and a collector plate, usually made of aluminium, which draws thin polymer filaments to the collector. A characteristic Taylor cone was formed at the nozzle and the nanofibers were deposited in random orientation on the collector. By using a moving nozzle holder and a rotating collector, the fibres can be given the preferred orientation. The nanofiber mat produced as such was measured using optical and scanning electron microscopy (SEM). In addition, a piece of the nanofiber mat was analysed through thermogravimetric analysis (TGA) to reach conclusions about the PAN to TiO_2 ratio. The nanofiber mat was further dip-coated in a solution of dissolved anthocyanins to dye the TiO_2 particles via covalent binding and then assembled as a component for a DSSC. In addition, a commercially available liquid electrolyte was used in order to investigate the rapid evaporation of the electrolyte in the usual comparison cells. The prepared DSSCs were subsequently measured over a period of about two months.

It should be noted that neither the carbonization of the nanofiber mat nor sintering of the TiO_2 was carried out. Since the front electrode is to be spun directly onto existing components of the DSSC in the workflow of future application, thermal treatment, which is necessary for both carbonization and sintering, would negatively affect or even destroy other components of the DSSC.

2 Materials and Methods

A suspension containing DMSO (min. 99.9%, obtained from S3 chemicals, Bad Oeynhausen, Germany) as solvent, X-PAN as co-polymer (93.5% acrylonitrile, 6% methylacrylate, 0.5% natrium-sodium-mythallylsulfonate, Dralon, Dormagen, Germany; Mn = 90,000 g/ml, Mw = 250,000 g/mol) and TiO_2 nanoparticles with an average size of 21 nm (P25 Titanium IV oxide nanopowder, 21 nm primary particle size, Sigma Aldrich, Saint Louis, MO, USA) in a weight ratio of 8:1:1 was prepared. For this purpose, the X-PAN was dissolved in DMSO for one hour at room temperature while stirring, TiO_2 was then added and mixed in. A homogeneous nanofiber mat was electrospun using a SpinBox (Bioinicia, Spain) needle-based electrospinning machine with a horizontally moving nozzle holder and a rotating collector. The spin parameters were as follows: voltage: 25 kV; pump speed: 1000 μl/h; distance nozzle to collector: 20 cm; collector rotation speed: 400 rpm; temperature 21.5 °C; relative humidity: 26%; outer nozzle diameter: 1.6 mm; and duration: 72 min. In addition, a spinning solution of 16 wt% X-PAN dissolved in DMSO was prepared and spun using the same parameters to produce a TiO_2-free reference nanofiber mat.

To extract the anthocyanins, 17 g of Maqui berry tea (Mayfair, Wilken Tee GmbH, Fulda, Germany) was mixed with 150 g of deionized water and 50 g of ethanol, stirred for half an hour and subsequently filtered. The now filtered anthocyanin dye solution was placed in a beaker that facilitated the sufficient dip-coating of the nanofiber mats. For immersion during dip-coating, the nanofiber mat was held with metal tongs. This also prevented the nanofiber mat from rolling up due to surface tension. To dye the nanofiber mat, it was then immersed in the dye solution for about 30 s with gentle stirring and afterwards placed on a commercial fluorine-doped tin oxide coated glass slide (ManSolar, Petten, Netherlands) and stored in the dark for drying. In the case of the TiO_2 nanofiber mat, this then facilitated direct use as a front electrode for a DSSC after drying.

The structure of the anthocyanin dye is shown in Figure 1. Since there are always many different anthocyanins present as colour, only the general mesomers have been shown. Sugars or similar large structures can be attached as residues, but mostly these are hydroxy or hydrogen groups.

Similar glass slides were used for the counter electrode. The slides were sprayed with a graphite spray (CP-Graphitprodukte GmbH, Wachtberg, Germany) for 1 s from a distance of 50 cm. In addition, the counter electrodes were heat treated for 30 min at 200 °C in a heating cabinet (B150 muffle oven, Nabertherm, Lilienthal, Germany). This procedure is known to form a graphite catalyst layer in the range of 2–4 μm [13].

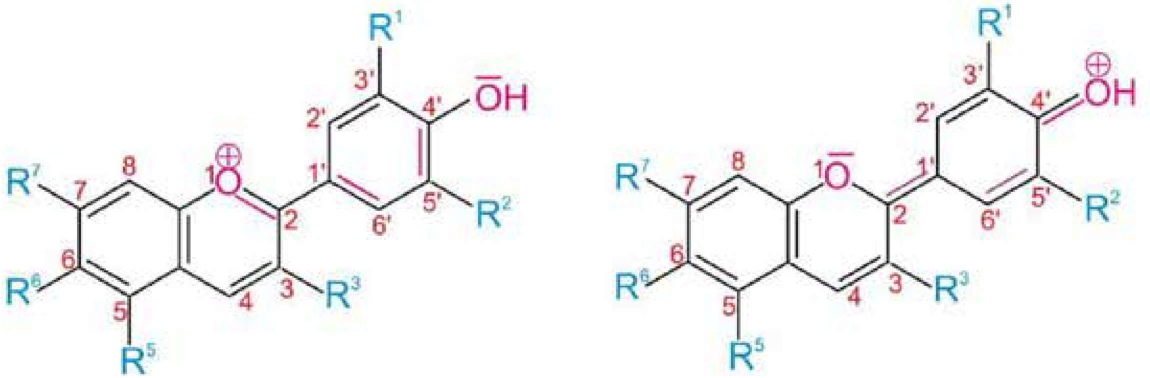

Figure 1: Mesomeric boundary structures of the anthocyanin backbone. Some of the residues may be bound sugars, for example. However, most of the residues consist of hydroxy groups or hydrogen.

For assembly, the two prepared glass plates were placed on top of each other with a slight offset for attaching the measuring clamps and fixed tightly by means of adhesive tape. This design provides a DSSC with a reactive area of 6 cm^2, which is quite large compared to common cells in literature [14]. A liquid, commercially available electrolyte (ManSolar, Petten, Netherlands) was applied to the cell by capillary force. A total of three DSSCs were built according to this design.

For measurement, the DSSCs were placed under a solar simulator LS0500 with an AM 1.5G spectrum (LOT-Quantum Design GmbH, Darmstadt/Germany) with a power of 100 mW/cm^2 and a black, non-reflecting background. The current-voltage characteristics were recorded by a Keithley 2450 sourcemeter. The DSSCs were stored for the rest of the time in the dark under laboratory conditions.

The macroscopic images were taken using a Sony Cybershot DSC-RX100 IV camera. Light microscope images were taken using a Zeiss Axio Observer Microscope in transmissive light mode.

To measure the nanofiber mat by means of SEM, the nanofiber mat was stuck on a Stub via a graphite adhesive pab and thinly sputtered with palladium. All measurements were performed at a high voltage of 10 kV, and secondary electrons were detected.

TGA measurement were made using a Hi-Res TGA 2950 Thermo-gravimetric Analyzer from TA Instruments (New Castle, DE, USA) under a constant air flow and a temperature increase of 10 K/min from 40 °C to 800 °C.

3 Results and discussion

Figure 2 shows a) an untreated TiO$_2$ nanofiber mat after the spinning process; b) a pure X-PAN mat after dip-coating in an anthocyanin dye solution and subsequent drying in the dark; and c) a TiO$_2$ nanofiber mat dyed analogously. The white colour of the untreated nonwoven is due to the polymer and TiO$_2$, which is also a known bleaching agent. In clear contrast, the dyed nonwovens show a distinct coloration. Nanofiber mat c) with TiO$_2$ shows a clearly darker coloration than sample b). This indicates the expected bathochromic shift, also known as red shift, in the spectrum due to the bond between anthocyanin and TiO$_2$ [4]. The smaller, even darker particles on the dyed nonwovens are solid residues from the dissolution process of the anthocyanin from the tea, which could not be completely filtered out.

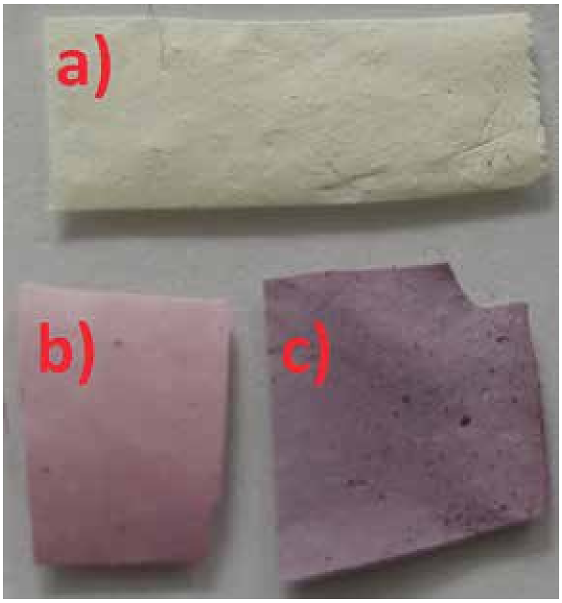

Figure 2: Photograph of differently treated electrospun nanofiber mats: a) PAN-TiO$_2$ without further treatment; b) pure PAN after dip-coating in a anthocyanin dye solution and drying; and c) PAN-TiO$_2$ after dyeing

Figure 3 shows light microscope images of the nanofiber mat in a) and b) untreated state and c) and d) after dip-coating, and drying in transmitted light mode with a magnification factor of around 10 between images a) and b) and c) and d). The thickness of the nanofiber mat appears to vary in different positions, which is evident from the lighter and darker areas in images a) and c), which acts as a background for the much darker particles. In Figures 2 b) and d), nanofibers are already visible, and have a diameter of up to 1.6 µm, although the diameter of most fibres is less than 1 µm. In addition, large accumulations of TiO$_2$ can be seen in the images, which in isolated cases have diameters of up to 50 µm.

In the optical comparison of the uncoloured nanofiber mats (Figure 3 a) and b)) with the coloured mat images (c) and d)), it is clear that the colouring and thus binding of the anthocyanin dye takes place on the TiO$_2$ particles and nanofibers containing TiO$_2$ nanoparticles.

Figure 4 shows SEM images of the untreated nanofiber mat containing PAN and TiO$_2$, with increasing magnification from a) to d). Here, TiO$_2$ accumulations can also be seen in all four images,

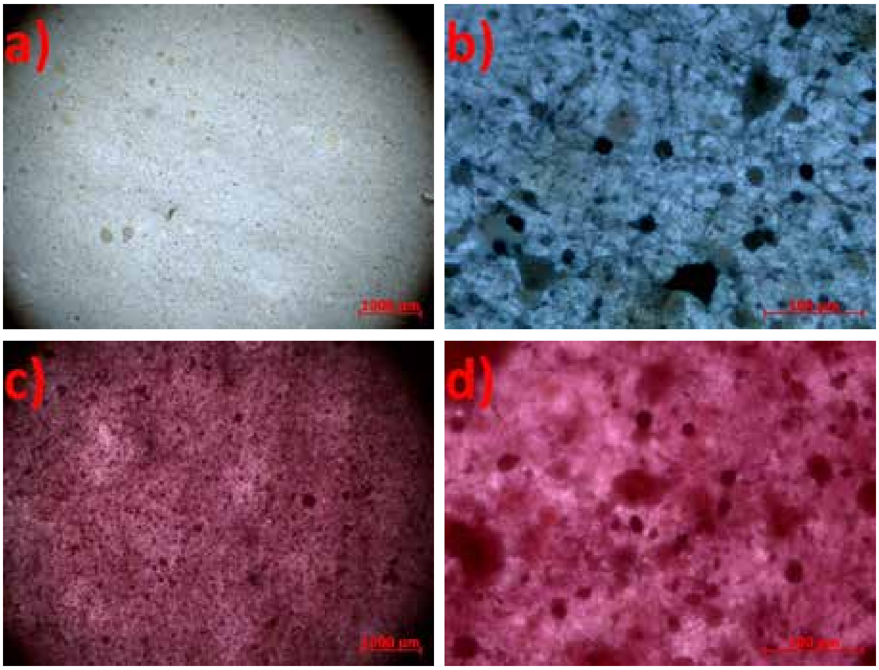

Figure 3: Light microscope images of the PAN-TiO$_2$ nanofiber mats a) and b) before dyeing; and c) and d) after dyeing with different magnifications

and appear to be very disordered and vary greatly in size. While the larger TiO$_2$ particles, which are up to 10 µm in size, are in the nanofiber mat and partly act as anchor and starting points for nanofibers, the smaller particles are located around and on the nanofibers, and do not interrupt the nanofiber structure.

The diameter of the nanofibers varies greatly, from 90 nm to about 1.5 µm, as previously suspected in Figure 3. Here, it is possible that even thinner fibres exist that either cannot be resolved or appear thicker due to a TiO$_2$ cladding. Particularly in needle electrospinning, particles seem to negatively influence the spin behaviour and thus lead to a large

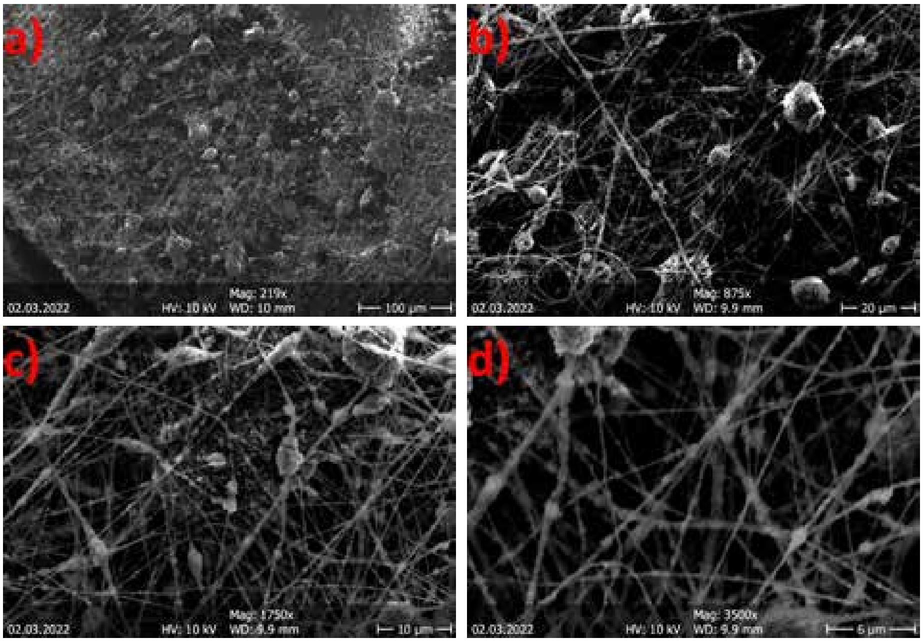

Figure 4: REM images of the undyed PAN-TiO$_2$ nanofiber mat with increasing magnification from a) to d).

variation in nanofiber diameter, while for a fixed DMSO:PAN ratio, the fibre thickness varies little, as described by Grothe et al [15, 16].

Due to the spinning process using a movable nozzle holder and rotating collector roll, the nanofibers should have a preferred direction. This cannot be identified with certainty on the basis of SEM images of Figure 4 a) to d), although in image a) the diagonal from bottom left to top right can be assumed to be the most probable.

Figure 5 shows the TGA measurement of the uncoloured PAN-TiO_2 nanofiber mat. The first range up to about 300 °C shows only a slight, steady decrease of 3 to 4 % due to the evaporation of water. At 300 °C, the melting point of PAN is reached and volatile gases are released, which lead to an abrupt decrease in weight by 18% [17, 18]. In this range and even up to 600 °C, the further combustion of organic components and evaporation of NH_3 and HCN takes place, resulting in a steady decrease of 32% [19]. Subsequently, 46% of the initial mass remains, which resembles the TiO_2 content, as this only melts and evaporates at significantly higher temperatures. Thus, the mass content of about 46% TiO_2 in the nanofiber mat corresponds to the ratio of the mass proportions of PAN and TiO_2 (1:1) in the spinning suspension.

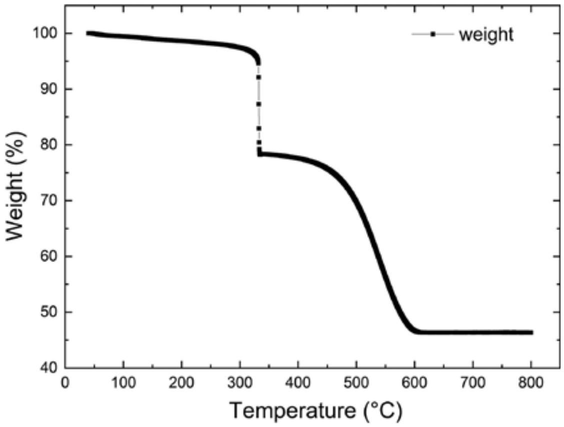

Figure 5: TGA measurement of the undyed PANTiO$_2$ nanofiber mat

Figure 6 shows the measured efficiencies of the three constructed DSSCs, where instead of the individual efficiencies per measurement day, the mean value of these is given with a standard deviation. This plot was chosen because there were isolated, presumably erroneous measurements of the respective cells as is known for the conductive glass plates used [9]. However, these measurement errors are taken into account and are reflected in the occasionally very large standard deviations. If the whole curve is considered in a physical context, a rather straight-line progression can be assumed, supported by several similar values with very small standard deviations.

Considering the pure mean values, efficiency increases during the first week from around 0.0003% to an average of 0.0012%, but fluctuates after three weeks with efficiencies ranging from 0.0002% to 0.0007%. Including the standard deviation, an efficiency of 0.0003% seems to be acceptable as a plausible value for the later course and is thus equal to the first measurement.

The fact that electrospinning can also be used to produce DSSCs with higher efficiencies has been shown several times in literature. Osfouri et al. describe a DSSC with electrospun TiO_2 nanofibers doped by bio-Ca nanoparticles with up to 1.48% efficiency [20]. DSSC efficiencies of a similar magnitude have been reported by Al-Alwani et al. [21] (0.23% effectivity) and Prabavathy et al. [22] with 0.99% to 1.17%. The impact of the pH value during extraction was shown by Ekpunobi et al. [23], with a pH value of three leading to an efficiency of 0.98%. Higher efficiencies can also be achieved with ruthenium dyes. Nien et al. [24] achieved efficiencies of between 3.11% and 7.92%, varying the light intensity on the one hand and the addition of $ZnFe_2O_4$ on the other.

In the work of Kohn et al. [3], DSSCs spun with dye and subsequently made conductive with PEDOT:PSS achieved efficiencies on the order of 10^{-3} %. A similar procedure to that described here by Mamun et al. [12], but in which the nonwovens were carbonized and then dyed, resulted in an efficiency of 0.0001%. In these two tests, however, the DSSC was measured at most up to the seventh day and no long-term stability was proven. We were able to confirm comparable efficiencies with the needle electrospinning and simpler production of the DSSCs over a period of 60 days. Furthermore, the efficiency is low compared to DSSCs with completely nontoxic, inexpensive materials that are known to have low efficiencies, whereby the measurement issues already mentioned above will have some influence in this regard [8, 9, 25]. To the best of our knowledge, this report is the first to show DSSCs that are made of a TiO_2 nanofiber mat that has not been subsequently sintered, carbonized or otherwise made conductive. In particular, the sintering of the TiO_2 layer is necessary for conventional cells.

It can be assumed that the future optimization of the nanofiber mat, especially with regard to contact to other layers of the cell, will lead to significant improvements in efficiency.

It is interesting to compare this with DSSCs that use the same commercial electrolyte and also have the same materials as components. With these normal cells, the efficiency is generally higher due to the fact that they were built as a comparison to other DSSCs, in which various aspects were changed and investigated. As a rule, these cells are significantly higher in terms of efficiency at the beginning of the measurements than other DSSCs, which, for example, test other electrolytes. However, these DSSCs with the commercial electrolyte already drop sharply after a few days and are sometimes no longer active after two months [9, 10, 25]. In contrast, Figure 6 shows a very low but nearly constant efficiency. In the optimum case, this could indicate that the evaporation of the electrolyte is reduced by this type of front electrode. As a negative interpretation, it would also be acceptable that the effect of evaporation would not play a major role at such a low efficiency. In any case, this is an observation that should be investigated through further long-term measurements.

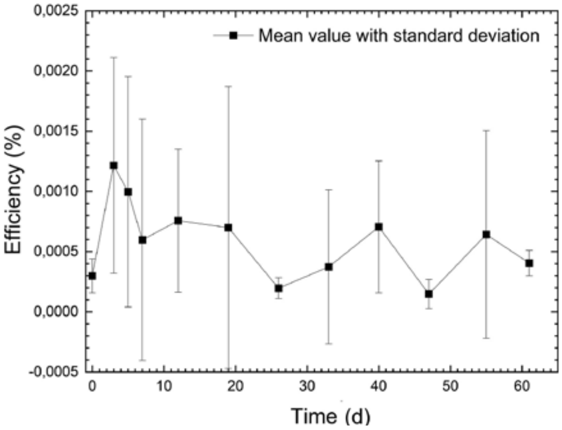

Figure 6: Mean values and standard deviations over 61 days of the three manufactured DSSCs with a needle electrospun and dyed nanofiber mat as front electrode

4 Conclusion

The electrospun nanofiber mat containing PAN as a polymer and TiO_2 nanoparticles was characterized via optical microscopy and REM, which showed that the nanofibers and TiO_2 nanoparticles varied greatly in size and distribution. The nanofiber mat was then dyed using a solution of water, ethanol and extracted anthocyanin. A comparison with a TiO_2-free, dyed nanofiber mat shows a clear red shift, confirming the bonding of the dye to the semiconductor material. The DSSCs built with the nanofiber mat as the front electrode showed a low but roughly constant efficiency over two months of measurement. Given that the nanofiber mat was not sintered and only low cost, non-toxic ingredients where used, the results are promising, but still require significant optimization.

For future studies, a comparison with a needleless electrospun nanofiber mat, whose spin solution has similar concentrations, would also be conceivable. The alignment of the nanofibers was not detected in anyway by the constellation used here.

Funding

This research was partly funded by the German Federal Ministry for Economic Affairs and Climate Action via the AiF, based on a resolution of the German Bundestag, grant number KK5044902SY0.

Conflicts of Interest

The authors declare no conflict of interest. The funders had no role in the design of the study, in the collection, analyses or interpretation of data, in the writing of the manuscript or in the decision to publish the results.

References

1. DRESSELHAUS, M.S., THOMAS, I.L. Alternative energy technologies. *Nature*, 2001, **414**, 332–337, doi: 10.1038/35104599.
2. *Renewables 2020*. Paris : OECD, 2020, doi: 10.1787/c74616c1-en.
3. KOHN, S., WEHLAGE, D., JUHÁSZ JUNGER, I., EHRMANN, A. Electrospinning a dye-sensitized solar cell. *Catalysts*, 2019, **9**(12), 1–9, doi: 10.3390/catal9120975.
4. O'REGAN, B., GRÄTZEL, M. A low-cost, high-efficiency solar cell based on dye-sensitized colloidal TiO_2 films. *Nature*, 1991, **353**, 737–740, doi: 10.1038/353737a0.
5. MUÑOZ-GARCÍA, A.B., BENESPERI, I., BOSCHLOO, G., CONCEPCION, J.J., DELCAMP, J.H., GIBSON, E.A., MEYER, G.J., PAVONE, M., PETTERSSON, H., HAGFELDT, A., et al. Dye-

sensitized solar cells strike back. *Chemical Society Reviews*, 2021, **50**(22), 12450–12550, doi: 10.1039/D0CS01336F.

6. SCHODEN, F., DOTTER, M., KNEFELKAMP, D., BLACHOWICZ, T., SCHWENZFEIER HELLKAMP, E. Review of state of the art recycling methods in the context of dye sensitized solar cells. *Energies*, 2021, **14**(13), 1–12, doi: 10.3390/en14133741.
7. EHRMANN, A., BLACHOWICZ, T. Recent coating materials for textile-based solar cells. *AIMS Materials Science*, 2019, **6**(2), 234–251, doi: 10.3934/matersci.2019.2.234.
8. GOSSEN, K., DOTTER, M., BROCKHAGEN, B., STORCK, J.L., EHRMANN, A. Long-term investigation of unsealed DSSCs with glycerol-based electrolytes of different compositions. *AIMS Materials Science*, 2022, **9**(2), 283–296, doi: 10.3934/matersci.2022017.
9. STORCK, J.L., DOTTER, M., BROCKHAGEN, B., GROTHE, T. Evaluation of novel glycerol/PEO gel polymer electrolytes for non-toxic dye-sensitized solar cells with natural dyes regarding long-term stability and reproducibility. *Crystals*, 2020, **10**(12), 1–15, doi: 10.3390/cryst10121158.
10. DOTTER, M., STORCK, J.L., SURJAWIDJAJA, M., ADABRA, S., GROTHE, T. Investigation of the long-term stability of different polymers and their blends with PEO to produce gel polymer electrolytes for non-toxic dye-sensitized solar cells. *Applied Sciences*, 2021, **11**(13), 1–14, doi: 10.3390/app11135834.
11. GROTHE, T., STORCK, J.L., DOTTER, M., EHRMANN, A. Impact of solid content in the electrospinning solution on the physical and chemical properties of polyacrylonitrile (PAN) nanofibrous mats. *Tekstilec*, 2020, **63**(3), 225–232, doi: 10.14502/Tekstilec2020.63.225-232.
12. MAMUN, A., TRABELSI, M., KLÖCKER, M., SABANTINA, L., GROßERHODE, C., BLACHOWICZ, T., GRÖTSCH, G., CORNELIßEN, C., STREITENBERGER, A., EHRMANN, A. Electrospun nanofiber mats with embedded non-sintered TiO$_2$ for dye-sensitized solar cells (DSSCs). *Fibers*, 2019, **7**(7), 1–10, doi: 10.3390/fib7070060.
13. JUHÁSZ JUNGER, I., GROSSERHODE, C., STORCK, J.L., KOHN, S., GRETHE, T., GRASSMANN, C., SCHWARZ-PFEIFFER, A., GRIMMELSMANN, N., MEISSNER, H., BLACHOWICZ, T., et al. Influence of graphite-coating methods on the DSSC performance. *Optik*, 2018, **174**, 40–45, doi: 10.1016/j.ijleo.2018.08.041.
14. UDOMRUNGKHAJORNCHAI, S., JUNGER, I.J., EHRMANN, A. Optimization of the TiO$_2$ layer in DSSCs by a nonionic surfactant. *Optik*, 2020, **203**, 163945, doi: 10.1016/j.ijleo.2019.163945.
15. GROTHE, T., WEHLAGE, D., BÖHM, T., REMCHE, A., EHRMANN, A. Needleless Electrospinning of PAN Nanofibre Mats. *Tekstilec*, 2017, **60**(4), 290–295, doi: 10.14502/Tekstilec2017.60.290-295.
16. STORCK, J.L., GROTHE, T., MAMUN, A., SABANTINA, L., KLÖCKER, M., BLACHOWICZ, T., EHRMANN, A. Orientation of electrospun magnetic nanofibers near conductive areas. *Materials*, 2019, **13**(1), 1–14, doi: 10.3390/ma13010047.
17. LEE, S., KIM, J., KU, B.-C., KIM, J., JOH, H.-I. Structural evolution of polyacrylonitrile fibers in stabilization and carbonization. *Advances in Chemical Engineering and Science*, 2012, **2**(2), 275–282, doi: 10.4236/aces.2012.22032.
18. KIM, H.M., CHAE, W.-P., CHANG, K.-W., CHUN, S., KIM, S., JEONG, Y., KANG, I.-K. Composite nanofiber mats consisting of hydroxyapatite and titania for biomedical applications. *Journal of Biomedical Materials Research Part B: Applied Biomaterials*, 2010, **94B**(2), 380–387, doi: 10.1002/jbm.b.31664.
19. ALARIFI, I.M., ALHARBI, A., KHAN, W.S., SWINDLE, A., ASMATULU, R. Thermal, electrical and surface hydrophobic properties of electrospun polyacrylonitrile nanofibers for structural health monitoring. *Materials*, 2015, **8**(10), 7017–7031, doi: 10.3390/ma8105356.
20. GOLSHAN, M., OSFOURI, S., AZIN, R., JALALI, T., MOHEIMANI, N.R. Efficiency and stability improvement of natural dye-sensitized solar cells using the electrospun composite of TiO$_2$ nanofibres doped by the bio-Ca nanoparticles. *International Journal of Energy Research*, 2022, **46**(11), 15407–15418, doi: 10.1002/er.8242.
21. AL-ALWANI, M.A.M., AL-MASHAAN, A.B.S.A., ABDULLAH, M.F. Performance of the dye-sensitized solar cells fabricated using natural dyes from *Ixora coccinea* flowers and *Cymbopogon schoenanthus* leaves as sensitizers. *International Journal of Energy Research*, 2019, **43**(13), 7229–7239, doi: 10.1002/er.4747.
22. PRABAVATHY, N., SHALINI, S., BALASUNDARAPRABHU, R., VELAUTHAPILLAI, D.,

PRASANNA, S., BALAJI, G., MUTHUKUMARASAMY, N. Algal buffer layers for enhancing the efficiency of anthocyanins extracted from rose petals for natural dye-sensitized solar cell (DSSC). *International Journal of Energy Research*, 2018, **42**(2), 790–801, doi: 10.1002/er.3866.

23. EKPUNOBI, U.E., OGBUEFI, S.I., EKPUNOBI, A.J. Dye pH effect on photoelectric parameters of natural photosensitizer pigment extracted from *Alstonia boonei* for dye-sensitized solar cells. *International Journal of Energy Research*, 2022, **46**(2), 1922–1933, doi: 10.1002/er.7307.
24. NIEN, Y.-H., WU, Y.-T., CHOU, J.-C., YANG, P.-H., HO, C.-S., LAI, C.-H., KUO, P.-Y., SYU, R.-H., ZHUANG, S.-W., CHEN, P.-F. Photovoltaic performance of dye-sensitized solar cells under low illumination by modification of a photoanode with $ZnFe_2O_4/TiO_2$ nanofibers. *IEEE Transactions on Nanotechnology*, 2022, **21**, 606–612, doi: 10.1109/TNANO.2022.3213278.
25. STORCK, J.L., DOTTER, M., ADABRA, S., SURJAWIDJAJA, M., BROCKHAGEN, B., GROTHE, T. Long-term stability improvement of non-toxic dye-sensitized solar cells ia poly(ethylene oxide) gel electrolytes for future textile-based solar cells. *Polymers*, 2020, **12**(12), 1–15, doi: 10.3390/polym12123035.

Cihat Okan Arikan[1], Samet Doğan[2], Deja Muck[3]
[1] Ege Üniversitesi, Emel Akın Vocational School, 35100, Bornova/İzmir
[2] Ege University, Faculty of Engineering, Textile Engineering, Erzene, 35100 Bornova/İzmir
[3] University of Ljubljana, Faculty of Natural Sciences and Engineering, Department of Textiles, Graphic Arts, and Design, Snežniška 5, 1000 Ljubljana, Slovenia

Geometric Structures in Textile Design Made with 3D Printing

Geometrične strukture v tekstilnem oblikovanju, izdelane s 3-D tiskom

Original scientific article/*Izvirni znanstveni članek*

Received/*Prispelo* 11-2022 • Accepted/*Sprejeto* 12-2022

Corresponding author/*Korespondenčni avtor:*
Samet DOĞAN
E-mail: sametdogan1299@gmail.com
ORCID ID: 0000-0002-3988-6799

Abstract

3D printing is a well-known technology for producing 3D objects by depositing successive layers of material. Among its many applications, the fashion industry has taken advantage of this technology to revolutionize its brands. Due to the unique properties of textiles, such as comfort, flexibility, etc., attempts have been made to create textile-like structures. Structures with different geometries were designed and printed using different materials ranging from rigid to flexible. In this study, three different basic geometric structures were designed using the Blender program (a free open-source 3D modelling software). Each geometric structure was designed in two different sizes with smaller and larger basic structural elements. In this case, six different models were created. The aim of this study was to compare the textile-like surfaces of different basic geometric shapes produced with 3D printers. It also aimed to investigate the use of surfaces designed with basic geometric shapes in the textile-like material for fashion industries. In the production phase, the fused deposition modelling (FDM) process was chosen, and ABS and TPU materials were used. Various tests were performed, such as mass tests, and tensile and flexural strength tests on models with different basic geometric shapes and sizes. An examination of the test results showed that the different geometric shapes of the various basic structures and the different materials used have an overall effect on the final properties of the structures. It was concluded that the obtained results can be used as a reference and could be helpful for researchers in the use of 3D printers in the textile-like material and fashion material industries.

Keywords: 3D printing, geometric structures, textile-like material design

Izvleček

3-D tiskanje je že dobro poznana tehnologija za izdelavo 3-D objektov z nanosom zaporednih slojev materiala. Med številnimi aplikacijami je tudi modna industrija to tehnologijo izkoristila za revolucioniranje svojih blagovnih znamk. Zaradi edinstvenih lastnosti tekstilij, kot so udobje, fleksibilnost itd., se poskušajo ustvariti tekstilu podobne strukture. V raziskavi so bile oblikovane strukture z raznovrstnimi geometričnimi vzorci in natisnjene z uporabo različnih materialov, od togih do fleksibilnih. S programom Blender (odprtokodna programska oprema za 3-D modeliranje) so bile modelirane tri različne osnovne geometrične strukture. Vsaka geometrična struktura je bila zasnovana v dveh različnih *velikostih z manjšimi in večjimi osnovnimi konstrukcijskimi elementi. Tako je nastalo šest različnih modelov. Cilj študije je bil primerjati tekstilu podobne površine različnih osnovnih geometričnih oblik, izdelanih s 3-D tiskalniki. Prav tako študija želi raziskati uporabo površin, oblikovanih z osnovnimi geometrijskimi oblikami, v materialih za modno industrijo. Za izdelavo geometričnih struktur je bil izbran postopek modeliranja s spajanjem slojev (FDM) in uporabljena materiala ABS in TPU. Na modelih z različnimi geometričnimi oblikami in velikostmi so bile opravljene različne meritve, kot so meritve mase in meritve natezne in upogibne trdnosti. Analiza rezultatov testiranja je pokazala, da različne geometrijske oblike različnih osnovnih struktur in različni uporabljeni materiali močno vplivajo na končne lastnosti omenjenih struktur. Ocenjujemo, da so dobljeni rezultati lahko dobra referenca in pomoč raziskovalcem pri uporabi 3-D tiskalnikov na področju oblikovanja tekstilu podobnih materialov v modni industriji.*

Ključne besede: 3-D tisk, geometrične strukture, oblikovanje tekstilu podobnih materialov

1 Introduction

The use of computer technologies in the design stages of the textile sector, as well as the use of new materials and production methods in design, bring a new approach to the design creation process. Textile surface designs have been developed by using new developments in design and production areas and materials developed for different purposes. 3D printers are one of the innovative processes that are claimed to lead to the industry 4.0 revolution. 3D printers allow the production of objects without the use of tools [1]. Textile and apparel designs developed in recent years have been influenced by technology and all the developments in design and production and have been produced using many materials and techniques developed for different purposes [2].

Various 3D production methods can be used for printing textile-like materials in the fashion industry. The most preferred methods are SLA (stereo lithography), SLS (selective laser sintering), FDM (fused deposition modelling) and Polyjet 3D [3].

We focused primarily on FDM as the most frequently used technology, as we found many interesting articles about the aforementioned process. It has been shown that the choice of pattern and material affects the properties of material surfaces. This study showed that the larger the pattern, the harder the textile-like surface becomes (Figure 1). The size of a repeating pattern also has a significant impact on the printing time of the pattern. The smaller the pattern, the longer the printing process will take. The flexibility of the surface can also be affected by the number of layers and especially the number of connecting wires. The more connecting wires a structure contained, the harder the surface became (Figure 2 A–C), while the tensile strength of the structure increased. In this study, a good compromise between the flexibility, elasticity and tensile strength of the textile-like surface was identified with a compression model consisting of 11 layers (Figure 2C) [4].

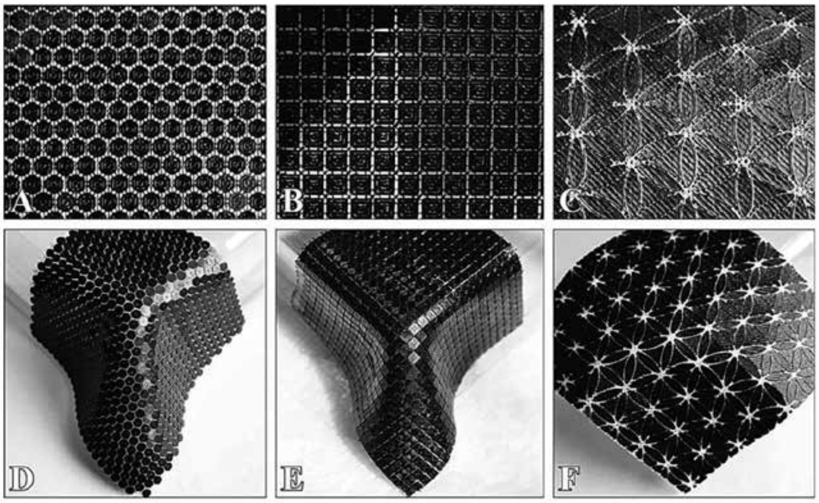

Figure 1: Illustration of various repeating patterns: A) polygon pattern, B) rectangle pattern, C) floral pattern, D) fabric-like curtain with polygon pattern, E) fabric-like curtain with rectangle pattern, F) curtain with large patterns [4]

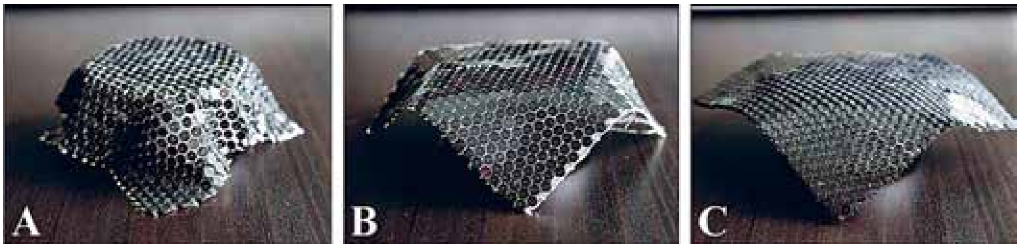

Figure 2: Different flexibilities based on the number of layers: A) five layers (three layers of PLA, two layers of LAY-FOMM 40), B) seven layers (four layers of PLA, three layers of LAY-FOMM 40), C) 11 layers (six layers of PLA, fives layers of LAY-FOMM 40) [4]

An important aspect of this work was to ensure the comfort of use of the textile-like surfaces. These properties can be achieved with the flexible and elastic printing material LAY-FOMM 40. Since LAY-FOMM 40 is harmless and food-safe according to the manufacturer, four layers of LAY-FOMM 40 are printed on each model (Figure 3). Basically, this is a printed lining layer that is also incorporated into conventional clothing. Special effects can be achieved by manually intervening in the Z-height of a layer during the printing process [4].

In collaboration with a PhD project at the University of Central Florida in Orlando, a glove with integrated sensors based on textile-like structures was printed (Figure 4). Sewing patterns were developed for the glove that are also used in the textile industry to produce garments (Figure 4A). It was printed using a X400 3D printer and PLA and LAY-FOMM 40 materials. As Figures 4B and 4C show, the surface of the glove was partially printed with polygons [4].

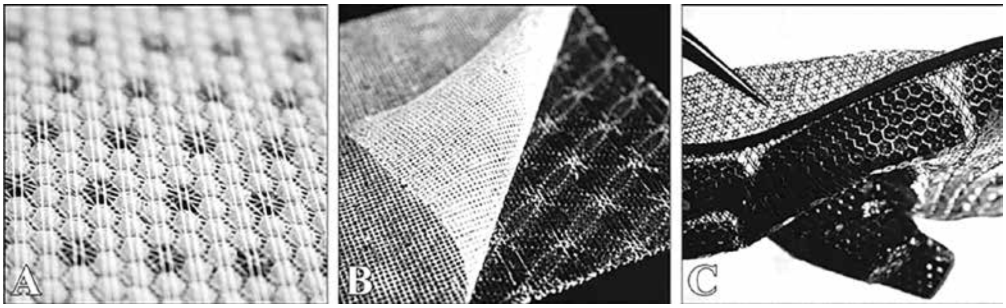

Figure 3: Printed lining: A) four layers of LAY-FOMM 40 on textile-like surface, B) and C) fusion of four layers[4]

Figure 4: 3D printed glove: A) sewing pattern printed from two materials, B) surface design of the glove, C) flexible sewing pattern with inner lining, D) pattern parts sewn together to form a three-dimensional garment [4]

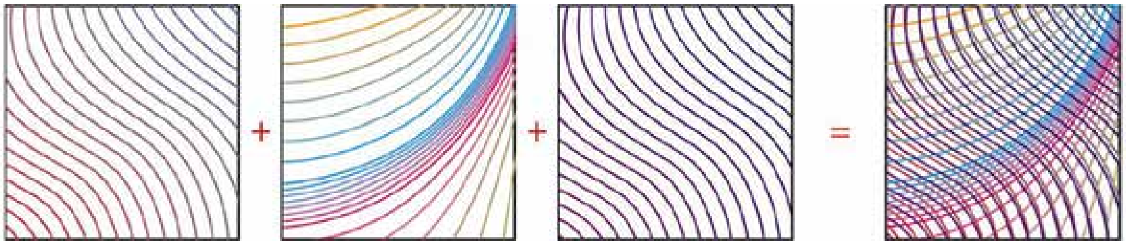

Figure 5: Test pattern for a layered structure consisting of three superimposed layers [5]

In the glove pattern, several layered structures were achieved using FDM technology [5]. Figure 5 shows a test structure used to investigate whether individual strings can be applied to relatively open structures without support structures [5].

The results of the FDM print in Figure 6 show that while this approach is mostly successful, the threads can sometimes break, even when a minimum diameter of 0.4 mm is maintained. Therefore, lace-like structures were created that also start with a partially open base layer but do not contain free-floating regions as the next approach to creating textile-based 3D printed patterns [5].

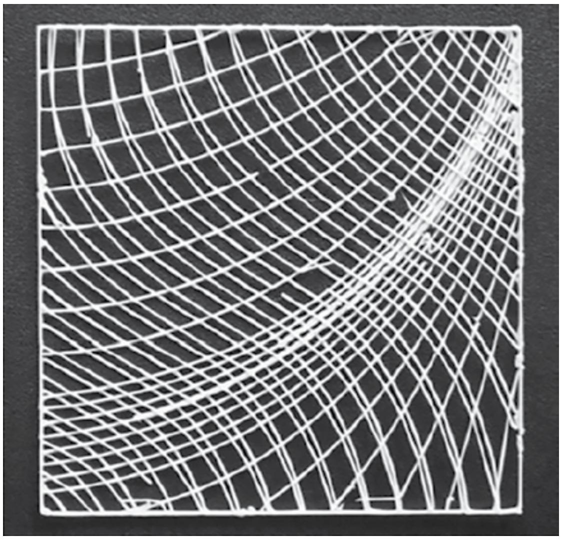

Figure 6: Results of the 3-layer structure printed using FDM (size 8 cm × 8 cm) [5]

Based on the well-known Plauen lace, lace patterns were designed, usually containing floral and circular elements on a base layer connecting these parts. One such pattern is shown in Figure 7a. Since there are no free-floating areas, printing using the FDM process is not problematic if all connecting lines have a sufficiently large diameter (Figure 7b) [5].

In addition to soft PLA, which was used for most of the lace patterns to avoid potential mechanical problems with harder material that could cause base joints to break, an experimental polymer was used: Lay Tekkks, one of four different types of porous filament from the PORO-Lay line. Lay Tekkks is a hard filament manufactured by Kai Parthy of CC-Products (Cologne, Germany) that can be transported to the nozzle without the transport problems that too-soft filaments can cause in some FDM printers. However, after printing is complete, it can be placed in warm water for a period of minutes to hours, which causes the hard part of the material to dissolve. The resulting sample thus becomes increasingly softer the longer it is immersed in water (Figure 8) [5].

a) b)

Figure 7: Multi-layer lace pattern shown in 'netfabb' (a), and the resulting 3D print (b). Detail size ~ 4 cm × 7 cm [5]

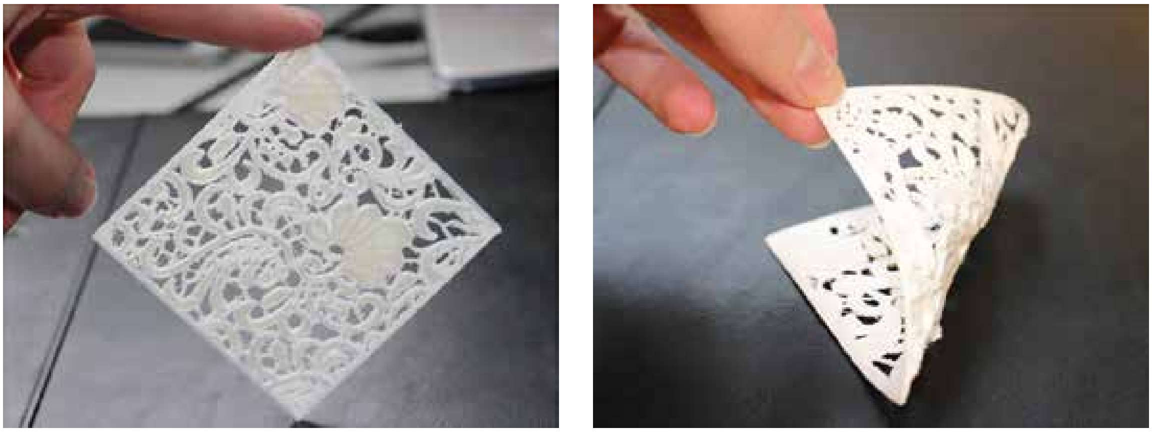

a) b)

Figure 8: Lace pattern from Lay Teks before (a) and after dissolving the hard material in warm water for three hours (b). The size of the pattern is 8 cm × 8 cm [5]

The aim of this study was to print textile-like surfaces with different geometric structures using 3D printing technologies based on thermoplastic extrusion. A fused deposition modelling (FDM) was used as the 3D production method. In this study, 6 different models were designed using 3 different basic geometric structures. These are small size hole square, large size hole square, small size hole triangle, large size hole triangle, small size hole hexagon, large size hole hexagon. All of the modeled samples were printed in the same size. Only the hole sizes and shapes of the models were different. These 6 different models were printed with ABS and TPU material. Three different tests were applied to total 72 samples. The effects of these basic geometric shapes on textile-like surfaces were investigated using mass, tensile and flexural strength measurements. In the study, it was also investigated which basic geometric shape is more useful and flexible in textile-like materials; which basic geometric structure could be more durable and what could affect the test results; and which thermoplastic material and basic geometrical structure can exhibit properties like a textile-like fabric.

2 Materials and methods

2.1 Sample preparation

2.1.1 ABS and TPU

ABS (also known as acrylonitrile-butadiene-styrene) has high hardness, good impact strength even at low temperatures, good insulating properties, good wear and tensile strength, high dimensional stability, and high surface gloss [6, 7].

Thermoplastic polyurethane (TPU) is a melt-processable thermoplastic elastomer with high durability and flexibility. TPU offers a wide range of physical and chemical property combinations for the most demanding applications, e.g., automotive, wire and cable, breathable films for leisure, sports and textile coatings, wearable non-yellowing films, etc. Its properties are between the characteristics of plastic and rubber. Thanks to its thermoplastic characteristic, it has several advantages that other elastomers cannot offer, such as excellent tensile strength, high elongation at break and good load-bearing capacity [8, 9].

2.1.2 Modelling of geometric structures

In this study, textile-like surfaces were printed based on three different basic geometric shapes: square, triangle and hexagon.

2.1.3 Printing

The printed models in this project were made using a Zmorph FAB 3D printer (Zmorph, Poland) (Figure 9), which uses the fused deposition modelling process. This high-quality semi-professional 3D printer processes thermoplastic filaments by melting them in the extruder immediately before printing. The maximum operating temperature at the extruder tip is 260 °C, while the maximum extrusion volume is 40 mm/s. The maximum working volume of the printer is 235 mm ×250 mm ×165 mm. The printer uses Voxelizer printing software. A file in Voxelizer format is transferred to the printer via a

USB memory stick or Wi-Fi. FDM is a process based on the formation of a new layer on another layer by melting the fibrous thermoplastic material.

The printing material used in this project was an ABS (acrylonitrile butadiene styrene) filament (AzureFilm, Slovenia), which is a lightweight, high-impact and high-creep polymer [10]. TPU (thermoplastic polyurethane) (AzureFilm, Slovenia) with high tensile strength was also used.

This system is based on the principle of extruding molten plastic from a heated injector onto a heated moving bed [11]. To obtain the model after printing from the pressure bed, the temperature of the bed must be lowered to a minimum temperature of 30 °C degrees.

The parameters used to print the models in this study on the Zmorph 3D printer are shown in Table 1 for ABS material and Table 2 for TPU material.

Figure 9: Photo during printing

Table 1: Printing parameters for printing with ABS material

Settings	Value
Extruder settings	
Default print speed	24 mm/s
Travel speed	90 mm/s
Layer settings	
First layer speed	40%
First layer height	0.42 mm
Maximum adhesion ratio	2.5
Height minimum multiplier	0.4
Height maximum multiplier	0.75
Temperature	
Hotbed temperature	100 °C
Extruder temperature	255 °C
Fan speed	40%
Other	
Filament diameter	1.75 mm
Extrusion diameter	m

Table 2: Printing parameters for printing with TPU material

Settings	Value
Extruder settings	
Default print speed	20 mm/s
Travel speed	120 mm/s
Layer settings	
First layer speed	100 %
First layer height	0.25 mm
Maximum adhesion ratio	2.25
Height minimum multiplier	0.3
Height maximum multiplier	0.85
Temperature	
Hotbed temperature	60 °C
Extruder temperature	250 °C
Fan speed	30 %
Other	
Filament diameter	1.75 mm
Extrusion diameter	m

2.1.4 Software

The models created in this study were modelled using the 3D Blender program. The modelled patterns are saved as *.stl files and transferred to the Voxelizer software for 3D printing. A *.stl file is easy to use for printing with this program. A G-code file is also created to transfer the models to the printer with the Voxelizer program for special head and print movements.

2.1.5 Models printed with ABS and TPU

To ensure the comparability of the test results, the sizes of the models were designed in basic geometric shapes that were most similar to each other. The models were designed on the basis of the dimensions 50 mm × 150 mm × 2 mm, so that they could be easily tested in a tensile and bending testing machine. The width of the lines forming the geometric shapes was 0.8 mm.

2.2 Samples

Sample 1

(a) Small size hole square

The width of all lines forming the figures in the patterns was 0.8 mm. The dimensions of this pattern, created in the form of small squares of horizontal and vertical lines, were 49.4 mm × 151.42 mm × 2 mm. The inner dimension of each square was 4.5 mm × 4.5 mm. A real, printed 'small size hole square' example is shown in Figure 10, while the 3D model drawing made using Blender software is shown in Figure 11.

(b) Large size hole square

The size of this model was 49.4 mm × 153.9 mm × 2 mm. However, in this example, the dimensions of the square holes were larger than in the previous model. In this model, the x and y length of the inner square was 8.8 mm × 8.8 mm. A real 'large size hole square' example is shown in Figure 12, while a 3D model drawing made using Blender software is shown in Figure 13.

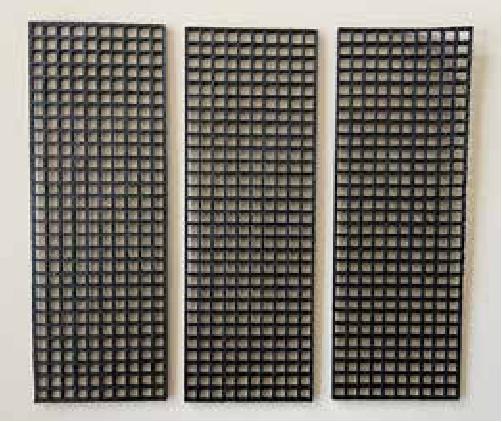

Figure 10: Structures printed with ABS small size hole square

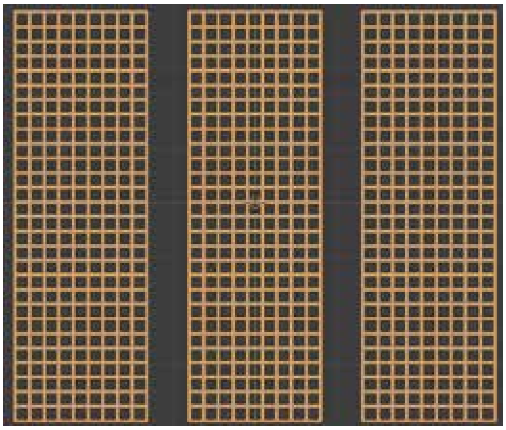

Figure 11: Screenshot of the 3D modelled square structure with small holes in Blender software

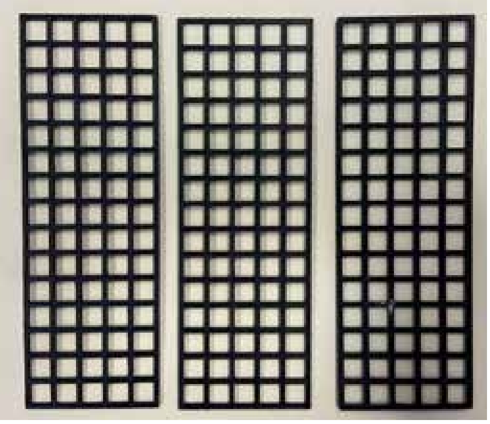

Figure 12: Structure printed with ABS large size hole square

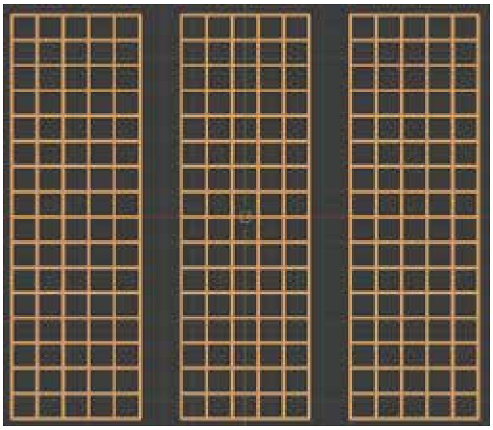

Figure 13: Screenshot of the 3D modelled large size hole square structure in Blender software.

Sample 2

(a) Small size hole triangle

In this model, small triangles with only one diagonal were formed on the small squares of the first example (Figure 14). The dimensions of this model were 49.4 mm × 151.2 mm × 2 mm. The 3D model prepared using Blender software is shown at Figure 15.

(b) Large size hole triangle

The size of this model was 49.4 mm × 153.9 mm × 2 mm. This model is similar to the small size hole triangle model. The model size was made larger and is shown in Figure 16, while 3D the drawing model using Blender software is shown in Figure 17, The difference in size and triangular area was obtained by adding a diagonal to each square.

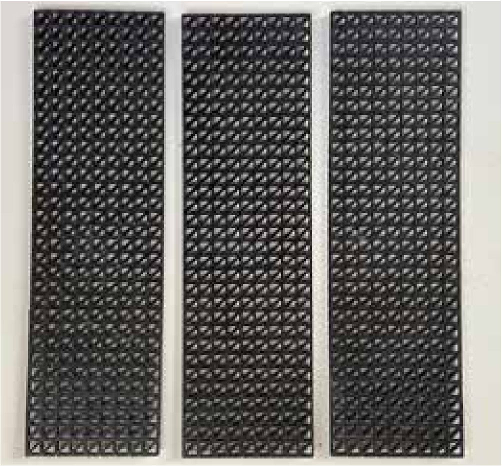

Figure 14: Structure printed with ABS small size hole triangle

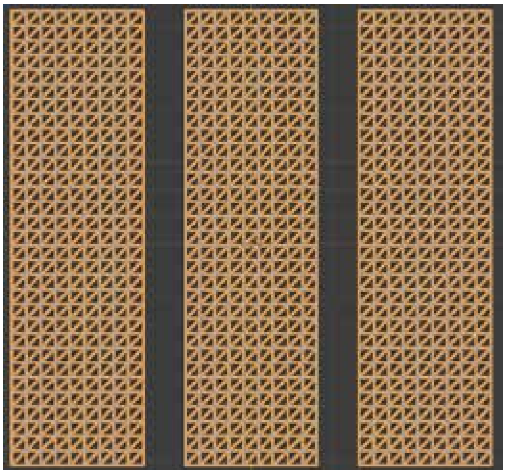

Figure 15: Screenshot of the 3D modelled small size hole triangle structure in Blender software

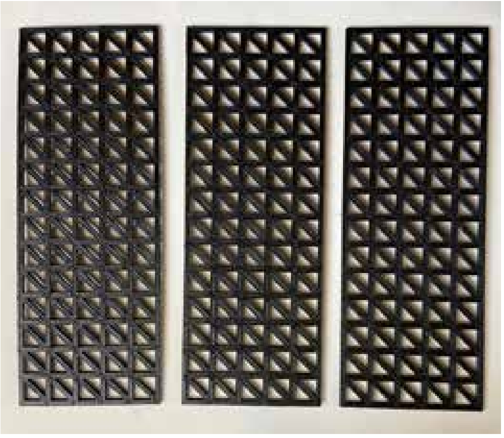

Figure 16: Structure printed with ABS large size hole triangle

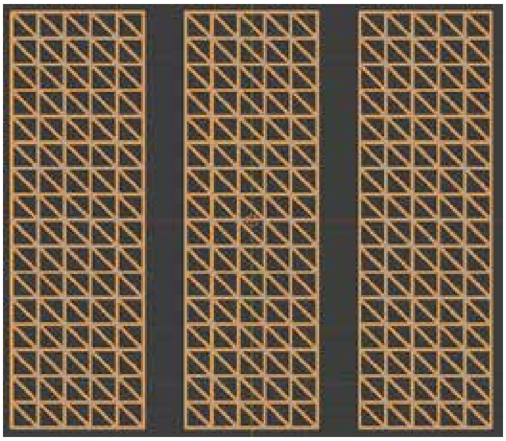

Figure 17: Screenshot of the 3D modelled large size hole triangle structure in Blender CAD software

Sample 3

(a) Small size hole hexagon

This model had a large diagonal dimension of 6.11 mm. The dimensions of this model were 51.8 mm × 147.7 mm × 2 mm. The real structure is shown in Figure 18, while the 3D model prepared using Blender software is shown in Figure 19.

(b) Large size hole hexagon

This model was designed with large hexagonal shapes with a large diagonal length of 12.22 mm. The dimensions of this model were 54.7 mm × 150.7 mm × 2 mm. This is similar to the small size hole hexagon model, but with larger sized holes. The real structure is shown in Figure 20, while the 3D model prepared using Blender software is shown in Figure 21.

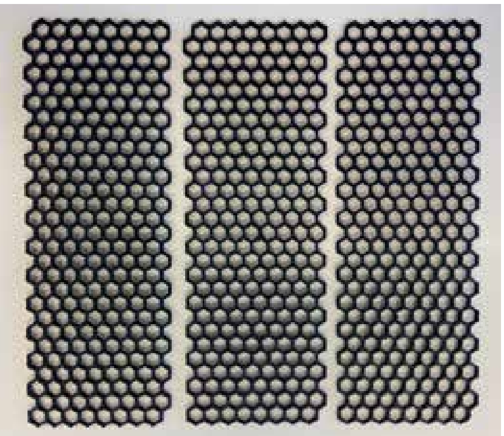

Figure 18: Structure printed with ABS small size hole hexagonal

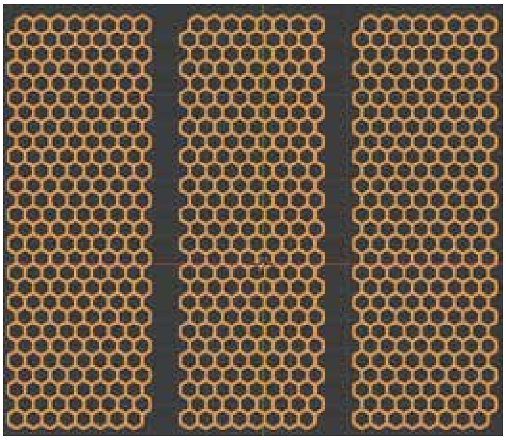

Figure 19: Screenshot of the 3D modelled small size hole hexagonal structure in Blender software

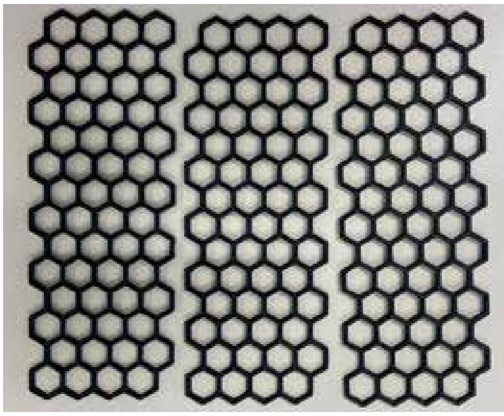

Figure 20: Structure printed with ABS large size hole hexagonal

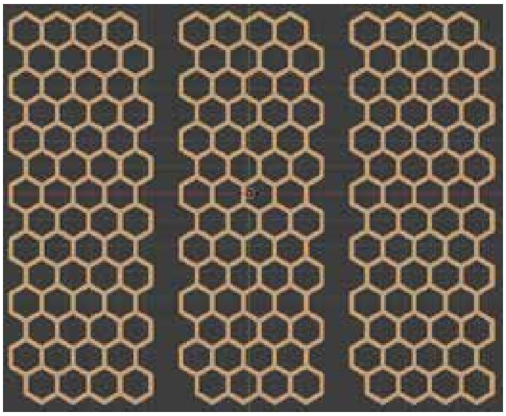

Figure 21: Screenshot of the 3D modelled large size hole hexagonal structure in Blender software

2.3 Methods

A mass of samples that were designed in similar dimensions was tested to understand effects of printed ABS and TPU materials in six different ways. The mass of the samples was measured with precision balance Mettler Toledo AE 200.

Mechanical properties have been tested on a dynamometer Instron 5567 (Instron, GB) (Figure 22a). The distance between the clamps was 5 cm. Tensile test applied to the samples with six different textile-like surfaces with three different basic geometric structures produced using ABS and TPU materials to investigate which basic geometric surface and which material would be more suitable for textile-like materials in the fashion industry. This test was performed to measure the wearability of a fabric or surface.

The aim of the flexural strength (Figure 22b) test was to examine the drape on the human body when a textile-like surface is worn. In this test, six different samples were printed with ABS and TPU materials using three different basic geometric patterns, followed by the relevant research.

While applying these tests, the dimensions of specimens of 150 mm × 50 mm × 2 mm were accepted as adequate for testing on the dynamometer. Therefore, all samples were designed to be closest to these dimensions. Laboratory values of ambient temperature was 23 °C ± 2 °C and relative humidity of 45% ± 10%. Measurements were made according to the ISO 13934-1 test standard.

3 Results and discussion

In this study, mass, tensile stress and flexural strength of samples with different geometric surfaces produced in the same dimensions with ABS and TPU materials was analyzed, compared and interpreted.

a) *b)*

Figure 22: Photos of a) tensile test and b) flexural test

72 printed textile-like surfaces were obtained from 12 different models for tensile strength testing. The obtained surfaces were compared in two different ways with different geometric surfaces and different materials.

3.1 Production times of models and mass measurement results

For all 3D-printed geometric structures presented, the manufacturing time and mass of the structures were first analyzed.

Table 3 shows that the printing times of the designed models vary depending on the model and material. This is because ABS and TPU materials have different printing parameters. For this reason, an exact comparison of the printing times is not possible.

Table 4 and Figure 23 clearly show that all models printed with TPU are heavier than those printed with ABS. Although the models with TPU and ABS materials are all made in the same dimensions, the reason why the models printed with TPU are heavier is that TPU and ABS materials have different specific densities. TPU material has a higher spe-

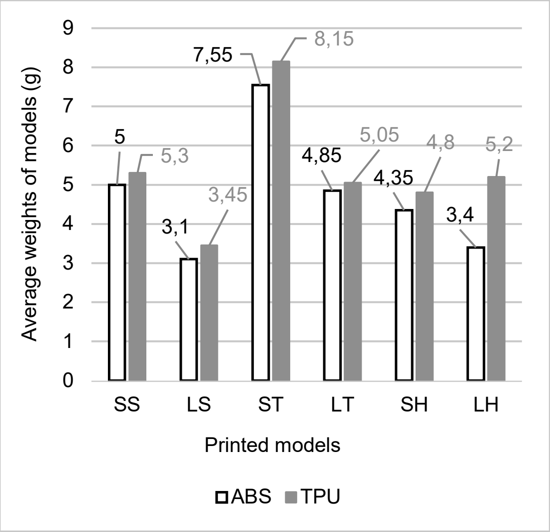

Figure 23: Average mass of models

Table 3: Production times of models

Geometric structure	Marked as	Production time with ABS (min)	Production time with TPU (min)
Small size hole square	SS	173	141
Large size hole square	LS	77	87
Small size hole triangle	ST	111	306
Large size hole triangle	LT	163	139
Small size hole hexagon	SH	164	126
Large size hole hexagon	LH	99	129

Table 4: Average weight of models

Geometric structure	Average weight and STDV of ABS models (g)	Average weight and STDV of TPU models (g)
SS	5.0 ± 0.21	5.3 ± 0.20
LS	3.1 ± 0.25	3.45 ± 0.21
ST	7.55 ± 0.28	8.15 ± 0.17
LT	4.85 ± 0.23	5.05 ± 0.20
SH	4.35 ± 0.27	4.8 ± 0.04
LH	3.4 ± 0.19	5.2 ± 0.26

cific gravity than ABS material. The density of TPU material is 1.15–1.17 g/cm^3, while the density of ABS material is 1.03–1.10 g/cm^3 [12, 13].

It is clearly seen that the large size hole square is the lightest and the small size hole triangle is the heaviest of samples produced using both materials.

Mass determination results provide important information on many performance properties, such as the strength, density, and softness of the material. At the same time, mass determination tests provide information about the density of textile surfaces [14].

3.2 Tensile strength test results

Maximum force applied to the samples, percentage of tensile strain (displacement) at maximum force and amount of displacement at maximum force are given in the Table 5 and 6, and Figures 24–26.

The tensile stress test results of six different samples printed with TPU material and created based on three different basic geometric patterns clearly shows that under maximum strength, hexagonal structure specimens have higher tensile stress performance than specimens produced in other structures. This is the same for hexagonal structures produced using both TPU and ABS materials. Since TPU material is more flexible than ABS material, the displacement percentages of the samples produced using TPU material under maximum force are quite high compared to ABS material. In the samples produced using TPU material, the highest displacement percentage was 317.53% under maximum force, while the highest value was obtained for ABS material, at 6.212%.

The displacement of the specimens at maximum force, tensile strain (displacement) at maximum force and maximum force at tensile stress were measured in this test. The speed of the measuring device was 025 mm/s.

Tensile strength results vary according to materials and sample structures. Since the material and basic geometric surface structure were investigated in this study, the samples were produced in the same dimensions and on the same model surfaces. The test results clearly show that the tensile stress (displacement) of TPU material at maximum strength demonstrated much higher values than ABS material.

Moreover, Figure 26 shows that the maximum force applied to ABS material is much higher than the maximum force applied to TPU material, since ABS material is much less flexible than TPU material.

Comparison of tensile strength results of samples with basic geometric structures produced using ABS material: LH > SH > ST > SS > LS > LT (Table 5).

Comparison of tensile strength results of samples with basic geometric structures produced using TPU material: LH > ST > SH > SS > LT > LS (Table 6).

It is clear that the hexagonal specimens have the highest tensile strength at both materials.

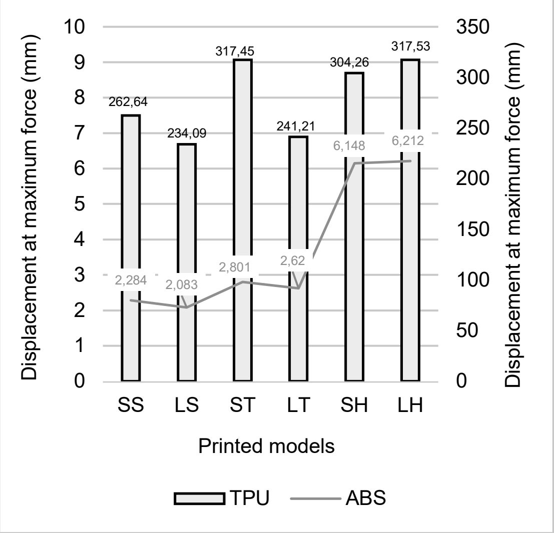

Figure 24: Displacement at maximum force

Table 5: Tensile strain test results applied to models produced using ABS

ABS models	Maximum force (N)	Tensile strain (displacement) at maximum force (%)	Displacement at maximum force (mm)
SS	674.858 ± 35.448	4.569 ± 0.704	2.284 ± 0.352
LS	435.340 ± 35.922	4.165 ± 0.407	2.083 ± 0.204
ST	766.462 ± 17.023	5.601 ± 0.402	2.801 ± 0.201
LT	437.367 ± 15.954	4.125 ± 0.448	2.062 ± 0.224
SH	310.827 ± 6.015	12.296 ± 1.824	6.148 ± 0.912
LH	194.244 ± 12.765	12.424 ± 1.872	6.212 ± 0.936

Table 6: Tensile strain test results applied to models produced using TPU

TPU models	Maximum force (N)	Tensile strain (displacement) at maximum force (%)	Displacement at maximum force (mm)
SS	382.696 ± 10.966	525.280 ± 10.448	262.640 ± 5.224
LS	231.116 ± 37.769	468.180 ± 76.292	234.090 ± 38.146
ST	556.948 ± 54.403	601.900 ± 69.924	300.450 ± 34.962
LT	273.418 ± 34.962	482.420 ± 4.052	241.210 ± 2.026
SH	331.192 ± 7.305	608.520 ± 25.904	304.260 ± 12.952
LH	355.691 ± 25.423	635.060 ± 16.080	317.530 ± 8.040

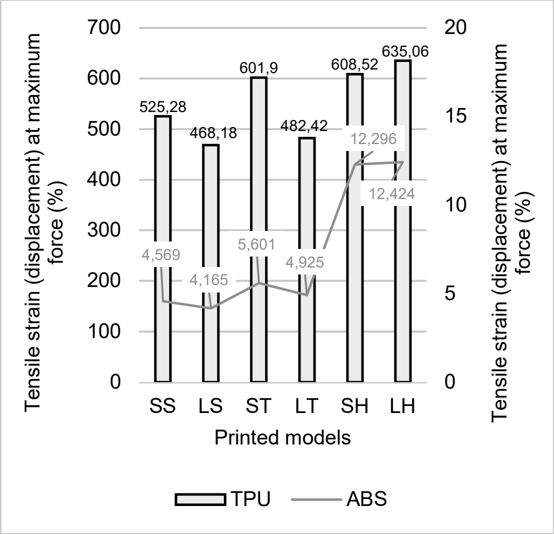

Figure 25: Tensile strain (displacement) at maximum force

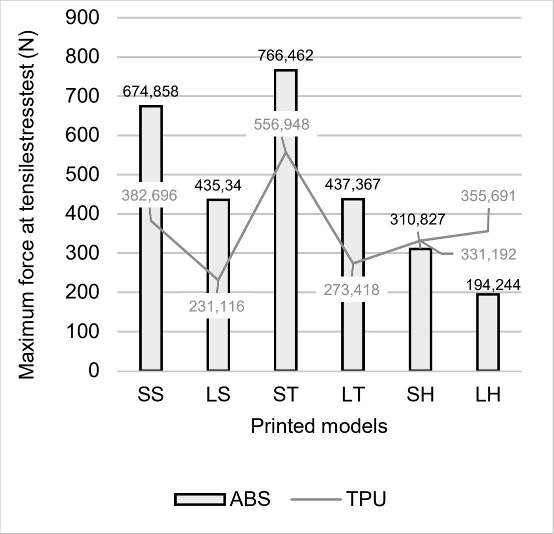

Figure 26: Maximum force at tensile stress test

Textile-like surfaces produced using different geometric shapes
According to Tables 5 and 6, the smaller the repeating pattern units on printed textile-like surfaces, the higher the tensile strength and vice versa: the larger the pattern, the harder the textile-like surface produced. If the patterns were printed in small repeat units, the mass of the models increased (Table 4). As a result of the tests conducted in this study, the order of tensile strength of different geometric models made with both ABS and TPU materials is as follows: SH > ST > SS, LH > LT>LS.
Tables 5 and 6 clearly show that textile-like surfaces printed with a hexagonal pattern have a much higher tensile strength.

Hexagons are ubiquitous in nature, from the largest planets to microscopic compounds. The reason for this prevalence, however, is not because hexagons have a special edge, but because the simplest shape that can be created in nature is the circle, and flexible circles spontaneously transform into hexagons under pressure. From honeycombs to giant clouds on planets, from geological formations to snowflakes, every hexagon can be illuminated using purely scientific explanations. For millennia, scientists and philosophers thought the hexagon was the shape that would most efficiently fill a plane. However, this idea was discussed earlier. Moreover, at the end of the 19th century, the Belgian physicist Joseph Plateau was able to calculate that the forces on 120-degree foils are all in equilibrium and that this geometry is the most mechanically stable arrangement [15].

3.3 Flexural strength test results

Flexural strength test results are given in Tables 7 and 8, and on Figures 27–29.

TPU material has a higher flexibility than ABS material. For this reason, Figure 28 clearly shows that TPU material requires much less force to bend than ABS material.

When evaluating the flexural strength of models made using the two different materials, no direct correlation can be established between the flexural strengths of different shapes.

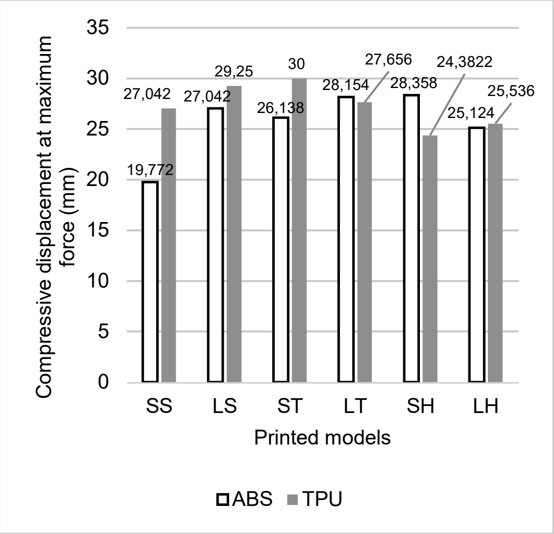

Figure 27: Compressive displacement at maximum force

Table 7: Flexural strength test results applied to models produced using ABS material

Models of ABS	Maximum force (N)	Compressive displacement at maximum force (mm)	Force at break (Standard) (N)
SS	9.112 ± 0.19	24.208 ± 2.24	8.364 ± 0.28
LS	5.341 ± 0.17	27.042 ± 3.96	5.140 ± 0.31
ST	12.743 ± 0.53	26.138 ± 2.83	11.933 ± 0.68
LT	8.386 ± 0.42	28.154 ± 0.72	7.438 ± 0.37
SH	5.744 ± 0.15	28.358 ± 3.84	5.297 ± 0.16
LH	4.786 ± 0.10	25.124 ± 1.09	4.537 ± 0.23

Table 8: Flexural strength test results applied to models produced using TPU material

Models of TPU	Maximum force (N)	Compressive displacement at Maximum Force (mm)	Force at break (Standard) (N)
SS	0.185 ± 0.01	27.042 ± 3.07	0.159 ± 0.01
LS	0.135 ± 0.01	29.250 ± 1.47	0.119 ± 0.00
ST	0.274 ± 0.01	30.000 ± 3.86	0.272 ± 0.03
LT	0.141 ± 0.00	27.656 ± 2.46	0.125 ± 0.01
SH	0.109 ± 0.01	24.822 ± 1.86	0.100 ± 0.01
LH	0.133 ± 0.01	25.536 ± 2.03	0.118 ± 2.03

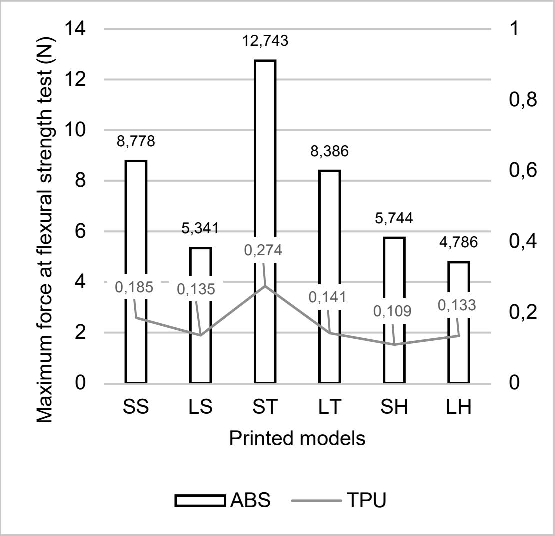

Figure 28: Maximum force at flexural strength test

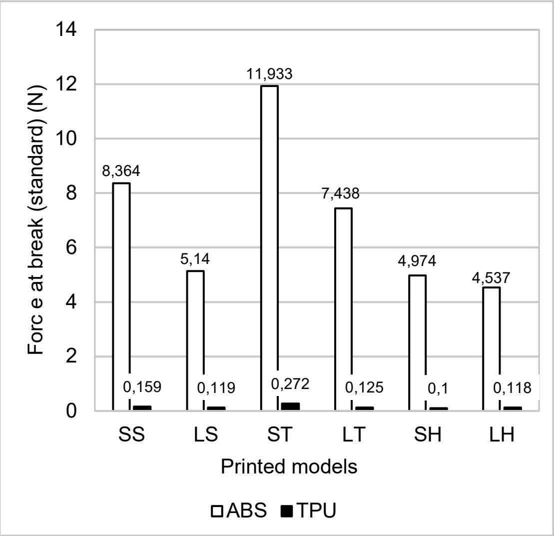

Figure 29: Force at break (standard)

4 Conclusion

3D printers are appearing in all aspects of our lives, including the textile and fashion industries. 3D printers, which have the potential to facilitate personalized production, are gaining momentum as the technology evolves. Manufacturing with 3D printers is an alternative to traditional manufacturing methods.

Defined as the manufacturing method of the 21st century, 3D printers allow the body to be wrapped like fabric, weaving together different shapes in different sizes. Textile designers can work with this technology as an alternative working method instead of traditional production methods.

For this article, six different patterns were designed using three different basic geometric shapes. A total of 72 patterns were made using six different models with two different materials. These patterns were subjected to mass, tensile strength and flexural strength tests. From the results of the tensile strength tests, it was determined that different geometric shapes affect tensile strength. Hexagonal structures have high values, while square structures have lower values. The hexagonal structures showed the highest resistance to the force applied to them when the tensile stress test was performed. This is due to the fact that the hexagons, because of their angle of 120°, were able to equally resist the force applied by all arms. Different models have an impact on the comfort of the products used in the textile-like material in fashion industries. The result in this case was that the hexagonal structures are more comfortable than others.

The results show that the tensile strength of TPU material is much higher than that of ABS material. In addition, textile-like surfaces made using TPU material have more flexibility and drape than textile-like surfaces made using ABS material.

Textile-like surfaces printed using TPU material have a softer feel than those made using ABS material. Therefore, textile-like surfaces made using TPU material are more suitable in terms of wearability. ABS material's hard handling, lower flexibility, and lack of drapability limit its use in the material in fashion industries.

However, ABS material can be used in the manufacture of accessories as an alternative material for the textile material and fashion industries, such as buckles, crown buttons, zippers, walking sticks, umbrella bags, fans, watch straps, etc.

The order of bending strength of the models made using ABS material according to their values under compression displacement at maximum force was as follows: shapes with small holes and shapes with large holes; triangle with small holes > square with small holes > hexagon with small holes, square with large holes > triangle with large holes > hexagon with large holes.

The order of bending strength of the models made using TPU material according to their values under compression displacement at maximum force was as follows: shapes with small holes and shapes with large holes; triangle with small holes > square with small holes > hexagon with small holes, square with large holes > triangle with large holes > hexagon with large holes.

No conclusion could be drawn from the results of the applied flexural strength tests, since the impact of shapes on flexural strength was not stable. However, comparing two different materials, the difference between the maximum forces can be clearly seen. According to the results of the bending strength test, we can conclude that the properties of the materials impact these test results rather than the moulds.

It can be seen from this study that, in the production of a wearable textile-like surface using 3D printers, the geometric shape of the unit patterns that form the surface and the size of the unit patterns affect the properties of the textile-like surface. In this study, three basic geometric shapes and two different materials (ABS and TPU) were used. It is therefore likely that the data from this study can serve as a reference for new studies when a textile-like surface with a geometric unit pattern is to be obtained.

References

1. AVCI, G., EREN, O., SEZER, H.K. Tekstil sektörüne eklemeli imalat yaklaşımı: 3B yazıcılar ile deneysel çalışma . In *Uluslararası Bilim, Teknoloji Ve Sosyal Bilimlerde Güncel Gelişmeler Sempozyumu, Ankara, Turkey*, 2019, 411–419.
2. ERBIYIKLI, N. Art and science in terms of textile and fashion design [online]. DergiPark Akademik [accessed 14 December 2022]. Available on World Wide Web: <https://dergipark.org.tr/tr/download/article-file/275338>.
3. YILDIRAN, M. Moda giyim sektöründe üç boyutlu yazıcılarla tasarım ve üretim. *Art-e Sanat Dergisi*, 2016, **9**(17), 155–172.
4. UYSAL, R., STUBBS, J.B. A new method of printing multi-material textiles by fused deposition modelling (FDM). *Tekstilec*, 2019, **62**(4), 248–257, doi: 10.14502/Tekstilec2019.62.248-257.
5. MELNIKOVA, R., EHRMANN, A., FINSTERBUSCH, K. 3D printing of textile-based structures by Fused Deposition Modelling (FDM) with different polymer materials. *IOP Conference Series: Materials Science and Engineering*, 2014, **62**(1), 1–7, doi: 0.1088/1757-899X/62/1/012018.
6. Comprehensive guide on Acrylonitrile Butadiene Styrene (ABS) [online]. Omnexus [accessed 11 August 2022]. Available on World Wide Web: <https://omnexus.specialchem.com/selection-guide/acrylonitrile-butadiene-styrene-abs-plastic>.
7. FILAMEON ABS HighFlow Filament [online]. FILAMEON [accessed 11 August 2022]. Available on World Wide Web: <https://www.filameon.com/urun/filameon-abs-filament/>.
8. Comprehensive Guide on Thermoplastic Polyurethanes (TPU) [online]. Omnexus [accessed 11 August 2022]. Available on World Wide Web: <https://omnexus.specialchem.com/selection-guide/thermoplastic-polyurethanes-tpu>.
9. FILAMEON TPU Filament [online]. FILAMEON [accessed 11 August 2022]. Available on World Wide Web: < https://www.filameon.com/urun/filameon-tpu-filament/>.
10. PARTSCH, L., VASSILIADIS, S., PAPAGEORGAS, P. 3D printed textile fabrics structures. In *5th International Istanbul Textile Congress 2015: Innovative Technologies "Inspire to Innovate", September 11th-12th 2015, Istanbul, Turkey*, 1–7.
11. REISS, D. *Complex processes and 3D printing*: BSc project. London : Imperial Collage London, 2013, 1–15.
12. ABS Plus. Safety data sheet [online]. Azurefilm [accessed 11 July 2022]. Available on World Wide Web: <https://www.azurefilm.com/media/uploads/Tehni%C4%8Dni%20listi/ABS/ABS_Plus_SDS.pdf>.
13. OĞULATA, R.T., KADEM, F.D. Prediction of regression analyses of fabric tensile strength of 100% cotton fabrics with yarn dyed in different constructions. *Textile and Apparel*, 2008, **18**(3), 185–191.
14. Flexible 98A TDS [online]. Azurefilm [accessed 11 July 2022]. Available on World Wide Web: <https://www.azurefilm.com/media/uploads/Tehni%C4%8Dni%20listi/FLEXIBLE/Flexible_98A_TDS.pdf>.
15. Doğada Altıgen Geometri Neden Bu Kadar Yaygın? (Why ıs hexagonal geometry so common in nature?) [online]. Evrim Ağacı [accessed 12 July 2022]. Available on World Wide Web: <https://evrimagaci.org/dogada-altigen-geometri-neden-bu-kadar-yaygin-11666>.
16. ÖZGÜN, C.A. N., ARABACI, H. 3 boyutlu yazicilarin moda aksesuarlari üretiminde kullanilmasi (The usage of 3D printers in the production of fashion accessories). *International Journal of 3D Printing Technologies and Digital Industry*, 2021, **5**(3), 445–456.
17. BULAT, F. BAŞARAN, F.N. Tekstil tasariminda yenilikçi yaklaşimlar: 3B yazicilarla deneysel çalişmalar (Innovative approaches in textile design: experimental practices with 3D printers). *Kesit Akademi Dergisi*, 2018, **4**(15) , 257–273.

Gilbert De Mey[1], Ilda Kazani[2, 3], Majlinda Hylli[2], Pellumb Berberi[4]
[1] Department of Electronics and Information Systems, Ghent University, Technologiepark 126, 9052 Ghent, Belgium
[2] Department of Textile and Fashion, Polytechnic University of Tirana, Sheshi Nënë Tereza 1, Tirana, Albania
[3] Albanian Young Academy, Shëtitoria Murat Toptani 1000, Tirana, Albania
[4] Department of Engineering Physics, Polytechnic University of Tirana, Bulevard Dëshmorët e Kombit 4, Tirana, Albania

Influence of Humidity on the Electric Resistivity of Leather: Mathematical Modelling

Matematično modeliranje vpliva vlažnosti na električno upornost usnja

Short scientific article/*Kratki znanstveni prispevek*

Received/*Prispelo* 11-2022 • Accepted/*Sprejeto* 12-2022

Corresponding author/*Korespondenčna avtorica:*
Assoc Prof dr. Ilda Kazani
E-mail: ikazani@fim.edu.al
ORCID ID: 0000-0002-5727-5553

Abstract

A mathematical model is presented to simulate the electric resistivity of leather samples as a function of humidity. It will be shown that absolute and not relative humidity is the crucial parameter. The model assumes that the leather includes channels that can absorb water from the surrounding environment. This effect primarily determines the electric conductivity of the leather samples. The theoretical results from the model are quite closely in line with experimental measurements.

Keywords: electric resistivity, leather, humidity, modelling

Izvleček

Predstavljen je matematični model za simulacijo električne upornosti vzorcev usnja kot funkcije vlažnosti. Poudariti je treba, da je odločilni parameter absolutna in ne relativna zračna vlažnost. Model predvideva, da usnje vsebuje kanale (kapilare), ki lahko absorbirajo vodo iz okolice. Ta učinek predvsem določa električno prevodnost vzorcev usnja. Teoretični rezultati modela se dobro ujemajo z eksperimentalnimi meritvami.

Ključne besede: električna upornost, usnje, vlaga, modeliranje

1 Introduction

Due to 21st century technology, we must adapt to smart products offered by the market where tablets, computers, most mobile screens and smartwatches operate with a capacitive touch screen (finger-touch method) [1]. One practical application is the use of a touch screen when wearing leather gloves. These screens use the electric conductivity of the fingertip to increase the electric capacitance in a certain area of the screen. If gloves are worn, they should also be electrically conductive. It will be shown later that pure leather is a poor electric conductor. Leather will however, become conductive by absorbing water from ambient humid air or by diffusion from the finger. This is also true, depending on weather, climate or different conditions, where the finger-touch method is not possible and a conductive glove is very important [2–4].

Furthermore, the rapid growth of electrical and electronic devices and accessories that emit electromagnetic energy in different frequency bands has led to an increase in exposure to EM radiation, which can be harmful for human health. It was determined from literature that electrically conductive textiles are preferred for shielding applications primarily due to their good shielding properties and numerous advantages [5]. Although there are different studies about electromagnetic shielding textiles in literature, there is an urgent need to develop electromagnetic interference (EMI) shielding materials [6].

Moreover, different groups have worked on textile antennas [7–10] and leather antennas [11] for wearables, in which the conductivity is a prerequisite. Therefore, in order to make resistive traditional leather conductive, different groups have worked with different methods [2–4, 12–14].

In previous contributions, sheep crust leather was coated with polypyrrole using the double in-situ polymerization method and the electrical resistivity of conductive leather using the “multiple-step method” [15–16] in different air temperature and humidity conditions was measured [17].

In this paper, a theoretical analysis of the influence of humidity on the electric resistivity of leather was performed. The mathematical theory of this method will be outlined in the next section.

2 Mathematical model

In order to set up a mathematical model, a closer look must be taken at the experimental results shown in Figure 1. If the two figures (Figures 1a and 1b) are compared, it is clear that relative humidity *RH* is no longer a suitable parameter. On the other hand, Figure 1b shows a good relationship with absolute humidity. In a previously published paper, these data were fitted to $H^{-1.042}$ or $H^{-1.059}$, depending on whether sheets were included or only strips were taken into account [17]. The measuring technique was especially designed for textile samples and has been described extensively in literature [15–16].

These results are not surprising at all. Relative humidity is used to describe the environmental effect of air on the human body. Moreover, relative humidity is rather easy to measure. However, this paper deals with the electric conductivity of leather. Electric conductivity is determined by the intrinsic conductivity of leather and the amount of absorbed water molecules. The latter is simply absolute humidity usually expressed in g/kg or grams of water per kilogram air. We must therefore limit our investigation to modelling electric resistivity as a function of absolute humidity *H*.

If we extrapolate the fitting $H^{-1.042}$ or $H^{-1.059}$ [17] to low values of *H*, it is clear that the resistivity of intrinsic leather must be very high. We would expect it should be at least one order of magnitude higher than the maximum value of 500 Ωm shown in Figure 1b.

Firstly, the experimental fittings $H^{-1.042}$ or $H^{-1.059}$ [17] suggest that, theoretically speaking, it could be just *1/H*. Secondly, a closer look at Figure 1b tells us that humidity *H* has a tremendous influence on resistivity. The values vary between 65 Ωm and 437 *Ωm*. The conclusion is obvious: electric conduction is mainly determined by the amount of absorbed water, and the

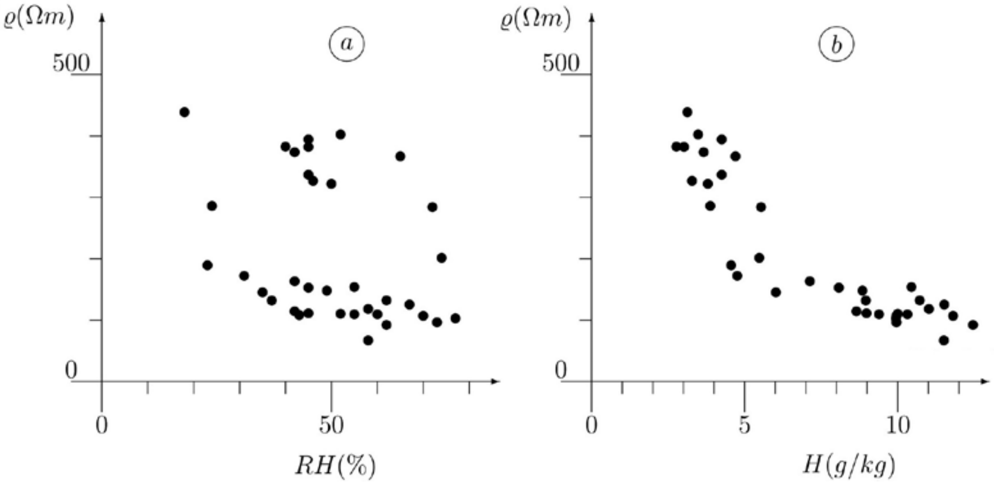

Figure 1: Variation of resistivity ρ vs. (a) relative humidity RH and (b) absolute humidity H [17]

conductivity of completely dry leather must be very low. These results also prove that there must be channels inside the leather filled with water. These channels provide electro conducting wires between the two electrodes. The word "channel" should be interpreted in a broad sense. A surface layer of water will also conduct electricity between the two electrodes.
A simple model is shown schematically in Figure 2. The two rectangular electrodes, with an area expressed as $S = b \times d$, are at distance a. Conducting channels now connect the two electrodes. Each channel has a cross section of ΔS and a length of a. It is obvious that the conductivity of the channel is proportional to absolute humidity: $\sigma_{channel} = \alpha H$. Conductance G between the two electrodes is then given by the equation:

$$G = G_{leather} + G_{Channels} = \sigma_{leather}\frac{bd}{a} + N\sigma_{channel}\frac{\Delta S}{a} \quad (1)$$

Conductivity σ, which is the inverse of resistivity *($\sigma = 1/\rho$)* is then found using the equation:

$$\sigma = G\frac{a}{bd} = \sigma_{leather} + N\sigma_{channel}\frac{\Delta S}{bd} = \sigma_{leather} + \frac{N\alpha\Delta S}{bd}H \quad (2)$$

Resistivity ρ is then the inverse of equation (2):

$$\rho = \frac{1}{\sigma} = \frac{1}{\sigma_{leather\;+N\sigma_{channel}\frac{\Delta S}{bd}}} = \frac{\rho_{leather}}{1+\beta H} \quad (3)$$

Where $\rho_{leather} = 1/\sigma_{leather}$. Parameter β is given by the equation:

$$\beta = \frac{N\alpha\Delta S\rho_{leather}}{bd} \quad (4)$$

As already stated, resistivity $\rho_{leather}$ is very high, so that (3) can be approximated using the equation:

$$\rho_{approx} = \frac{\rho_{leather}}{\beta H} \quad (5)$$

This result is quite close to the fittings $H^{-1.042}$ or $H^{-1.059}$ used in [17]. Although this mathematical model is very simple (all channels have an equal length and cross section), it will help us explain the experimental results, as will be seen below.
The experimental results shown in Figure 1b have been redrawn in Figure 3 on a double logarithmic scale. A *1/H* curve, such as (5), is then represented by a straight line. The experimental data can be fitted quite well to the equation 6, where the resistivity ρ is expressed in Ωm and the absolute humidity H in g/kg::

$$\rho_{approx} = \frac{1148}{H} \rightarrow \frac{\rho_{leather}}{\beta} = 1148 \quad (6)$$

A second fitting using (3) was only possible for $\rho_{leather}$ values > 10000 Ωm, as also shown in Figure 3. We can thus conclude that the fitting using (3) helps us to achieve a lower limit for the resistivity of intrinsic leather. If we assume for a moment $\rho_{leather}$ = 10000 Ωm, we can determine the parameter β to be given by β = 8.7108. Note that higher values of $\rho_{leather}$ also provide good fittings with the measurements.

3 Conductivity plot

Equations (2) and (3) suggest that it might be more obvious to plot conductivity σ as a function of absolute humidity H. We should then expect a straight line in a linear plot as shown in Figure 4. A linear fitting has been performed using the least squares approximation. The result is:

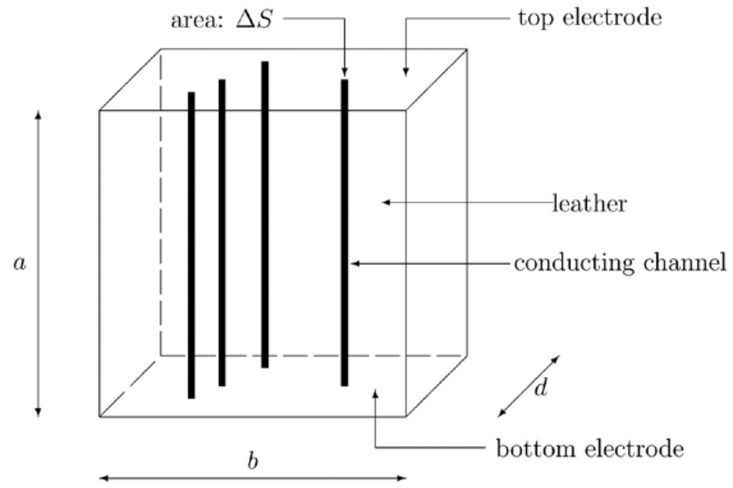

Figure 2: Model used to explain the electric resistivity of leather samples

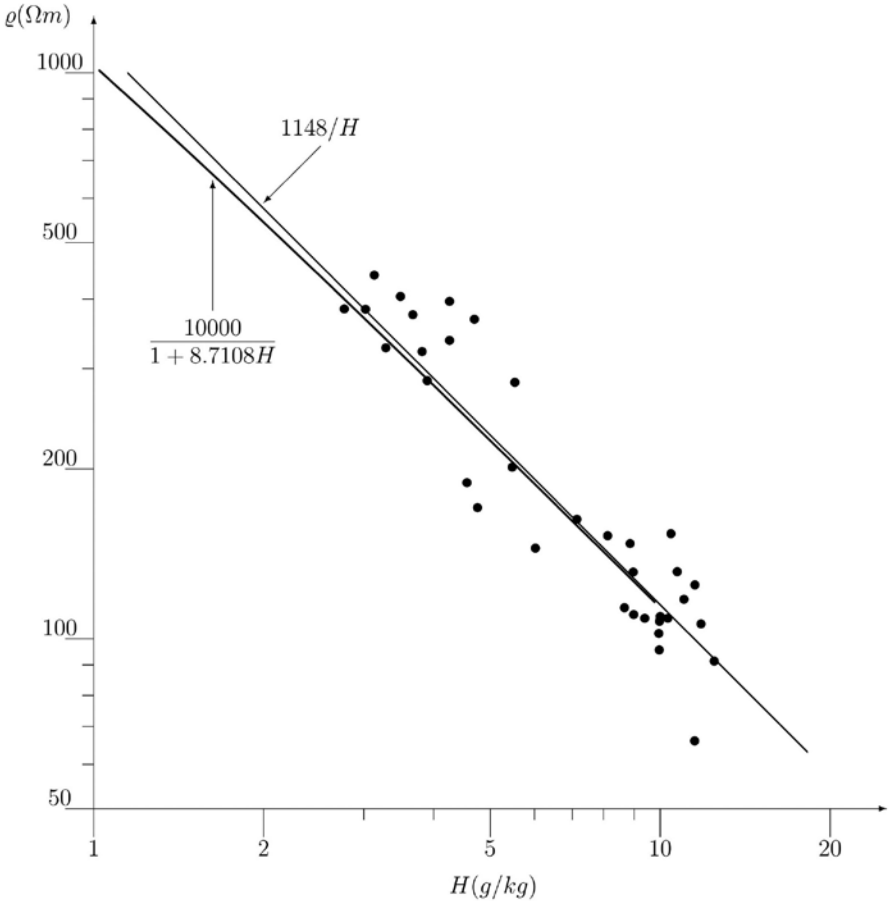

Figure 3: Double logarithmic plot of resistivity ρ vs. absolute humidity H

$$\sigma_{approx} = -0.0001975 + 0.00090883\,H \left(\frac{\mathrm{S}}{\mathrm{m}}\right) \quad (7)$$

As in the previous section, an extrapolation towards $H \to 0$ should inform us about the intrinsic conductivity of the leather. However, the fitting (7) gives us a negative number, which physically makes no sense. However, a closer view of Figure 4 reveals that the negative number in (7) is caused by inevitable errors due to the fitting procedure. We can also interpret these results as the zero conductivity of completely dry leather. Nevertheless, the conductivity plot is not suitable for obtaining a limiting value of leather conductivity.

For higher values of H, we can omit the negative number so that:

$$\sigma_{approx} = 0.00090883\,H \left(\frac{\mathrm{S}}{\mathrm{m}}\right) \quad (8)$$

from which we get easily:

$$\frac{1}{\sigma_{approx}} = \frac{10^4}{9.0833\,H} = \frac{1100.3}{H} \quad (\Omega\mathrm{m}) \quad (9)$$

which is very close to the approximation *1148/H* found in (6).

The conclusion is thus obvious: the conductivity plot is suitable for finding a simple relation such as (7), but we cannot find an upper limit for the conductivity of pure intrinsic leather. Using the resistivity plot presented in the previous section, it was possible to find a lower limit for leather resistivity of 10000 Ωm, which corresponds to a conductivity of 0.0001 S/m.

4 Discussion

In order to set up a mathematical model, a closer look must be taken at the experimental results shown in Figure 1. If we compare the model outlined so far, it is a highly simplified version of the real situation. In practice, not all conducting channels will connect two electrodes by a straight line. Some channels will be wider, and thus able to absorb more water from the surrounding air. We assume, for example, that half of the channels have a

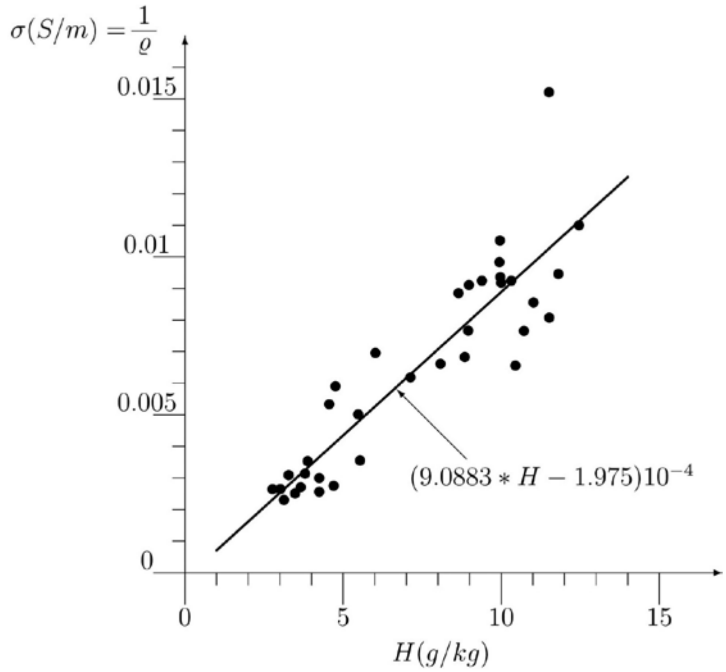

Figure 4: Plot of conductivity σ as a function of absolute humidity H

length of *a* and the other half have a double length of *2a*, as shown schematically in Figure 5.

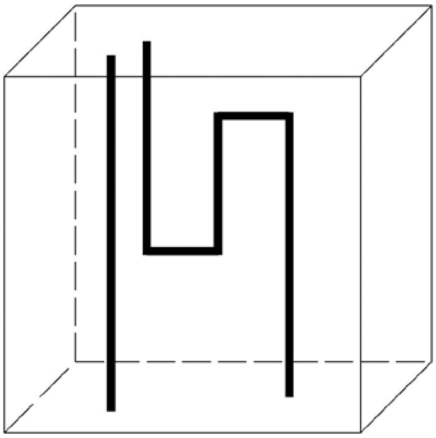

Figure 5: Channels with different lengths: a and 2a

Equation (1) must then be replaced by the equation:

$$G = G_{leather} + G_{channels} = \sigma_{leather}\frac{bd}{a} + \frac{N}{2}\sigma_{channel}\frac{\Delta S}{a} + \frac{N}{2}\sigma_{channel}\frac{\Delta S}{2a} \tag{10}$$

Equation (3) still remains valid. The difference is that coefficient β is now given by the equation:

$$\beta = \frac{3N\alpha\Delta S\rho_{leather}}{4bd} \tag{11}$$

This proves that the theory outlined above remains valid, and only the numerical value of β must be adjusted.

Obviously, the actual situation is much more complicated than channels with lengths of *a* and *2a*. In practice, channels are randomly distributed, may have different lengths and sections, and are oriented in all possible directions. Only channels connecting two electrodes can contribute to detectable resistivity. Even when probability distributions are introduced for channels lengths as the cross-sections in equation (2), we still arrive at the same result (3), except that the expression for coefficient β will be much more complicated than (4). The only assumption that may not be changed is: $\sigma_{channel} = \alpha H$. In other words: electric conductivity $\sigma_{channel}$ is proportional to absolute humidity *H*, and remains the basic assumption of our model.

5 Conclusion

A theoretical investigation of the electric conductivity of leather samples as a function of the absolute humidity is presented in this paper. In order to set up a mathematical model, a closer look must be taken at the experimental results. A mathematical model was presented to explain the electric conductivity of leather samples as a function of absolute humidity. It was also made clear that there is no direct correlation between resistivity and relative humidity. Moreover, it was possible to find a lower limit for the resistivity of intrinsic leather samples. It is clear that the same approach can be used to model the resistivity of other solid materials with channels that can absorb water from ambient humid air. Alternatively, such a method can also be used to indicate the porosity of a material.

References

1. NAM, H., SEOL, K.H., LEE, J., CHO, H., JUNG, S.W. Review of capacitive touchscreen technologies: overview, research trends, and machine learning approaches. *Sensors*, 2021, **21**(14), 4776, doi: 10.3390/s21144776.
2. YANG, C., WANG, J., LI, L. A novel approach for developing high thermal conductive artificial leather by utilizing smart electronic materials. *Textile Research Journal*, 2017, **87**(7), 816–828, doi: 10.1177/0040517516641356.
3. WEGENE, J.D., THANIKAIVELAN, P. Conducting leathers for smart product applications. *Industrial & Engineering Chemistry Research*, 2014, **53**(47), 18209–18215, doi: 10.1021/ie503956p.
4. HONG, K.H. Preparation of conductive leather gloves for operating capacitive touch screen displays. *Fashion & Textile Research Journal*, 2012, **14**(6), 1018–1023, doi: 10.5805/KSCI.2012.14.6.1018.
5. DURAN, D., KADOĞLU, H. Electromagnetic shielding characterization of conductive woven fabrics produced with silver-containing yarns. *Textile Research Journal*, 2015, **85**(10), 1009–1021, doi: 10.1177/0040517512468811
6. WANG, Y., PENG, H.K., LI, T.T., SHIU, B.C., ZHANG, X., LOU, C.W., LIN, J.H. Layer-by-layer assembly of low-temperature in-situ polymerized pyrrole coated nanofiber membrane for high-efficiency electromagnetic interference shielding. *Progress in Organic Coatings*, 2020, **147**, 105861, doi: 10.1016/j.porgcoat.2020.105861.
7. HERTLEER, C., ROGIER, H., VALLOZZI, L., VAN LANGENHOVE, L. A textile antenna for off-body communication integrated into protective clothing for firefighters. *IEEE Transactions on Antennas and Propagation*, 2009, **57**(4), 919–925, doi: 10.1109/TAP.2009.2014574.
8. VALLOZZI, L., VAN TORRE, P., HERTLEER, C., ROGIER, H., MOENECLAEY, M., VERHAEVERT, J. Wireless communication for firefighters using dual-polarized textile antennas integrated in their garment. *IEEE Transactions on Antennas and Propagation*, 2010, **58**(4), 1357–1368, doi: 10.1109/TAP.2010.2041168.
9. DEL-RIO-RUIZ, R., LOPEZ-GARDE, J.M., MACON, J.L., ROGIER, H. Design and performance analysis of a purely textile spiral antenna for on-body NFC applications. In *2017 IEEE MTT-S International Microwave Workshop Series on Advanced Materials and Processes for RF and THz Applications (IMWS-AMP)*, 2017, 1–3, doi: 10.1109/IMWS-AMP.2017.8247427.
10. JIANG, Y., XU, L., PAN, K., LENG, T., LI, Y., DANOON, L., HU, Z. e-Textile embroidered wearable near-field communication RFID antennas. *IET Microwaves, Antennas & Propagation*, 2019, **13**(1), 99–104, doi: 10.1049/iet-map.2018.5435.
11. MITILINEOS, S.A., KALLIVRETAKI, A.E., VASSILIADIS, S., KAZANI, I., GUXHO, G., DASSONVILLE, F., KONCAR, V. A wearable NFC antenna sewn on leather substrate for immersive IoT applications. *Textile & Leather Review*, 2022, **5**, 70–84, doi: 10.31881/TLR.2022.03.
12. SHIN, E.J., HAN, S.S., CHOI, S.M. Fabrication of highly electrical synthetic leather with polyurethane/poly(3,4-ethylene dioxythiophene)/poly(styrene sulfonate). *The Journal of The Textile Institute*, 2018, **109**(2), 241–247, doi: 10.1080/00405000.2017.1337296.
13. BAO, Y., FENG, C., WANG, C., MA, J., TIAN, C. Hygienic, antibacterial, UV-shielding performance of polyacrylate/ZnO composite coatings on a leather matrix. *Colloids and Surfaces A: Physicochemical and Engineering Aspects*, 2017, **518**, 232–240, doi: 10.1016/j.colsurfa.2017.01.033.
14. HYLLI, M., SHABANI, A., KAZANI, I., BEQIRAJ, E., DRUSHKU, S., GUXHO, G. Application of double in-situ polimerization for changing the leather properties. In *Book of Proceedings of 8th International Textile Conference*, Tirana, Albania, 2018, 42–47.
15. BERBERI, P.G. A new unified method for measurment of electrical resistivity of textile assemblies. In *Proceedings of ESA Annual Meeting, Boston University, June 23–25, 1999*, 121–134.
16. BERBERI, P.G. Effect of processing on electrical resistivity of textile fibers. *Journal of Electrostatics*, 2001, **51–52**, 538–544, doi: 10.1016/S0304-3886(01)00112-7.
17. KAZANI, I., HYLLI, M., BERBERI, P. Electrical resistivity of conductive leather and influence of air temperature and humidity. *Tekstilec*, 2021, **64**(4), 298–304, doi: 10.14502/Tekstilec2021.64.298-304.

SHORT INSTRUCTIONS FOR AUTHORS OF SCIENTIFIC ARTICLES

Scientific articles categories:

- **Original scientific article** is the first publication of original research results in such a form that the research can be repeated and conclusions verified. Scientific information must be demonstrated in such a way that the results are obtained with the same accuracy or within the limits of experimental errors as stated by the author, and that the accuracy of analyses the results are based on can be verified. An original scientific article is designed according to the IMRAD scheme (Introduction, Methods, Results and Discussion) for experimental research or in a descriptive way for descriptive scientific fields, where observations are given in a simple chronological order.
- **Review article** presents an overview of most recent works in a specific field with the purpose of summarizing, analysing, evaluating or synthesizing information that has already been published. This type of article brings new syntheses, new ideas and theories, and even new scientific examples. No scheme is prescribed for review article.
- **Short scientific article** is original scientific article where some elements of the IMRAD scheme have been omitted. It is a short report about finished original scientific work or work which is still in progress. Letters to the editor of scientific journals and short scientific notes are included in this category as well.

Language: The manuscript of submitted articles should be written in UK English and it is the authors responsibility to ensure the quality of the language.

Manuscript length: The manuscript should not exceed 30,000 characters without spacing.

Article submission: The texts should be submitted only in their electronic form in the format *.doc (or *docx) and in the format *.pdf (made in the computer program Adobe Acrobat) to the address: tekstilec@a.ntf.uni-lj.si. The name of the document should contain the date (year-month-day) and the surname of the corresponding author, e.g. 20140125Novak.docx. The articles proposed for a review need to have their figures and tables included in the text. The article can also be submitted through a cloud-based file transfer service, e.g. "WeTransfer" (www.wetransfer.com).

Publication requirements: All submitted articles are professionally, terminologically and editorially reviewed in accordance with the general professional and journalistic standards of the journal Tekstilec. Articles are reviewed by one or more reviewers and are accepted for publication on the basis of a positive review. If reviewers are not unanimous, the editorial board decides on further proceedings. The authors can propose to the editorial board the names of reviewers, whereas the editorial board then accepts or rejects the proposal. The reviewers' comments are sent to authors for them to complete and correct their manuscripts. The author is held fully responsible for the content of their work. Before the author sends their work for publication, they need to settle the issue on the content publication in line with the rules of the business or institution, respectively, they work at. When submitting the article, the authors have to fill in and sign the Copyright Statement (www.tekstilec.si), and send a copy to the editors by e-mail. They should keep the original for their own personal reference. The author commits themselves in the Copyright Statement that the manuscript they are submitting for publication in Tekstilec was not sent to any other journal for publication. When the work is going to be published depends on whether the manuscript meets the publication requirements and on the time reference the author is going to return the required changes or corrections to the editors.

Copyright corrections: The editors are going to send computer printouts for proofreading and correcting. It is the author's responsibility to proofread the article and send corrections as soon as possible. However, no greater changes or amendments to the text are allowed at this point.

Colour print: Colour print is performed only when this is necessary from the viewpoint of information comprehension, and upon agreement with the author and the editorial board.

More information on: www.tekstilec.si